GOLD OPEN ACCESS

THE GEOLOGICAL SOCIETY OF AMERICA®

Evaluating the Shinumo-Sespe drainage connection: Arguments against the "old" (70–17 Ma) Grand Canyon models for Colorado Plateau drainage evolution

Karl E. Karlstrom[1], Carl E. Jacobson[2,3], Kurt E. Sundell[4], Athena Eyster[5], Ron Blakey[6], Raymond V. Ingersoll[7], Jacob A. Mulder[8], Richard A. Young[9], L. Sue Beard[10], Mark E. Holland[11], David L. Shuster[12,13], Carmen Winn[1], and Laura Crossey[1]

[1]Department of Earth and Planetary Sciences, University of New Mexico, Albuquerque, New Mexico 87131, USA
[2]Department of Geological and Atmospheric Sciences, Iowa State University, Ames, Iowa 50011-3212, USA
[3]Department of Earth and Space Sciences, West Chester University of Pennsylvania, West Chester, Pennsylvania 19383, USA
[4]Department of Geosciences, University of Arizona, Tucson, Arizona 85721, USA
[5]Earth, Atmospheric and Planetary Sciences, Massachusetts Institute of Technology, Cambridge, Massachusetts 02139, USA
[6]Colorado Plateau Geosystems, Phoenix, Arizona 85032, USA
[7]Department of Earth, Planetary, and Space Sciences, University of California, Los Angeles, California 90095-1567, USA
[8]School of Earth, Atmosphere and Environment, Monash University, Clayton, Victoria 3168, Australia
[9]Department of Geological Sciences, State University of New York at Geneseo, New York 14454, USA
[10]United States Geological Survey, Flagstaff, Arizona 86001, USA
[11]Department of Life, Earth, and Environmental Sciences, West Texas A&M University, 2403 Russell Long Boulevard, Canyon, Texas 79015, USA
[12]Department of Earth and Planetary Science, University of California, Berkeley, Berkeley, California 94720-4767, USA
[13]Berkeley Geochronology Center, 2455 Ridge Road, Berkeley, California 94709, USA

ABSTRACT

The provocative hypothesis that the Shinumo Sandstone in the depths of Grand Canyon was the source for clasts of orthoquartzite in conglomerate of the Sespe Formation of coastal California, if verified, would indicate that a major river system flowed southwest from the Colorado Plateau to the Pacific Ocean prior to opening of the Gulf of California, and would imply that Grand Canyon had been carved to within a few hundred meters of its modern depth at the time of this drainage connection. The proposed Eocene Shinumo-Sespe connection, however, is not supported by detrital zircon nor paleomagnetic-inclination data and is refuted by thermochronology that shows that the Shinumo Sandstone of eastern Grand Canyon was >60 °C (~1.8 km deep) and hence not incised at this time. A proposed 20 Ma (Miocene) Shinumo-Sespe drainage connection based on clasts in the Sespe Formation is also refuted. We point out numerous caveats and non-unique interpretations of paleomagnetic data from clasts. Further, our detrital zircon analysis requires diverse sources for Sespe clasts, with better statistical matches for the four "most-Shinumo-like" Sespe clasts with quartzites of the Big Bear Group and Ontario Ridge metasedimentary succession of the Transverse Ranges, Horse Thief Springs Formation from Death Valley, and Troy Quartzite of central Arizona. Diverse thermochronologic and geologic data also refute a Miocene river pathway through western Grand Canyon and Grand Wash trough. Thus, Sespe clasts do not require a drainage connection from Grand Canyon or the Colorado Plateau and provide no constraints for the history of carving of Grand Canyon.

Instead, abundant evidence refutes the "old" (70–17 Ma) Grand Canyon models and supports a <6 Ma Grand Canyon.

■ INTRODUCTION

Sedimentary provenance studies are used extensively in paleogeographic and tectonic reconstructions. Ideally, the goal of a provenance study is to characterize the depositional system from source-to-sink using as many diagnostic features as possible, including sources of detritus, constraints on sediment transport, and depositional settings. This goal challenges current methods that often have non-unique interpretations. Here, we critically examine a provocative hypothesis for the provenance of Cenozoic deposits of the southwestern Colorado Plateau region of the United States. This provides a good case study because the accumulated detrital zircon data for sources and sinks are voluminous, and the provenance interpretations have high-profile tectonic and paleogeographic ramifications.

■ THE SHINUMO-SESPE HYPOTHESIS

Recent papers have evaluated whether the Mesoproterozoic Shinumo Sandstone, exposed only deep in Grand Canyon, was the source of some clasts in the Sespe Formation of the Los Angeles basin area (Wernicke, 2011; Ingersoll et al., 2013, 2018; Sabbeth et al., 2019). If even a single such clast could be positively verified, this would provide an important source-to-sink

Karl E. Karlstrom https://orcid.org/0000-0003-2756-1724

"nail" for reconstructing a past drainage connection between a Grand Canyon source and a Sespe Formation sink, and hence for refining paleogeographic and tectonic reconstructions of the Colorado Plateau and southern California regions. Specifically, this hypothesis requires that Grand Canyon had been carved in its present position and to near its modern depth so that the Shinumo Sandstone, which is only exposed in the depths of Grand Canyon within a few hundred meters of the modern river, was acting as the source for clasts in downstream basins. Wernicke (2011) proposed this connection for the entire Sespe Formation, which ranges from middle Eocene to early Miocene in age. Sabbeth et al. (2019) tested this hypothesis through zircon U-Pb dating and paleomagnetic analysis of conglomerate clasts in the Sespe Formation and potential source rocks, including the Shinumo Sandstone. They found no evidence of an Eocene connection but did posit that clasts in the Miocene part of the Sespe Formation were derived from Grand Canyon. However, both Eocene and Miocene connections conflict with recent thermochronologic and geologic evidence that indicates that the Shinumo Sandstone was not likely exposed in Grand Canyon during either of these timeframes (Karlstrom et al., 2014; Young and Crow, 2014; Fox et al., 2017; Winn et al., 2017; Lamb et al. 2018) such that the "Shinumo-Sespe hypothesis" needs thorough evaluation.

Wernicke (2011, p. 1301) proposed that the drainage connection between southern California and Grand Canyon initiated at ca. 55 Ma through an "Arizona River" that "carved Grand Canyon to within a few hundred meters of its modern depth." This river would have fed lower to middle Eocene marine formations now exposed in the Los Angeles and surrounding areas, followed by the nonmarine Sespe Formation beginning at ca. 42 Ma. In contradiction, Ingersoll et al. (2013, p. 311) concluded, based on an extensive Mesozoic to Cenozoic detrital zircon record for southern California, that: "Although Paleogene headwaters of southern California rivers extended into the eastern Mojave Desert, Sonoran Desert, and Mogollon Highlands, our results indicate that these headwaters did not extend as far as the Colorado Plateau." This conclusion is consistent with the failure of Sabbeth et al. (2019) to find a Sespe-Shinumo connection in the Eocene, although they have continued to use the name "Arizona River" for their inferred connection at ca. 20 Ma. Specifically, they concluded (Sabbeth et al., 2019, p. 1973) that: "The Shinumo Formation, presently exposed only within a few hundred meters elevation of the bottom of eastern Grand Canyon, thus remains the only plausible, known source for the moderate- to high-inclination clast population [in the Miocene part of the Sespe Formation]. If so, then the Upper Granite Gorge of the eastern Grand Canyon had been eroded to within a few hundred meters of its current depth by early Miocene time (ca. 20 Ma)."

The first goal of this paper is to evaluate both the 50 and 20 Ma iterations of the "Arizona River" hypothesis in the context of current understanding of the age of Grand Canyon. The second goal is to synthesize the Eocene through Miocene drainage evolution and paleogeography of this region. For both goals, we provide a more extensive inventory of detrital zircon characteristics of potential quartzite and sandstone sources as well as the preserved remnants of paleoriver deposits and depositional basins in the region.

■ SESPE FORMATION PROVENANCE

Quartzite pebbles and cobbles are notoriously durable and persistent in rivers, and it is a commendable (and elusive) goal to try to parse source terranes for far-traveled quartzite clasts. The Sespe Formation (Howard, 1987, p. 13) consists of "sequences of unfossiliferous strata lying above fossiliferous marine Eocene rocks and overlain by fossiliferous marine Miocene rocks." It contains far-traveled quartzite clasts defined by Howard (2000, p. 1635) as quartzose sedimentary rocks (not necessarily quartz arenites) that fracture across grain boundaries. This property may be the result of diagenesis (orthoquartzite) or metamorphism (metaquartzite). These terms are difficult to apply in detail and further petrographic subdivisions are needed for detailed provenance work (e.g., Howard, 2000; his tables 2 and 3; Sabbeth et al., 2019; their supplementary figure 3). Descriptions from both papers suggest that quartzose clasts of the Eocene (ca. 42 Ma) to Miocene (ca. 20 Ma) components of the Sespe Formation include a diverse population of white, black, red, and green pebbles and cobbles that include metaquartzite and silica-cemented orthoquartzite that range in composition from quartz arenite to arkose.

Figure 1 shows potential source regions for the orthoquartzite clasts in the Sespe Formation. These regions contain diverse types of quartzose rocks. Paleoproterozoic to lower Mesoproterozoic (1.78–1.50 Ga) metaquartzites are common in the Mojave (Barth et al., 2009; Holland et al., 2018) and central Arizona areas (e.g., Cox et al., 2002; Doe et al., 2012; Mako et al., 2015; Spencer et al., 2016b). Lower Mesoproterozoic (1.5–1.45 Ga) metaquartzites are present in central Arizona (Doe et al., 2012, 2013). Metaquartzites range from lower greenschist to amphibolite facies and tend to have polygonal and interlocking grain boundaries. Orthoquartzites occur in the Mesoproterozoic (1.25–1.1 Ga) Pahrump, Apache, and Unkar Groups in the Mojave, central Arizona, and Grand Canyon regions (Timmons et al., 2005; Mahon et al., 2014a, 2014b; Mulder et al., 2017, 2018). Neoproterozoic orthoquartzite is present in Grand Canyon and Death Valley (Mahon et al., 2014a; Dehler et al., 2017), and Phanerozoic orthoquartzite is known in several units such as the Permian Coconino Sandstone and Jurassic Navajo and/or Aztec sandstones. These sandstones are generally unmetamorphosed and show diagenetic quartz overgrowths and pressure solution. Less mature Paleozoic sandstone also occurs across the Southwest; for example, the Tapeats Sandstone and its correlatives are dominantly arkosic to subarkosic (McKee and Resser, 1945; Hereford, 1977; Stewart et al., 2001; Karlstrom et al., 2018) and rarely quartz arenite (e.g., Zabriskie Quartzite, Howard, 2000). Several of the orthoquartzite lithologies were variably metamorphosed in the Maria fold and thrust belt and Death Valley region (Labotka, 1980; Hamilton, 1987; Applegate and Hodges, 1995; Salem, 2009), potentially blurring the use of metamorphic versus diagenetic textures. Some samples depicted in Sabbeth et al. (2019; their supplementary figure S3) display textures similar to those of the region's metaquartzites (e.g., 14LS02 and 14LS05), and others are similar to the Mesoproterozoic silica-cemented sandstones (e.g., 14LS08, 14LS09, and BW1614). Overall, the textures of many Sespe clasts remain ambiguous for source correlations.
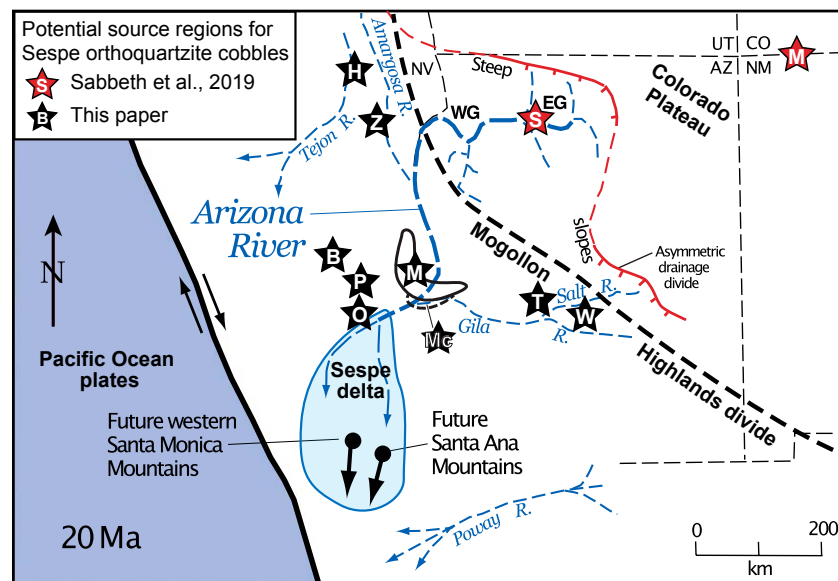
Figure 1. Index map of the southwestern United States showing the proposed Arizona River hypothesis (modified from Sabbeth et al., 2019). Potential source regions for orthoquartzite clasts in the Sespe Formation are shown by stars. Red star source regions and the red asymmetric drainage divided favored by Sabbeth et al. (2019) are not favored here. Instead, a more southerly Mogollon Highlands drainage divide and the black source regions are favored by our detrital zircon analysis. Abbreviations: B—Big Bear Group; EG—eastern Grand Canyon; H—Horsethief Springs Formation; red M—Morrison Formation; black M and outline—metamorphosed Paleozoic rocks of Maria fold and thrust belt; black dash—area of McCoy (Mc) Mountains Formation; O—Ontario Ridge metasedimentary rocks; P—Pinto Mountain Group; S—Shinumo Sandstone; T—Troy Quartzite; W—White Ledges Formation; WG—western Grand Canyon; Z—Zabriskie Quartzite.

The potential Shinumo Sandstone source in Grand Canyon has the smallest areal extent of any of the possible sources for Sespe clasts shown in Figure 1. Tilted sandstone of the Unkar Group occurs only in several small areas (total <100 km²) in the inner gorge of eastern Grand Canyon, from river mile 78–108 (Fig. 2A). The Shinumo Sandstone (Timmons et al., 2005), previously called the Shinumo Quartzite (Elston et al., 1993), is a strongly cross-bedded, silica-cemented quartz arenite containing a thick interval of convolute bedding. Its age is 1150–1104 Ma, as constrained between the age of the youngest detrital zircon grains (Mulder et al., 2017) and the age of the stratigraphically overlying 1104 Ma Cardenas Basalt and intrusive 1100 Ma diabase dikes and sills (Timmons et al., 2005). Its detrital zircon spectra contain peaks at 1.8–1.7, 1.45–1.40, and 1.3–1.1 Ga. Older grains suggest it was derived in part from unroofing of the underlying Vishnu Schist, but there was also appreciable input of detritus in the foreland of the 1.3–1.0 Ga Texas-Grenville suture to the south (Mulder et al., 2017, 2018). Outcrops of the Shinumo Sandstone extend to as high as 1260 m elevation in eastern Grand Canyon near river miles 80 and 88 (up to 530 m above the river), and 1120 m near River Mile 109 (450 m above the river), but most of Shinumo Sandstone outcrop is less than 300 m above the river. As such, it would be a potential source rock following carving of eastern Grand Canyon to within ~300 m of its modern depth.

The Sespe Formation in southern California restores ~310 km across the San Andres fault system to a 20 Ma position west of the modern Colorado River delta. It was deposited within what Howard (2000) and Ingersoll et al. (2013, 2018) termed the Sespe delta (Fig. 1). The Sespe Formation is predominantly Oligocene, although it is as old as middle Eocene (42 Ma) and as young as early Miocene (20 Ma). Based on integrated study of conglomerate clast assemblage, sandstone petrography, and detrital zircon ages, Ingersoll et al. (2018) concluded that most sediment of the Sespe delta was sourced from the Mesozoic Cordilleran arc, with subequal amounts of Cretaceous and Jurassic detritus and lesser Triassic detritus, plus Proterozoic framework rocks (ca. 1.7 and ca. 1.4 Ga) of southern California, southwestern Arizona, and northwestern Sonora, Mexico. Far-traveled quartzite clasts may have been sourced on the southern slopes of the Mogollon highlands of central Arizona and transported by rivers that came across the arc. But the near absence of detrital zircon ages of 300–1000 Ma (distinctive ages in upper Paleozoic through Cretaceous strata of the Colorado Plateau; e.g., Dickinson and Gehrels, 2003, 2009; Gehrels et al., 2011) is inconsistent with derivation of Sespe detritus from the Grand Canyon area. Rather, the oldest record of the distinctive 300–1000 Ma signature corresponds with the arrival of Colorado River detritus to the Salton Trough area at 5 Ma (Kimbrough et al., 2015; Crow et al., 2019a). Thus, Ingersoll et al. (2013, 2018) argued that diverse provenance data from the Sespe Formation and detrital zircon age spectra from Cretaceous through Pliocene strata of southern California do not support the cutting of Grand Canyon prior to the Pliocene. The range of possible source rocks and areas shown in Figure 1 indicates that finding one or more definitive Shinumo Sandstone clasts from the Grand Canyon within the Sespe Formation has a low probability. This paper challenges the Wernicke (2011) and Sabbeth et al. (2019) statement that Shinumo Sandstone is "the only plausible" source for a subset of Sespe clasts.
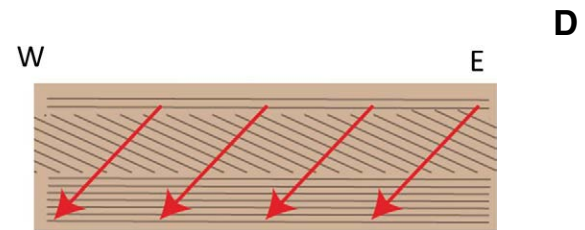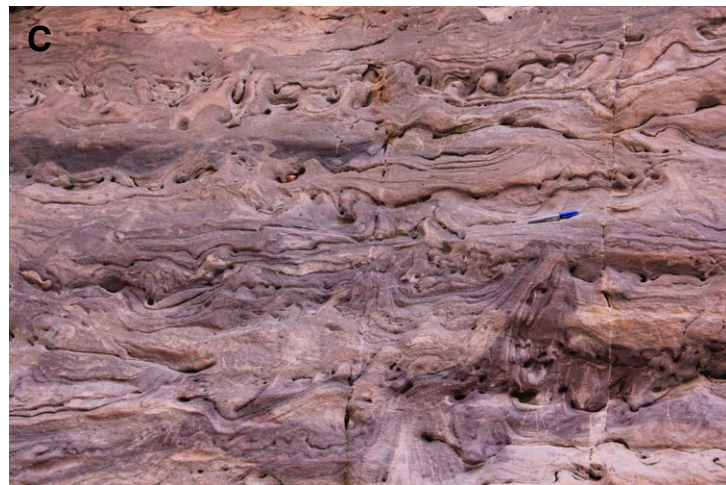
Figure 2. (A) 300-m-thick Shinumo Sandstone in Grand Canyon extends several hundred meters above the river in tilted fault blocks. (B) Correlative Mesoproterozoic Troy Quartzite of central Arizona is another potential source for Sespe cobbles. (C) Convolute bedding and bi-polar foresets in outcrops of Shinumo Sandstone of Grand Canyon show that sedimentary lamination in cobbles need not be horizontal bedding. (D) Illustration of how a 50°W–plunging paleomagnetic inclination relative to bedding would be measured as a 70° inclination relative to E-dipping cross bedding; modified from Sabbeth et al. (2019), their supplementary figure S4. (*Continued on following page.*)
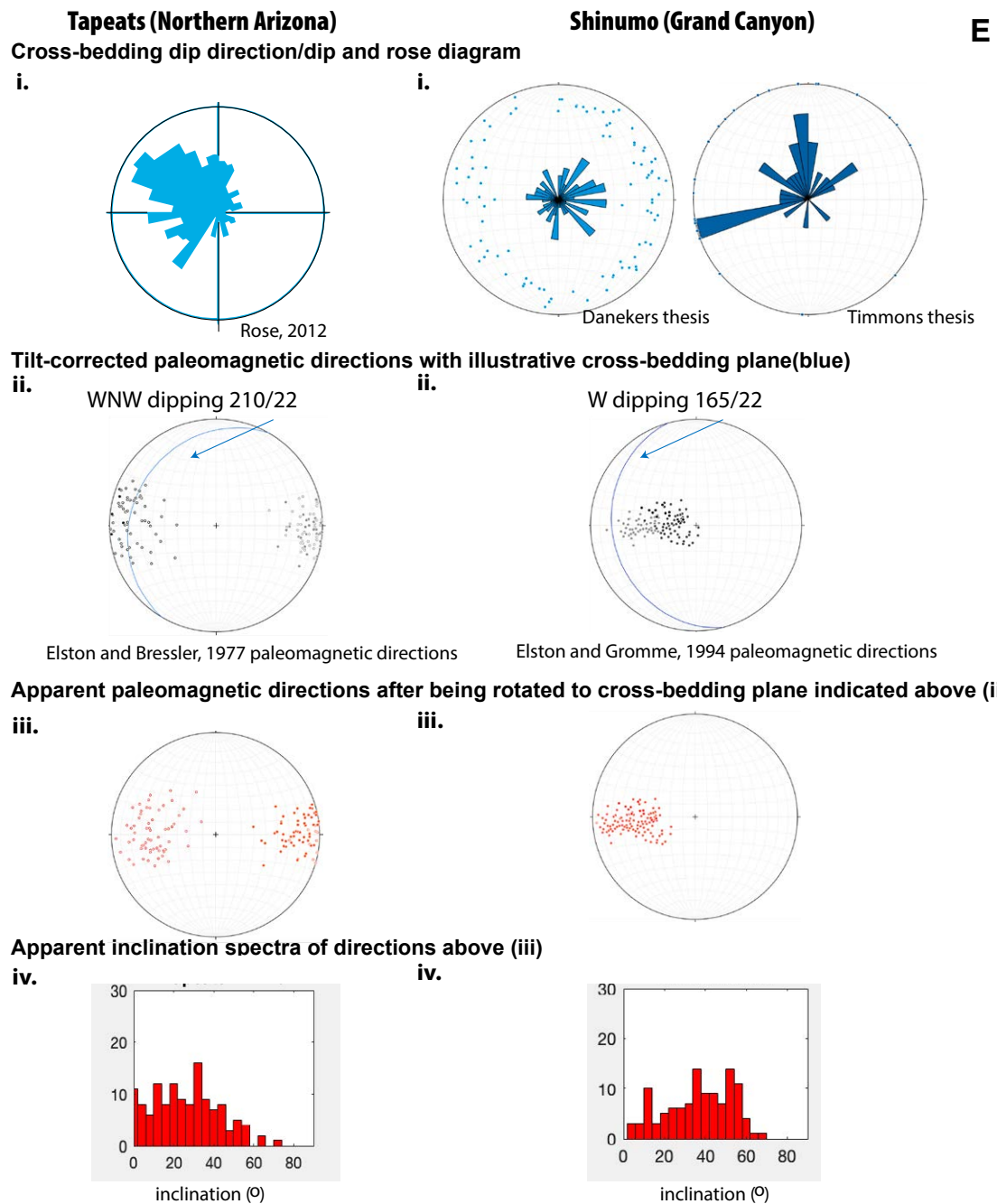
E

Tapeats (Northern Arizona)

Cross-bedding dip direction/dip and rose diagram

i.

Rose, 2012

Shinumo (Grand Canyon)

i.

Danekers thesis   Timmons thesis

Tilt-corrected paleomagnetic directions with illustrative cross-bedding plane(blue)

ii.
WNW dipping 210/22

Elston and Bressler, 1977 paleomagnetic directions

ii.
W dipping 165/22

Elston and Gromme, 1994 paleomagnetic directions

Apparent paleomagnetic directions after being rotated to cross-bedding plane indicated above (ii)

iii.

iii.

Apparent inclination spectra of directions above (iii)

iv.

inclination (º)

iv.

inclination (º)

Figure 2 (*continued*). (E) Illustration of non-uniqueness of inclination data when cross-bedding versus bedding laminations cannot be distinguished. For both Tapeats (left) and Shinumo (right) sandstones of Grand Canyon, E.i. plots of paleoflow directions and dips (blue), E.ii. plots of the sample paleomagnetic directions (black) and an illustrative bedding plane (210/22 for Tapeats and 165/22 for Shinumo, both in blue), E.iii. plots of the apparent paleomagnetic directions, i.e., the measured paleomagnetic directions relative to horizontal (as plotted in E.ii) having been rotated about the strike of the indicated cross-bedding plane, resulting in the apparent paleomagnetic directions one might measure if bedding were confused with this orientation of cross bedding. E.iv. illustrates the overall inclination spectra of these apparent directions and shows the non-uniqueness of inclination data when cross bedding cannot be distinguished from bedding lamination.

■ PALEOMAGNETISM OF CLASTS AS A PROVENANCE CONSTRAINT

Applying paleomagnetic analyses to clasts for provenance studies is a unique and unconventional approach because all geographic context is lost in transport. The main constraint obtainable from pebbles is the magnetic paleoinclination relative to "sedimentary lamination" (Sabbeth et al., 2019, their figure 4). This could be a meaningful constraint if the magnetization is demonstrated to be primary (syn-depositional) relative to bedding in the cobbles. Sabbeth et al. (2019) suggest that Mesoproterozoic source rocks would contain moderate primary inclinations and hence be distinguishable from Neoproterozoic and Cambrian source regions that would contain shallow inclinations.

Primary or Secondary Magnetization in Cobbles

The approach of Sabbeth et al. (2019) relies on inclination data from clasts, without verifying that the clasts actually carry a pre-depositional magnetization via a positive conglomerate test. The conglomerate test is one of the fundamental field tests in paleomagnetism and tests two alternate hypotheses: (1) that the rock has been remagnetized such that the matrix and clasts all display the same direction representing a non-primary postdepositional direction; versus (2) that the rock has not been remagnetized and that the matrix displays a primary syn-sedimentary direction, whereas the clasts preserve distinct pre-depositional magnetizations that are generally random. Unfortunately, as Sabbeth et al. (2019) noted, a conglomerate test was not conducted. Other paleomagnetic work conducted on the Sespe Formation has demonstrated that it carries an early chemical remanent magnetization (CRM) (Hillhouse, 2010), but its effect on clasts, if any, cannot be evaluated using the Sabbeth et al. (2019) data.

Primary or Secondary Magnetization in Source Regions

The question of whether the magnetization is primary in the source region is also untestable from the clast data because of the possibility of steep overprints on lower-inclination primary directions. For example, any of the orthoquartzites could have been remagnetized in the Late Cretaceous to Cenozoic in the Maria fold and thrust belt, core complexes, or Death Valley regions to give moderate secondary inclinations similar to today's magnetic field. For example, samples from Neoproterozoic–Cambrian sandstones from Grand Canyon and the Uinta Mountains have been completely remagnetized with steep recent chemical remanent magnetizations carried by hematite (Weil et al., 2004, 2006; Eyster et al., 2020). Some of the Zijderveld diagrams from these remagnetized samples (Eyster et al., 2020) look similar to those depicted as primary in Sabbeth et al. (2019). Hence, it is possible that some of the Sespe clasts could include a primary direction carried by magnetite (or lower-coercivity hematite) and then

a steep overprint carried by high-coercivity hematite (Sabbeth et al., 2019; their supplementary figure S2). The Cambrian Zabriskie Quartzite was proposed by Howard (2000) as a potential source of Sespe clasts. It locally displays steep overprints or pervasive steep remagnetization, and, in one study, about half of the samples displayed steep natural remanent magnetization (NRM) directions near the present axial dipole field that changed only slightly upon thermal demagnetization to 680 °C (Van Alstine and Gillett, 1979). The development of steep remagnetizations has been documented in a variety of units and has the potential to occur in many of the possible source locations. Thus, it is problematic to assume and inaccurate to claim (Sabbeth et al., 2019, p. 1973) that moderate to steep inclinations are a unique fingerprint of the Mesoproterozoic Shinumo Sandstone of Grand Canyon.

Complexity of Cross Bedding

The measured paleoinclination data of clasts would only distinguish among different age sources if it is certain that the reference lamination is original horizontal bedding rather than cross bedding. However, convolute layering and polymodal cross bedding are very common in the Shinumo Sandstone (Fig. 2A; Daneker, 1975) as well as many other potential source rocks such as the Troy Quartzite (Fig. 2B). Cross bedding is generally defined by oxide-rich laminae (Fig. 2C) and would likely be indistinguishable from original horizontal bedding in isolated clasts. Thus, inclinations in the clasts could be mistakenly measured relative to cross bedding, not horizontal bedding. Sabbeth et al. (2019) claimed, too optimistically, that they can guess the most likely foreset dip for the Shinumo Sandstone and Tapeats Sandstone, and hence guess the more likely ± ~30° dispersion. But their assumed dominant foreset dip directions (Sabbeth et al., 2019; their supplementary figure S4) oversimplify the reported paleocurrent data for the Shinumo Sandstone, which includes trough cross beds with a dominant transport direction toward ~350° but with planar-tabular cross beds suggesting bipolar current directions to NE and SW (Fig. 2E.i; Daneker, 1975; Timmons et al., 2005; Mulder et al., 2017). Tapeats Sandstone (Rose, 2011) exhibits bi-polar (tidally influenced) cross beds, and other sandstones such as the Troy Quartzite are also pervasively cross bedded (Burns, 1987).

Figure 2D shows the reasoning of Sabbeth et al. (2019; their supplementary figure S4) that 50°W–plunging paleoinclinations relative to bedding in the Shinumo Sandstone would yield steeper (~70°) apparent paleoinclinations, relative to east-dipping foresets dominated. However, foreset planes have more diverse orientations in both Tapeats and Shinumo sandstones than they reported (Fig. 2E.i), as do measured paleomagnetic paleopoles (Fig. 2E.ii). To illustrate the complexity for a given illustrative foreset plane (e.g., Fig. 2E.ii), the apparent paleomagnetic inclination relative to that foreset is rotated by the dip of the foreset (Fig. 2E.iii), and the resulting apparent inclination spectra are quite dispersed (from 0° to 70°; Fig. 2E.iv). Once the numerous multiple foreset orientations are considered (Table S1[1] in the Supplemental Material), inadvertently mistaking cross bedding for bedding as the datum in clasts

Karlstrom et al. | Shinumo-Sespe drainage connection

for both Tapeats and Shinumo clasts results in apparent paleoinclinations ranging from 0° to 80° for either Mesoproterozoic or Cambrian cross-bedded sandstones. This is another potentially fatal caveat of using paleoinclination data for provenance studies of the Sespe clasts.

Evaluating the Sespe Clast Paleomagnetic Data

Figure 3 further explores the data reported by Sabbeth et al. (2019). They obtained paleoinclinations from 44 of 92 orthoquartzite pebbles with inclination values ranging from 0° to 78° (Fig. 3A). The range and distribution of clast paleoinclinations from both Eocene and Miocene parts of the Sespe Formation are similar, with maxima at ~16° and 40°. Although their small data set may not be statistically defendable, and disregarding the marked overlap (0°–55°) of values, Sabbeth et al. (2019) concluded that the Eocene clasts had a "stronger peak" at 15° and no steep (>55°) inclination clasts, whereas Miocene clasts had peaks at 15° and 45° and several values >60°. The potential sources they characterized are also shown in Figure 3A and included the Shinumo Sandstone (1.15–1.0 Ga), yielding dominantly mid-value (20°–80°) inclinations (from unpublished data of Elston and Grommé, 1994), and the Tapeats Sandstone (0.51 Ga), yielding dominantly lower inclinations (0°–40°; from Elston and Bressler, 1977). They concluded that their Miocene clasts, but not the Eocene clasts, may have been sourced from the Shinumo Sandstone. However, this is unconvincing given the substantial (14°–44°) overlap within and between these potential sources. Both the Tapeats and Shinumo inclination data in Figure 3A are more dispersed than would be expected in modern

data sets such that there also may be problems with overprints. Thus, similar to detrital zircon studies, future clast-inclination provenance studies will need to involve larger sample sizes and statistical treatment (e.g., >100 samples) to derive potential fingerprints of various sources.

Laurentia's apparent polar-wander path during Mesoproterozoic to Cambrian time is shown in Figure 3B (Swanson-Hysell et al., 2019). Data sets from North America support the conclusion by Sabbeth et al. (2019) that Mesoproterozoic source rocks would contain moderate primary inclinations and Neoproterozoic and Cambrian source regions would contain shallow inclinations. However, there have been very few paleomagnetic studies conducted with demagnetization data, and no paleomagnetic poles are available from Mesoproterozoic quartzites of the Southwest outside the Grand Canyon Unkar Group. The incomplete characterization of the wider possibilities of potential source rocks shown in Figure 1 is a fatal weakness for uniquely interpreting the paleoinclination data. Even if one accepted that the 40°–80° paleoinclinations of pebbles of the Miocene Sespe reflect primary source-rock inclinations relative to bedding, and therefore that 17 of 44 orthoquartzite samples could have come from a Mesoproterozoic source such as the Shinumo Sandstone, there are other equally plausible potential Mesoproterozoic source regions. These include regional correlatives of the Shinumo Sandstone such as the Troy Quartzite of the Apache Group, quartzites of the Lower Crystal Springs Formation of Death Valley (Timmons et al., 2005; Mulder et al., 2017), and quartzite of the Transverse Ranges (Barth et al., 2009).

Mesoproterozoic quartzites from elsewhere in this region likely carry similar paleomagnetic inclinations to those displayed in the Shinumo. For the Troy Quartzite, although there is no direct paleomagnetic data, there are poles
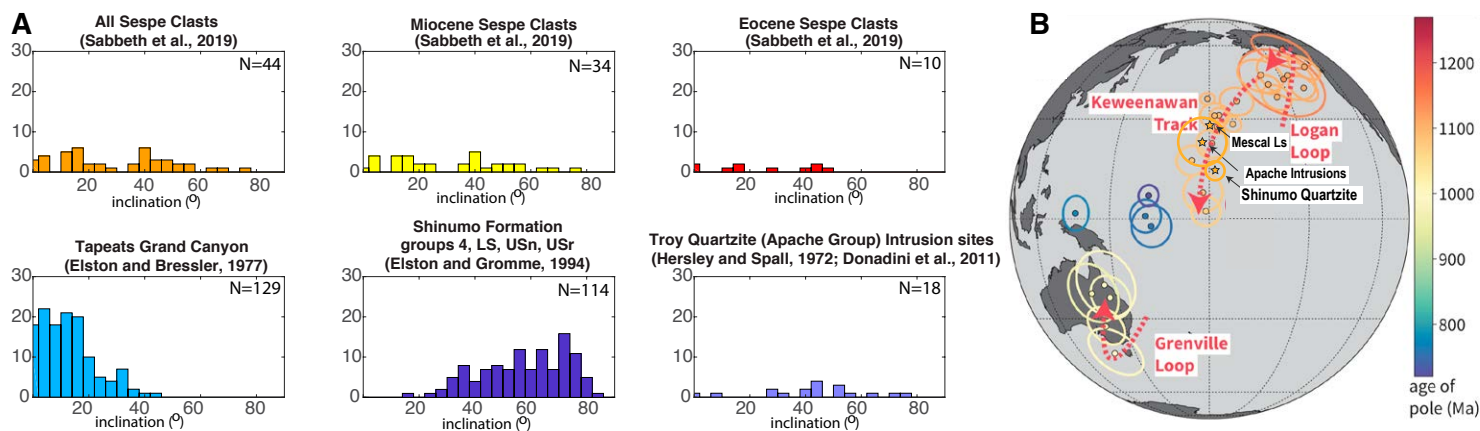

Figure 3. Paleomagnetic arguments and data. (A) Histograms of inclinations from Sabbeth et al. (2019) for the Sespe clasts and potential source rocks. Data sources indicated in the figure. (B) Key Laurentian poles and parts of its apparent polar wander path (adapted from Swanson-Hysell et al., 2019). Also shown are the Mescal Limestone pole (Elston et al., 1993), Shinumo pole (Elston et al., 2002), and the Apache Group intrusions (Donadini et al., 2011).

reported from the underlying Mescal Limestone, as well as from the intrusions into the Apache Group (Fig. 3A; replotted from Elston et al., 1993). Despite the lack of published demagnetization data, these poles suggest that the Troy Quartzite direction would be similar to the Shinumo Sandstone. Examination of the inclinations from other published site data from 1100 Ma diabase intrusions (Helsley and Spall, 1972; Donadini et al., 2011) suggests that mid-inclination spectra found in the Miocene Sespe clasts, if primary, could as readily have come from the Troy Quartzite as the Shinumo Sandstone.

In summary, the Sabbeth et al. (2019) approach was to minimize the potentially fatal and untestable complexities, such as multiple magnetizations; unrecognized dispersion caused by diverse cross-bedding orientations; and the expected overlap in values from other unstudied potential source regions. Their inclination data are permissive that some of the clasts were derived from Mesoproterozoic sedimentary sources such as the Shinumo, Troy and correlative units, but they could also be from remagnetized orthoquartzites of any age. Their assertion that a 30°–80° mode pinpoints the Shinumo as the only known "plausible" source region is rejected here and hence does not provide unambiguous evidence for a drainage connection between a Shinumo Sandstone source region and Sespe Formation deposition.

■ DETRITAL ZIRCON SIGNATURES OF POTENTIAL SOURCE ROCKS FOR SESPE CLASTS

Characterizing sedimentary rocks via their detrital zircon (DZ) populations is a more promising method by which the proposed Shinumo-Sespe connection can be tested. Our experience is that specific source-to-sink interpretations of such data sets are often non-unique, but we now have more sophisticated tools with which to quantitatively compare DZ age distributions (e.g., Vermeesch, 2013; Saylor and Sundell, 2016). Furthermore, the presence or absence of distinctive ages can provide definitive constraints.

Detrital zircon spectra from many Proterozoic rocks of the Southwest have one or more of the "three towers" of 1.8–1.6 Ga (Yavapai-Mazatzal provinces); 1.48–1.35 Ga (Picuris orogeny), and 1.25–1.0 Ga (broadly from the time of the Grenville orogeny). The modes and relative proportions of these age ranges may be diagnostic for high "n" analyses of >300–500 grains (Pullen et al., 2014). Distinctive zircon age groups may include: (1) 1.85 Ga and older grains that are common in the Mojave Province and Vishnu Schist (Holland et al., 2015); (2) 1.60–1.50 Ga "tectonic gap" age zircon that is now known from the Yankee Joe and related strata of central Arizona (Doe et al., 2012); (3) 1.38 Ga early Mesoproterozoic plutons of the Kingman uplift area that are slightly younger than the usual 1.45–1.43 Ga peaks (Winn, 2019); and (4) 1.2 Ga late Mesoproterozoic peaks that may have been derived from the Texas-Grenville foreland deposits of southwestern Laurentia (Mulder et al., 2017, 2018) and/or the San Gabriel anorthosite-syenite suite of southern California (Barth et al., 2000); these contrast with 1.1–1.0 Ga age group that dominates in Neoproterozoic to Mesozoic strata from much of western North America that may have

been derived in large part from Appalachian-Grenville sources (e.g., Gehrels et al., 2011; Gehrels and Pecha, 2014). For the latter group, we use the term Grenville age for 1.25–1.0 Ga grains irrespective of alternate potential provenance for these grains (Farmer et al., 2005).

To evaluate the Shinumo-Sespe hypothesis of Sabbeth et al. (2019), we compiled detrital zircon U-Pb ages from 15 studies in the literature (Table S2 [footnote 1]). The analyses were performed in nine different laboratories, two using ion microprobes and seven using laser-ablation–inductively coupled plasma mass spectrometry. The analytical approaches between laboratories vary in choice of primary standards, methods for correcting isotope fractionation, common-Pb correction, etc. Some studies report internal errors; others propagated errors. Some have eliminated certain analyses using a fixed-percentage U-Pb discordance filter, as has been commonly employed in detrital zircon studies (e.g., Gehrels and Pecha, 2014), whereas others have utilized a more recent approach of retaining only those analyses that are statistically concordant (cf. Spencer et al., 2016a). We have chosen the fixed-percentage approach because: (1) The disparities between the various data sets, both in accuracy and precision, preclude a consistent determination of statistical concordance. (2) Discordance is a geologically significant feature in potential source terranes of rocks considered here (e.g., Barth et al., 2009); ignoring such grains can obscure important signal. (3) Several rock units considered here have undergone medium- to high-grade metamorphism that led to significant Pb loss in zircon (Barth et al., 2009; Zylstra, 2017); using only statistically concordant zircon from these samples would disqualify an excessive number of analyses. Accordingly, we re-filtered any data sets (with one exception to be described below) that did not already adhere to the following criteria, which follow the widely used protocol of the Arizona LaserChron Center (e.g., Gehrels et al., 2006, 2008): (1) Rejection of analyses with concordance of <80% or >105%, where concordance is defined as the ratio of $^{206}Pb/^{238}U$ age to $^{207}Pb/^{206}Pb$ age. (2) Use of the $^{206}Pb/^{238}U$ age where that age is <900 Ma, and the $^{207}Pb/^{206}Pb$ age for those analyses where the $^{206}Pb/^{238}U$ age is ≥900 Ma.

In Figure 4, using the above data set, we re-plotted detrital zircon ages from the 12 orthoquartzite Sespe clasts presented by Sabbeth et al. (2019; their figure 8) using the detritalPy software package of Sharman et al. (2018). Colored age divisions at 300, 800, 1300, 1540, 1855, and 2450 Ma are used to highlight the "three towers" and other characteristic age populations. These subdivisions are somewhat arbitrary but were derived by empirical observation of natural breaks in most of our age distributions and closely follow those used by Dickinson et al. (2012).

Figure 4 shows that four of the 12 Sespe Formation clasts (red stars and red cumulative plots in Fig. 4) have tri-modal age distributions, and their youngest zircon grains are older than or within analytical error of the 1150–1104 Ma depositional age of the Shinumo Sandstone (gray bar in Fig. 4). These are considered the "best" potential matches to a Shinumo Formation source, and our focus is on these four of 12 of their clasts because they have moderate paleoinclinations, unambiguous >1.1 Ga maximum depositional ages (but see discussion below), and petrographic characteristics that resemble silica-cemented sandstone

(Sabbeth et al., 2019, their supplementary figure S3). Three of 12 clasts (bottom of Fig. 4 and blue cumulative plots) have unimodal age distributions unlike the Shinumo Sandstone but similar to many Paleoproterozoic samples in the region; their potential sources are discussed below.
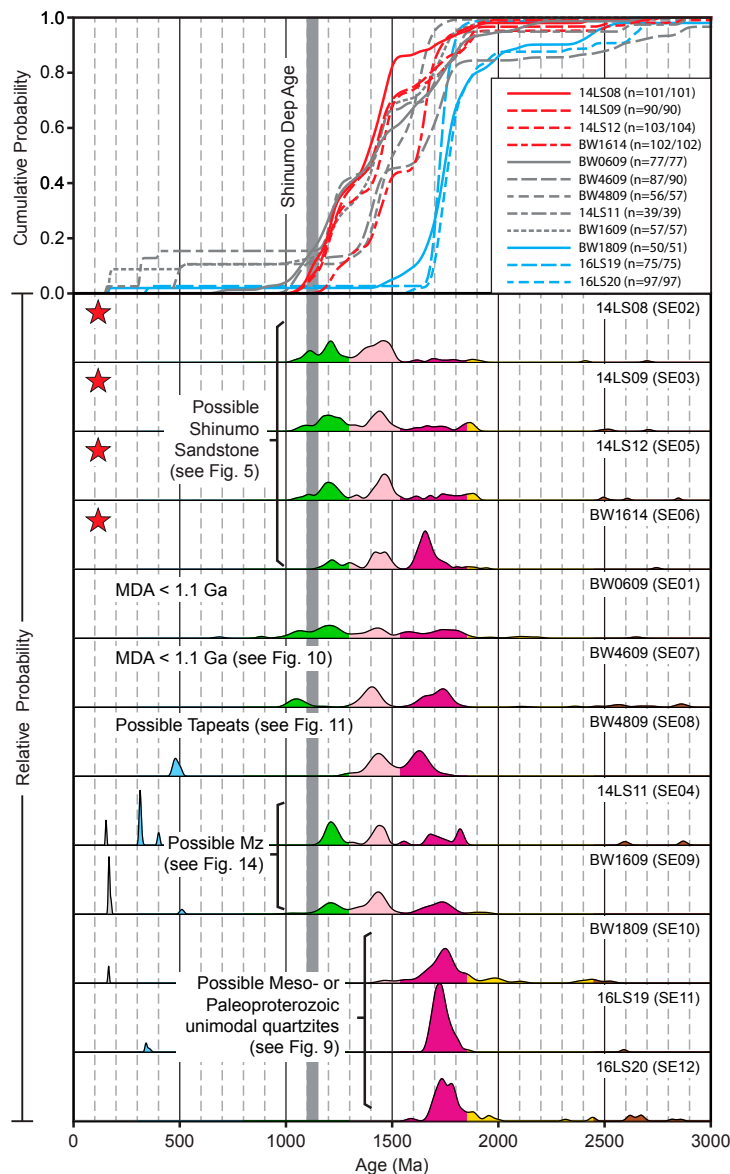
Seven of 12 have small to moderate numbers of post–1.1 Ga grains that would seem to preclude a Shinumo Sandstone source. For most of these (14LS11 excluded), Sabbeth et al. (2019, p. 1991) invoked an "allochthonous" argument that rationalizes young populations as spurious contamination, as likely also applies to their sample (IC-1-35) of the Shinumo Sandstone. Our new probability density plots try to address this by filtering out any grains with high discordance that can be due to lead loss or mixing of core and rim ages, but "allochthonous" contamination remains possible, although untestable. The following discussions consider this allochthonous interpretation, as well as the alternative that the young ages may be real.

Comparison of Best Sespe Clasts to Shinumo Sandstone

Figure 5 plots the four "best" (most Shinumo-like) clasts from the Sespe Formation to allow closer comparison with the proposed Shinumo Sandstone source. The Shinumo samples are arranged in stratigraphic order, with younger samples at the top. Three of the Sespe clasts (Samples 14LS08, 14LS09, and 14LS12) exhibit similar age distributions defined by abundant 1.25–1.0 Ga and 1.48–1.35 Ga zircon, modest numbers of 1.8–1.6 Ga grains, and small percentages of 3.0–1.85 Ga ages. The 1.25–1.0 Ga age population exhibits two subpeaks, a larger one at 1.2 Ga and a smaller one at 1.1 Ga. The 1.2 Ga peak is notable, as the Grenville-age population in many sedimentary sequences in the Southwest tends to be dominated by younger, ca. 1.1 Ga, ages (Dickinson and Gehrels, 2008a, 2008b, 2009; Gehrels and Pecha, 2014; Chapman et al., 2018). We refer to these three samples as the hybrid "Grenville-Picuris Sespe

Figure 4. Sabbeth et al. (2019) Sespe clast detrital zircon spectra re-plotted using the detritalPy software package of Sharman et al. (2018); the spectra in this and subsequent figures are probability density plots (PDPs). Vertical gray band at 1150–1100 Ma shows the upper and lower depositional age bounds of the Shinumo Sandstone based on ages of stratigraphically overlying and intrusive igneous rocks (Timmons et al., 2005) and detrital zircon ages (Bloch et al., 2006; Mulder et al., 2017), excluding some anomalously young ages (see Fig. 5). For the cumulative probability plots: the 5/7 samples with young grains that would potentially preclude clasts being from the >1.1 Ga Shinumo Sandstone are shown in gray, the 3/13 clasts with unimodal spectra similar to late Paleoproterozoic to early Mesoproterozoic samples are shown in blue. This leaves 4/13 samples (red stars and red cumulative probability paths) that have moderate paleoinclinations and unambiguous >1.1 Ga maximum depositional ages (within analytical uncertainty), and that petrographically look like silica-cemented sandstones in supplementary figure S3 of Sabbeth et al. (2019). Sample names in the legend for the cumulative probability curves and their equivalents in the panels for the PDPs are those used in the original sources. The names in parentheses in the PDP panels are abbreviations defined here to improve readability of Figure 8. The numbering sequence for the abbreviated names follows the ordering of samples used in Figure 8 of Sabbeth et al. (2019). We reordered the samples here to group those with similar detrital zircon age spectra. The letter "n" and numbers in parentheses in the legend for the cumulative probability curves indicate the number of ages <3000 Ma (before the slash) and the total number of ages (after the slash) for each sample. See Table S2 (text footnote 1) for detrital zircon ages used.

clasts." This group is broadly like sample K1275L-1 from the middle part of the Shinumo Formation, although sample K1275L-1 lacks the subpeak at 1.1 Ga. The fourth of the best Sespe clasts (BW1614) has less Grenville-age zircon overall than the other three samples, with no 1.1 Ga zircon, but a much higher
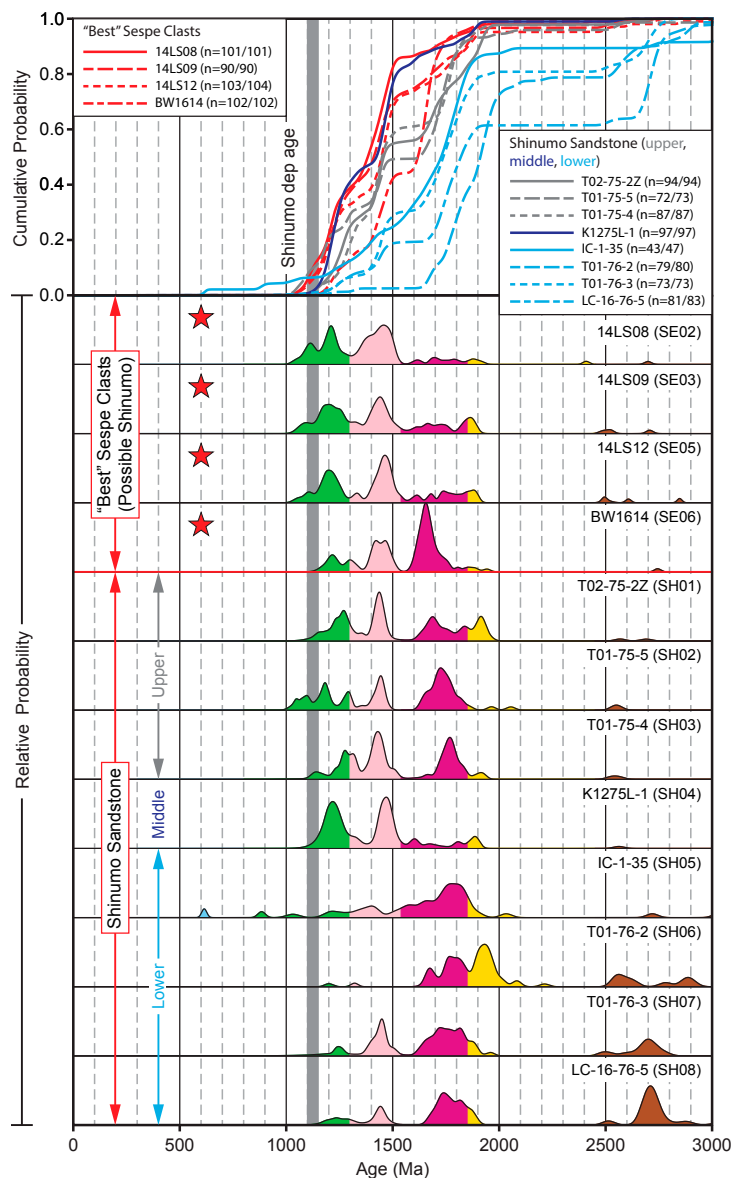
abundance of late Paleoproterozoic zircon (peak at 1.65 Ga). This Sespe clast somewhat resembles samples from the upper part of the Shinumo Sandstone, although the latter do not exhibit a consistent 1.2 Ga peak. In addition, the Paleoproterozoic peak in the upper Shinumo samples is older (1.8–1.7 Ga) than the Paleoproterozoic peak in Sespe sample BW1614. The lower Shinumo Sandstone exhibits the least similarity to the Sespe clasts. These samples have smaller numbers of Grenville-age and Picuris-age grains, but higher numbers of pre–1.8 Ga zircon, particularly Archean zircon.

Note that each of the three Grenville-Picuris Sespe clasts yielded several zircon ages younger than the 1104 Ma minimum depositional age of the Shinumo Formation (as young as 1042 Ma; Table S2 [footnote 1]). These ages are manifested in Figures 4 and 5 by a young tail (ca. 1.1–1.0 Ga) on the Grenville-age age range. However, a similar tail is present in Shinumo sample T01-75-5, and Shinumo sample IC-1-35 likewise exhibits several ages inconsistent with the depositional age of the formation. These anomalies in the Shinumo results preclude using the <1.1 Ga ages in the Grenville-Picuris Sespe clasts as evidence against derivation from the Shinumo Formation. We attribute the 1.1–1.0 Ga tails to Pb loss or analytical uncertainty.

Comparison of Best Sespe Clasts to Other Potential Sources

In Figure 6, we combine similar Sespe clasts and Shinumo samples, respectively, from Figure 5 and compare these composite spectra with alternative potential sources for the Sespe clasts. Among these are the Troy and Dripping Springs quartzites of the Apache Group of central Arizona (Stewart et al., 2001; Mulder et al., 2017), a region previously suggested as a potential source area for quartzite clasts in the Sespe conglomerate (Howard, 2000). Sabbeth et al. (2019, p. 1992) rejected the Troy Quartzite as a source for the Sespe clasts based on a K-S test comparing Sespe clasts 14LS08 and 14LS12 (both part of our Grenville-Picuris group) with a limited set of analyses for the Troy Quartzite (131 analyses from three samples from Stewart et al., 2001; Mulder et al., 2017). Here, we use a more comprehensive Troy age distribution that includes two new samples from Mulder et al. (2018) in addition to the samples plotted by Sabbeth et al. (2019); this age distribution contains the mode of Grenville-Picuris grains also seen in Sespe clasts (Fig. 6; note that, as explained in the figure caption, we use $^{206}Pb/^{238}U$ ages exclusively for the Mulder et al., 2018

Figure 5. Individual spectra for samples of Shinumo Sandstone from Upper Granite Gorge of Grand Canyon arranged stratigraphically with oldest at bottom compared with four "best" matches among Sespe conglomerate clasts (red stars). Note that there is a distinct 1.2 Ga peak in many Sespe clasts that is also present in some samples from the upper Shinumo Sandstone but that there is a higher proportion of pre–1.8 Ga grains in the Shinumo Sandstone versus a higher proportion of post–1.5 Ga grains in Sespe cobbles. K1275L-1 from the middle Shinumo Sandstone is one of the better possible matches for the Sespe clasts. Number of grains ("n") defined as in Figure 4. See Table S2 (text footnote 1) for data sources.
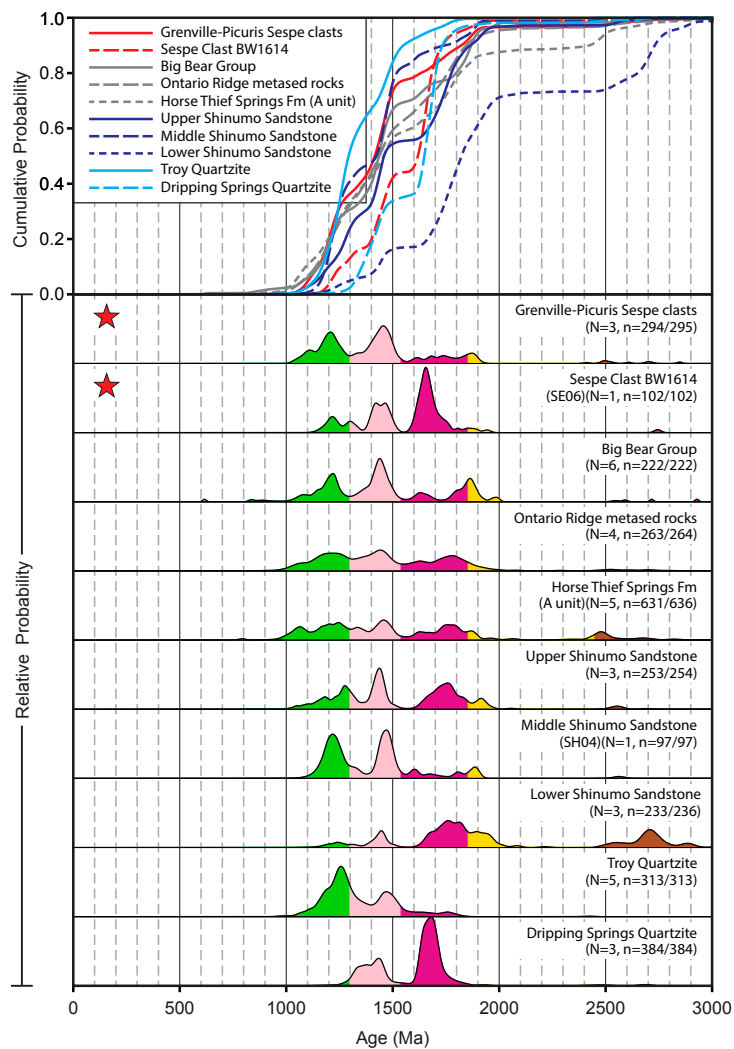
Figure 6. Alternative possible source regions for the best Sespe clasts compared to composites for lower, middle, and upper Shinumo Sandstone, Troy Quartzite, Dripping Springs Quartzite, Big Bear quartzite, Ontario Ridge quartzite, and Horse Thief Springs sandstone. Three of the four best Sespe clasts with similar release spectra (Figs. 4 and 5) have been combined into a single group ("Grenville-Picuris Sespe clasts"). Note that Sespe clasts are qualitatively most similar to middle Shinumo, Troy, and Big Bear quartzites. Analyses for two of samples of Troy Quartzite were optimized for trace-element analysis; they yielded acceptable errors for $^{207}Pb/^{235}U$ and $^{206}Pb/^{238}U$ ages but excessively high errors for $^{207}Pb/^{206}Pb$ ages. For these samples, we utilized $^{206}Pb/^{238}Pb$ ages for all analyses (see Table S2 [text footnote 1] for further explanation). "N" indicates the number of samples included in each group; "n" is as defined in Figure 4.

analyses). Sespe clast BW1614 is not a good match to the Troy Quartzite but somewhat resembles the stratigraphically underlying Dripping Springs Quartzite. Sespe clast BW1614, however, has a moderate proportion of Grenville-age zircon, which is not observed in the Dripping Springs Quartzite.

Figure 6 indicates that the detrital zircon age distribution for the Grenville-Picuris Sespe clasts is qualitatively similar to that of the Big Bear Group in the San Bernardino Mountains of the eastern Transverse Ranges in southern California (Barth et al., 2009). Both have strong 1.2 Ga and Picuris peaks, along with modest numbers of Yavapai-Mazatzal grains, and similar small percentages of 3.0–1.85 Ga grains. On the other hand, Sespe clasts tend to have a higher abundance of 1100 Ma ages than the Big Bear Group (Fig. 6). Also note that the Big Bear Group is metamorphosed (Barth et al., 2009) so that the Grenville-Picuris Sespe clasts could not have been derived directly from the current outcrops of the Big Bear Group (see also Howard, 2000). Nonetheless, these clasts could have been eroded from a lower-grade correlative of the Big Bear Group. Furthermore, the Big Bear Group is likely of Neoproterozoic age and might yield shallow paleoinclination vectors, if not remagnetized. Note also that one of the Big Bear samples includes a ca. 600 Ma age. This seems to be a reliable detrital age; so ultimately we need to reconcile this age with the scattering of young ages in some of the Sespe clasts and Shinumo sample IC-1-35.

The age spectrum for the Grenville-Picuris Sespe clasts also resembles that of quartzites within the Ontario Ridge metasedimentary complex in the eastern San Gabriel Mountains of southern California (Fig. 6; Zylstra, 2017). The age and significance of the sedimentary protoliths of the Ontario Ridge rocks are not well constrained owing to metamorphism within the upper-amphibolite facies, strong deformation, and intrusion by pre- and postmetamorphic Cretaceous granitoids. Nonetheless, these rocks are considered a potential correlative of the Big Bear Group (Zylstra, 2017). The relatively weak separation of the Grenville, Picuris, and Yavapai-Mazatzal–age peaks in the Ontario Ridge quartzites is likely the result of Pb loss during metamorphism.

Finally, we note some similarity in zircon age distributions between the Grenville-Picuris Sespe clasts and the basal part (A unit) of the Neoproterozoic Horse Thief Springs Formation of the Death Valley area (Mahon et al., 2014a, 2014b). The Horse Thief Springs Formation exhibits a distinct peak at 1050 Ma, which potentially sets it apart from the Grenville-Picuris Sespe clasts (Fig. 6), but which might also reflect Pb loss or analytical uncertainty. The Horse Thief Springs Formation is also distinguished by scarce ca. 800 Ma zircon. The best Sespe clasts were chosen specifically for comparison with the Shinumo Sandstone, and, by definition, exclude zircon younger than 1100 Ma that cannot plausibly be attributed to lead loss or analytical uncertainty. Nonetheless, the amount of 800 Ma zircon in the Horse Thief Springs Formation is just a fraction of a percent, which suggests that further analysis of Sespe clasts could reveal zircon of this age.

In summary, even based on qualitative visual comparisons (Fig. 6), the Troy and Dripping Springs Quartzites of the Apache Group, Big Bear Group, Ontario Ridge metasedimentary rocks, and middle to upper Shinumo Sandstone

cannot be ruled out as potential sources for Sespe cobbles. Although each of the units is limited in present areal extent, their occurrence across a wide expanse of southern California and southwestern Arizona, along with their cosmopolitan zircon suites, suggests they are remnants of (multiple) regional-scale sand systems. Hence, similar sequences may be present in other ranges, but not yet recognized, or have been removed by erosion or excised by extensional faulting, the latter of which fundamentally altered the landscape of southeastern California and southwestern Arizona subsequent to deposition of the Sespe Formation (Spencer and Reynolds, 1991; Jacobson et al., 2007). Consequently, we reject the notion that the Shinumo Sandstone is the "only plausible" source for orthoquartzite cobbles in the Sespe Formation.

Quantitative Comparison of Zircon Distributions

As noted above, the detrital zircon analyses considered here were collected on multiple instruments with a range of operating conditions and data reduction methods. These disparities indicate the need for caution when applying statistical techniques to compare the various sample groups. Nonetheless, quantitative comparison of probability density plots (PDPs) and cumulative distribution functions (CDFs) is an objective way to assess the dissimilarity between detrital age distributions, within the constraints of the data set. Dissimilarity measures yield a range of dissimilarity values between 0 and 1, with larger numbers corresponding to more dissimilar distributions

and 0 corresponding to identical distributions. To quantitatively compare detrital age distributions, Sabbeth et al. (2019, p. 1992) relied on p values calculated using the K-S test to assess correspondence between age distributions. However, p values are statistical hypothesis tests that are not well suited for quantitative comparison of detrital data because they produce too many Type-II errors (erroneously accepting a false null hypothesis that two samples were drawn from the same population), which mainly stems from p-values being highly sensitive to sample size and mixing sample size with effect size, where the former is the number of ages in a distribution, and the latter is "the degree to which the null hypothesis is false" (Cohen, 1977; Vermeesch, 2013); in other words, p values will often produce the opposite result of what is actually supported by the data. Therefore, p values are unsuitable measures of dissimilarity (Vermeesch, 2013, their appendix B). We have generated dissimilarity matrices using four *relative* measures of dissimilarity including Mismatch (1—Likeness) and Nondetermination (1—Cross-correlation) for comparison of PDPs (Amidon et al., 2005; Saylor et al., 2012; Satkoski et al., 2013), and the K-S and Kuiper test D and V values (not p values) for comparison of CDFs (Massey, 1951; Kuiper, 1960). All dissimilarity matrices were calculated and are presented in Table S3 using DZstats version 2.30 for macOS (Saylor and Sundell, 2016; www.github.com/kurtsundell/DZstats).

The results of the above analysis are presented in Figure 7. As explained in both Figures 7 and 8, we use abbreviated sample names because of space considerations (see Table S3 [footnote 1] for the definitions for all samples). Figure 7 shows the pairwise dissimilarity matrix generated using Mismatch
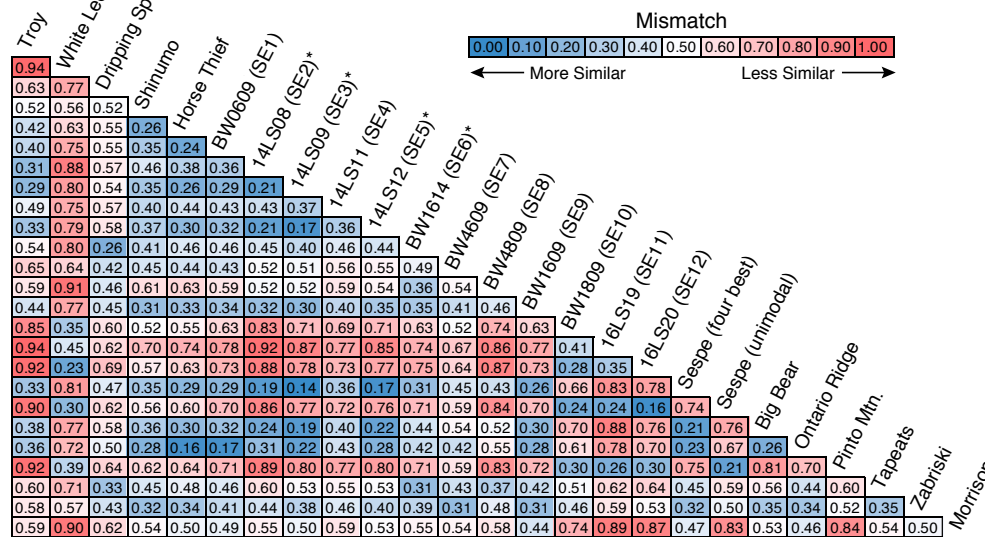

Figure 7. Dissimilarity matrix generated using Mismatch of probability density plots (PDPs) (Amidon et al., 2005) for individual Sespe clasts and subset composites compared to composite samples of Shinumo, Troy, Big Bear, Dripping Springs, White Ledges, Pinto Mountain, Horse Thief, Ontario Ridge, Pinto Mountain, Tapeats, and Zabriskie quartzites. All of the Sespe clasts are dissimilar to the Shinumo composite with Mismatch values ranging from 0.35 to 0.46 and also dissimilar to all of the individual Shinumo samples with Mismatch values ranging from 0.32 and 0.84 and with a mean of 0.55 ± 0.15 (1σ) (see the Supplemental Material [text footnote 1] for further quantitative comparison of individual samples and composite samples using each measure of dissimilarity. None of the four most Shinumo-like Sespe clasts (samples with asterisks) has a definitive or even moderately likely derivation from Shinumo Sandstone. See Table S3 for a full matrix that includes all individual clasts discussed herein.
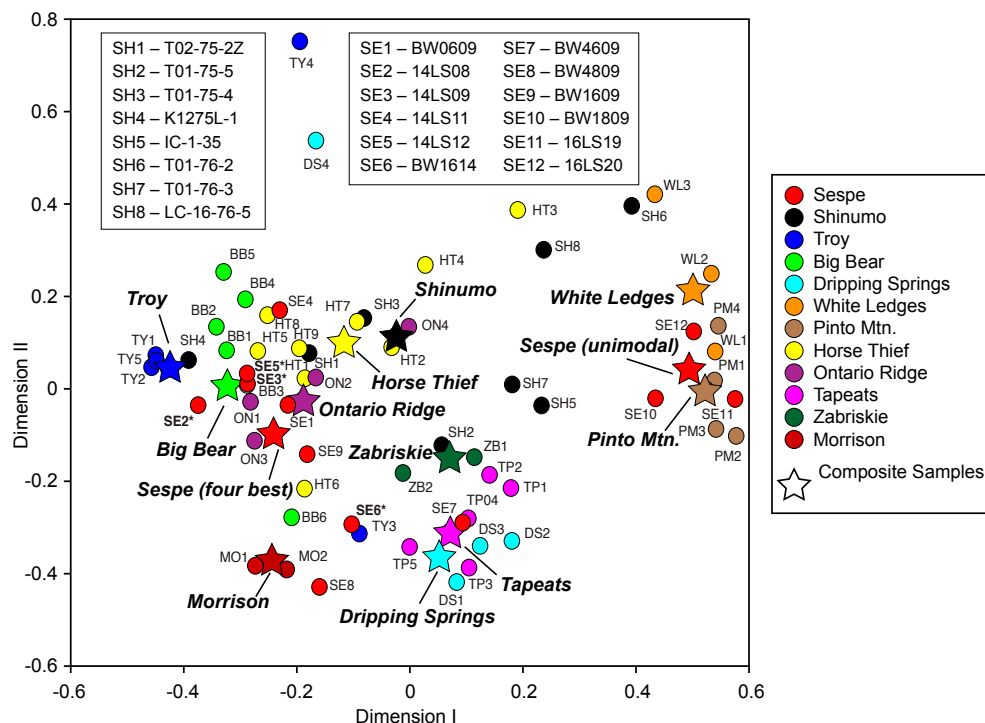
Figure 8. Multi-dimensional scaling (MDS) plot of all Sespe clasts facilitates comparison of detrital age distributions by producing a Cartesian 2-D plot through conversion of intersample dissimilarity to disparity via linear transformation and iterative reengagement in Cartesian space. Points closest together have lowest dissimilarity. Mismatch suggests Sespe clasts are likely derived from multiple sources and Shinumo is an unlikely source for even the four best Sespe clasts. MDS plots generated using alternate metrics show similar results and are presented in Table S3. See Figures 4 and 5 for definitions of the Sespe (SE) and Shinumo (SH) sample-name abbreviations. See text and Supplemental Material item for definitions of the other abbreviations.

of PDPs (Amidon et al., 2005) for the four best Sespe clasts compared to composite samples of the Troy, White Ledges, Dripping Springs, Shinumo, Horse Thief Springs, Big Bear, Ontario Ridge, and Pinto Mountain units, which have been discussed above, as well as the White Ledges Formation, Tapeats Sandstone, Zabriskie Quartzite, and Morrison Formation, whose detrital zircon spectra are presented below. Results are consistent regardless of which measure of dissimilarity is used (see color-coded tables in the Supplemental Material). The Sespe clasts show substantial internal variability with respect to one another, with Mismatch values ranging from 0.17 to 0.45. The three Grenville-Picuris Sespe clasts (14LS08, 14LS09, and 14LS12, abbreviated as SE2, SE3, and SE5, respectively, in Fig. 7) are generally self-similar, with relatively low Mismatch values ranging from 0.17 to 0.21, and are also similar to Troy, Ontario, and Big Bear units, with relatively low values ranging from 0.19 to 0.33. SE6 (BW1614) is the least similar to the other best Sespe clasts, with Mismatch values of 0.40–0.45 and is most similar to Dripping Springs Quartzite and Tapeats Sandstone, with Mismatch values of 0.26 and 0.31, respectively. All of the Sespe clasts are considerably dissimilar to the Shinumo composite, with Mismatch values ranging from 0.35 to 0.46 (Fig. 7) as well as dissimilar to all of the individual Shinumo samples, with Mismatch values ranging from 0.32

and 0.84 and with a mean of 0.55 ± 0.15 (1σ) (see Table S3 of the Supplemental Material [footnote 1] for further quantitative comparison of individual samples and composite samples using each measure of dissimilarity). In summary of Figure 7, none of the four most Shinumo-like Sespe clasts, nor the composite, has Shinumo Sandstone as the statistically most likely source.

Measures of dissimilarity can be visualized spatially using multi-dimensional scaling (MDS) (Vermeesch, 2013), which facilitates comparison of detrital age distributions by producing a Cartesian plot in N dimensions (usually 2 or 3) through conversion of intersample dissimilarity to disparity via linear transformation and iterative reengagement in Cartesian space. Multi-dimensional scaling seeks to minimize the misfit between distance and disparity (stress). Low stress (e.g., ~0.1) indicates a reasonable transformation. Although MDS was originally adapted for detrital data by Vermeesch (2013), here we use DZmds (Saylor et al., 2018; github.com/kurtsundell/DZmds) because it implements all of the dissimilarity measures discussed above. We use two-dimensional (2D) MDS to facilitate the visualization and interpretation of inter-sample dissimilarity.

Figure 8 shows that most individual sample sets tend to cluster around their respective composites, indicating they are distinct populations, with the only exception being the Sespe clasts. The four best Sespe clasts show

internal variability by plotting in varying locations in MDS space. As alluded to above, Sespe samples SE2 (14LS08), SE3 (14LS09), and SE5 (14LS12) are most similar (closest together in MDS space) to composite samples and most individual samples of Troy Quartzite, Ontario Ridge rocks, and Big Bear Group, whereas Sespe sample SE6 (BW1614) is most similar to Dripping Springs Quartzite and Tapeats Sandstone (Fig. 8). The unimodal Sespe clasts SE10 (BW1809), SE11 (16LS19), and SE12 (16LS20) are most similar (smallest distance on the MDS plot) to White Ledges Formation and Pinto Mountain Group. None of the best Sespe clasts show similarity in MDS space to any of the individual Shinumo samples nor to the composite Shinumo sample. In fact, the individual Sespe clasts show more internal variability than any other group by plotting over the most variable range in MDS space. This variability points to likely derivation of the Sespe clasts from multiple sources, including the four best Sespe clasts, which have a minimum of two different sources based on MDS, neither of which is likely to be Shinumo Sandstone (Fig. 8). Multi-dimensional scaling plots generated using alternate metrics show similar results, as presented in Table S3 of the Supplemental Material (footnote 1). In summary of Figure 8, MDS using Mismatch suggests, within the limits of our data set, that Sespe clasts were likely derived from various sources, and Shinumo Sandstone is an unlikely source for even the four best (most Shinumo-like) Sespe clasts.

Unimodal Sespe Clasts

Our prior discussion focused on those Sespe clasts that most closely match the Shinumo Sandstone. We here consider sources for the remainder of the clasts, beginning with the three samples with a near-unimodal Paleoproterozoic age distribution (Fig. 4; samples BW1809, 16LS19, and 16LS20). Two of the three samples include a total of three $^{206}Pb/^{238}U$ ages younger than 400 Ma, although two of these are highly discordant. For the purposes of discussion, we discount these three ages and assume that the unimodal Sespe clasts may have a Paleoproterozoic (or early Mesoproterozoic) depositional age. A composite probability plot for the three samples (Fig. 9), combined with Mismatch values of Figure 7, provides permissive matches with both the Pinto Mountain Group (Mismatch value of 0.21) of the Transverse Ranges (Barth et al., 2009) and the White Ledges Formation (Mismatch value of 0.30) of central Arizona (Doe et al., 2012). The Shinumo Sandstone, with its distinct 1.4 and 1.2 Ga peaks, has a Mismatch value of 0.56 with the unimodal Sespe clast composite and is a much less likely source.

Sespe Clasts Potentially Derived from Cambrian Strata

Figure 10 examines permissive source-region matches for Sespe clast BW4609, which has a Grenville-age peak at ca. 1050 Ma and hence is too young to be derived from the >1100 Ma Shinumo Sandstone (we consider this distinct
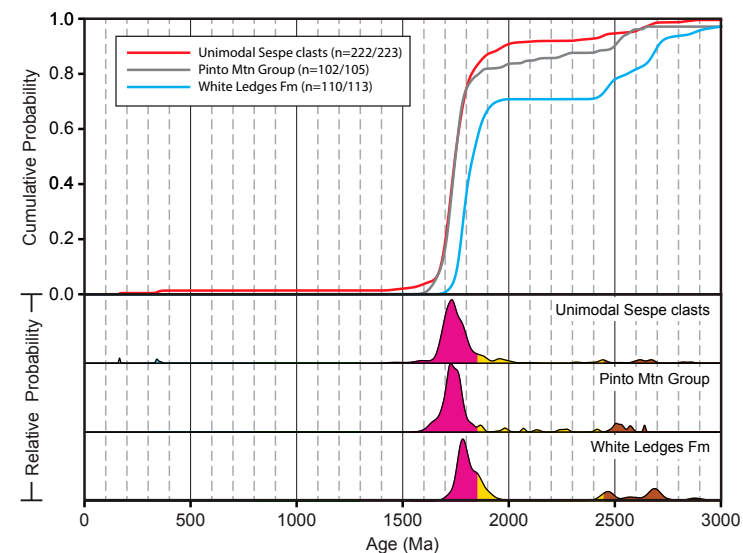

Figure 9. Comparison of the three Sespe clasts with dominantly unimodal spectra with the latest Paleoproterozoic–early Mesoproterozoic Pinto Mountain Group of the Transverse Ranges and White Ledges Formation of central Arizona. Note similar 1.8–1.7 Ga peaks and similar percentages of pre–1.8 Ga grains in all three. "N" and "n" as in previous figures.

peak to be more significant than the 1.1–1.0 tails on the Grenville-Picuris Sespe clasts). Further, BW4609 has essentially no 1200 Ma grains and a Mismatch value of 0.45 with the Shinumo Sandstone. Cambrian Tapeats Sandstone from Gehrels et al. (2011; their Tapeats 2) is the closer match (Mismatch of 0.43) to BW4609 in terms of the Grenville-age peak, but lacks significant pre-2000 Ma zircon. The Cambrian Zabriskie Quartzite, a miogeoclinal equivalent of the cratonal Tapeats Sandstone, also shows some similarities with Sespe clast BW4609 (Mismatch value of 0.31), including similar abundance of pre–2000 Ma ages. However, the Grenville-age peak in the Zabriskie Quartzite, at 1100 Ma, is older than that in the Sespe clast. The upper (E and F units) and lower (A unit) of the Neoproterozoic Horse Thief Springs Formation are also somewhat similar to Sespe clast BW4609 but have more grains in the 2100–1850 Ma range and a generally older Grenville-age component; the Mismatch value of 0.44 between BW4609 and Horse Thief Springs Formation suggests this is a less likely match than the Zabriskie Cambrian sample.

Figure 11 compares sample BW4809 with the composite spectrum for three samples of Tapeats Sandstone, one each from the Las Vegas Area, Grand Canyon, and central Arizona (Matthews et al., 2018; Karlstrom et al., 2018). The Sespe clast has a somewhat younger Paleoproterozoic peak of 1620 Ma compared to the Tapeats (>1680 Ma) and its Mismatch value is 0.37, but its ca. 500 Ma peak, defined by six grains, provides a compelling argument for
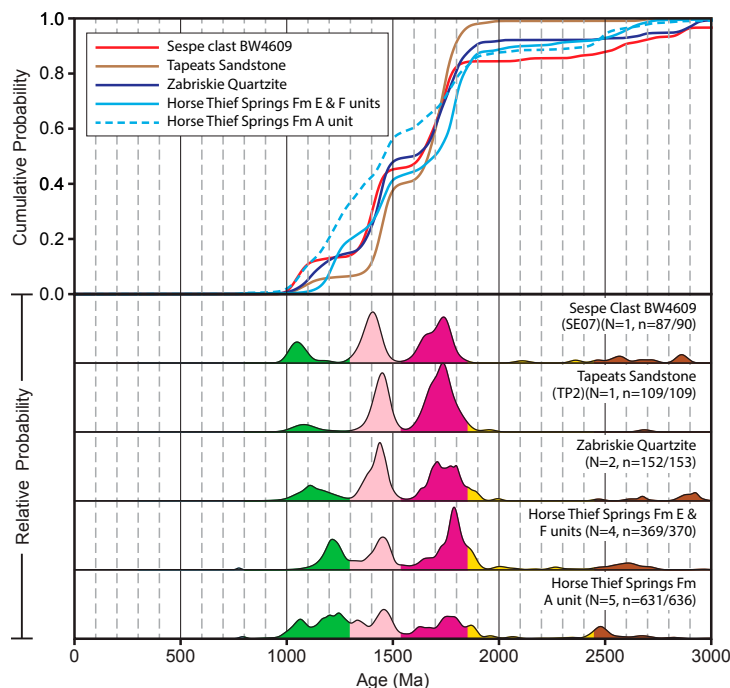
Figure 10. Comparison of Sespe clast BW4609 to potential sources. Zabriskie Quartzite or Tapeats Sandstone are reasonable matches except that the Grenville-age peak in these units is somewhat older than that in the Sespe clast. Note the absence of ca. 500 Ma zircon from the sample of Tapeats Sandstone shown here (from Gehrels et al., 2011) in contrast to the Tapeats samples plotted in Figure 11. "N" and "n" as in previous figures.
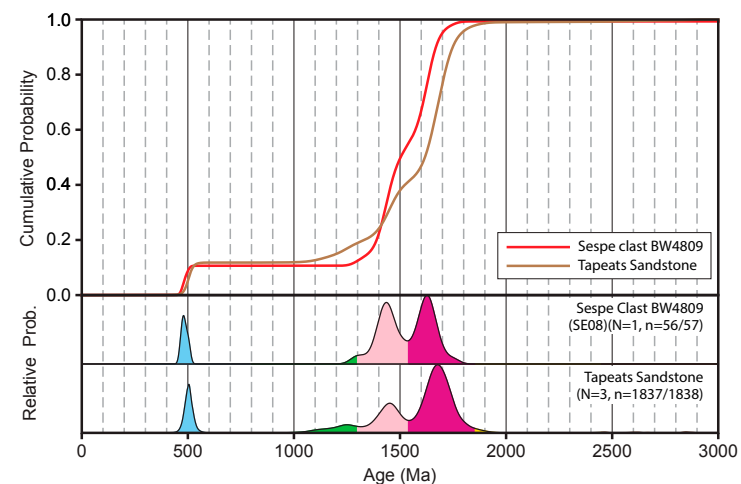

Figure 11. Comparison of Sespe clast BW4809 with a composite of three samples of Tapeats Sandstone from Frenchman Mountain of southern Nevada, Grand Canyon, and the central Arizona highlands (Karlstrom et al., 2018). The ca. 500 Ma peak in both the Sespe clast and Tapeats Sandstone is notable, as zircon of this age is uncommon in sedimentary sequences of the Southwest, including other parts of the Tapeats Sandstone (e.g., Dickinson and Gehrels, 2008b; Gehrels et al., 2011; Karlstrom et al., 2018). "N" and "n" as in previous figures.

derivation from the Tapeats Sandstone, as this is not a common age in the Southwest. The ca. 500 Ma grains in BW4809 are unlikely to be "allochthonous" given that no other young grains are present.

■ GRAND WASH TROUGH

An additional test for the proposed Shinumo-Sespe drainage connection would be to find clasts and/or detrital zircon from the inner Grand Canyon along the proposed Eocene or Miocene pathway of the hypothetical "Arizona River" (Fig. 12). This test has already been performed as part of continued examination of the "Muddy Creek constraint." As initially noted by Blackwelder (1934) and Longwell (1946), the "Muddy Creek constraint" is that sediments from Grand Wash trough, where the Colorado River exits the Grand Canyon at its west end, contain no far-traveled river deposits or sediment sourced

from the Colorado Plateau. Instead, as shown in Figure 12, this area was an internally drained basin prior to 6 Ma (Lucchitta, 1966, 1972, 2013; Crossey et al., 2015; Lamb et al., 2018). The late Paleocene–early Eocene (ca. 65–55 Ma) Music Mountain Formation (Young and Hartman, 2014), Oligocene–early Miocene (34–18 Ma) Buck and Doe Conglomerate (Young and Crow, 2014), and 25–17 Ma Rainbow Gardens Formation (Beard, 1996) and its correlative Jean Conglomerate (Beard, 1996; Lamb et al., 2018) were locally derived from the Kingman Uplift just tens of km to the south. Generally northeastward flow of 34–18 Ma paleorivers, 20–16 Ma basalt, and the 18.8 Peach Spring Tuff is opposite the proposed southward flow direction of the "Arizona River," in conflict with the Eocene or Miocene Shinumo-Sespe connection.

An additional argument (Fig. 13) follows the reasoning that if Shinumo detritus reached the Sespe delta at any time prior to 6 Ma, then there should be other diagnostic detritus from along the flow path, including zircon from other rocks in Grand Canyon and Grand Wash trough basins. Spectra representing the detrital grains that would have been contributed along this path, arranged downstream along the proposed "Arizona River," would be the Vishnu Schist, Unkar Group, Paleozoic strata, and (for the Miocene part of the Sespe Formation) the Rainbow Gardens Formation. The Rainbow Gardens Formation has peaks at 1.7 and 1.1 Ga, little 1.4 Ga detritus, and a syn-depositional peak at 23–20 Ma. It is interpreted to have been derived from nearby exposures of
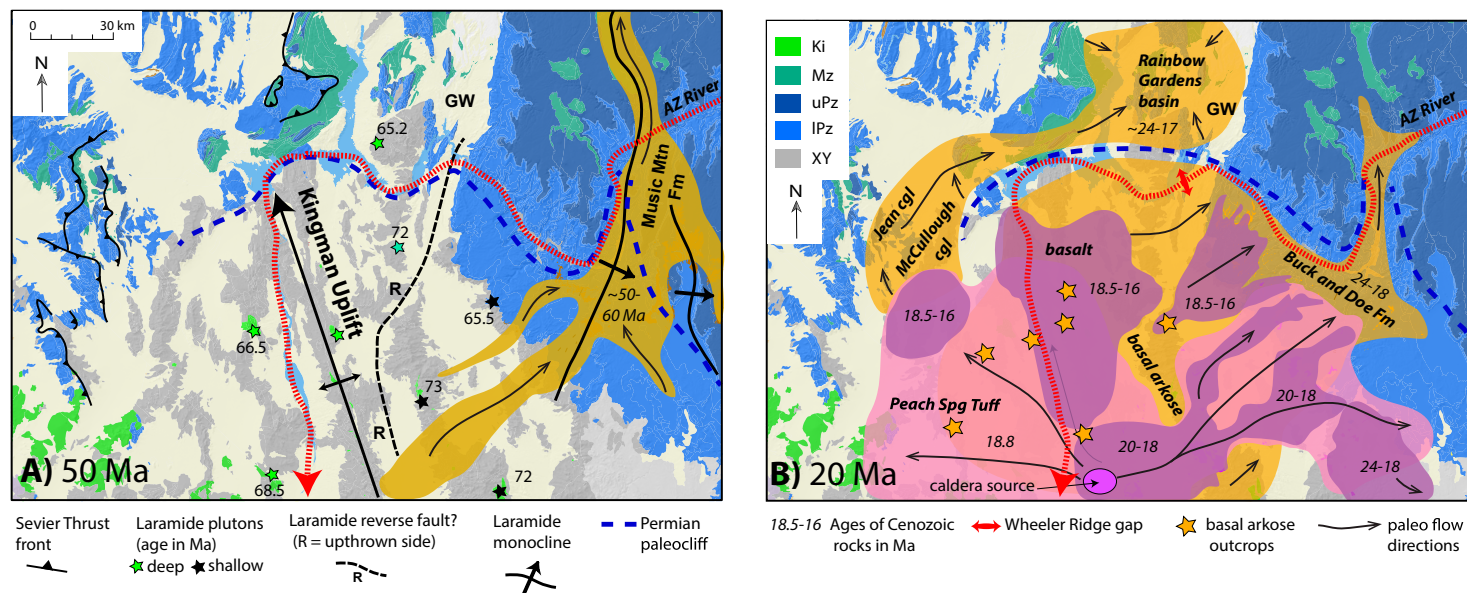
Karlstrom et al. | Shinumo-Sespe drainage connection

Figure 12. Geologic map of the Grand Wash (GW) trough area of western Grand Canyon prior to ca. 17 Ma extension. Gray (XY)—Precambrian; light blue (lPz)—lower Paleozoic; dark blue (uPz)—upper Paleozoic; dark green (Mz)—Mesozoic; light green (Ki)—Cretaceous intrusions; brown/orange/purple—Cenozoic rocks as labeled. Generalized geology is modified from Mackey et al. (2012) overlain on 30 m digital elevation model; north is up. Note that geology is not corrected for extension. (A) At ca. 50 Ma, the Music Mountain Formation paleoriver flowed northerly off the Kingman uplift and across the modern Grand Canyon, and the modern surface was 75–100 °C (depths of 2–3 km) based on thermochronology (Fitzgerald and Malusà, 2019, p. 183); both characteristics falsify the proposed south-flowing "Arizona River" (red dashed line). (B) At ca. 20 Ma, both paleoriver deposits and volcanic flows (24–16 Ma) continued to flow north, opposite to the proposed S-flowing "Arizona River" drainage. Note that the 18.8 Ma Peach Spring was widely distributed directly across the path of the "Arizona River." Red arrows show the location of the proposed Wheeler Ridge "paleocanyon" (Wernicke, 2011); this gap contains no paleo–Colorado River deposits and is interpreted here to be a structural gap formed during 17 Ma extension. Ages of Laramide plutons as reported in Beard and Faulds (2011) sourced from Lang and Titley (1998), Miller et al. (1997), Bouse et al. (1999), Brady et al. (2000), Faulds et al. (2001), Young (2001), Kapp et al. (2002), and Chapman et al. (2018).

Precambrian, upper Paleozoic, and lower Mesozoic strata in fault blocks adjacent to Grand Wash trough, with the notable addition of volcanic detritus from the Caliente volcanic field (ca. 28–19 Ma) to the north, but with no significant input from the paleo–Colorado River from the east (Lamb et al., 2018). The 25–15 Ma detritus in Grand Wash trough does not contain >2.0 Ga grains as found in the Shinumo Sandstone or Vishnu Schist, nor the full range of Paleozoic detritus from the walls of Grand Canyon, all of which would have been exposed if the canyon was cut to within a few hundred meters of its modern depth. Sespe Formation detrital zircon spectra also are missing several age modes from along the proposed "Arizona River" flow path: pre–1.8 Ga grains, latest Neoproterozoic (Gondwanan), Paleozoic (Appalachian), and 25–17 Ma Rainbow Gardens Formation detritus. Pre-Sespe Eocene strata throughout southern California similarly lack any significant detritus that would signal a source from Grand Canyon (Jacobson et al., 2011; Ingersoll et al., 2013).

An additional aspect of the Miocene "Arizona River" hypothesis is a proposed Miocene "paleocanyon" on Wheeler Ridge in Grand Wash trough (red arrows in Fig. 12B), which is posited to have "calved off" of Grand Wash Cliffs during 17 Ma faulting on the Grand Wash fault (Wernicke, 2011). This break in Wheeler Ridge is onlapped by 15 Ma ash beds (Wallace et al., 2005) draping topography and may represent a subsidiary fault in the hangingwall of the Grand Wash fault. But there is no evidence for Colorado River or Colorado Plateau–derived deposits in this gap. This absence precludes using this feature as evidence for a 20 Ma paleo–Grand Canyon.

■ CONNECTION TO THE COLORADO PLATEAU

Sabbeth et al. (2019) argued that their sample 14LS11, which includes zircon as young as 153 Ma (Fig. 14), is similar to the Upper Jurassic Morrison Formation, and hence implies a Colorado Plateau source for the Sespe Formation, compatible with the "Arizona River" hypothesis. Their argument is based on a comparison with two samples of the Westwater Canyon Member of the Morrison
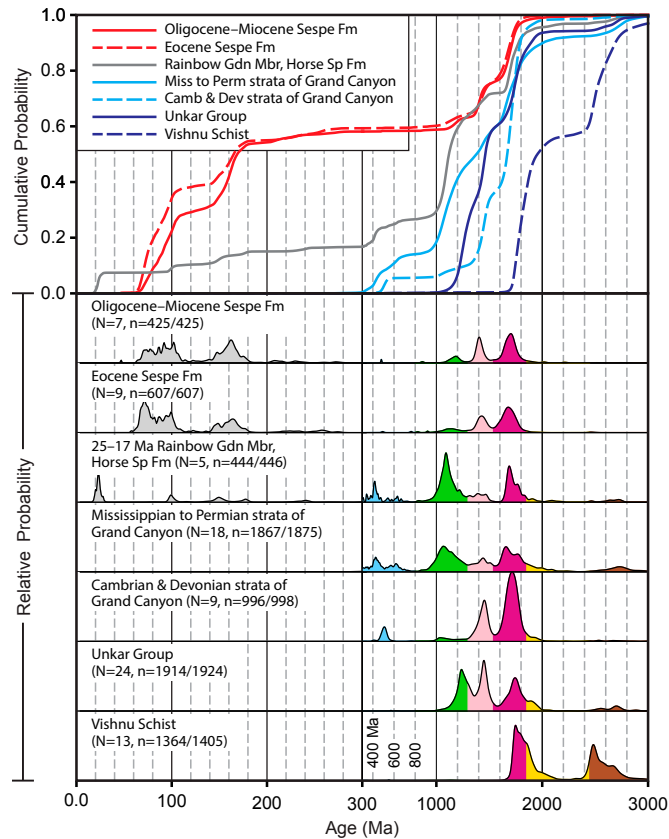
Figure 13. Illustration that if the Sespe Formation includes clasts derived from Shinumo Sandstone, then it should also include zircon populations found in the Proterozoic basement and Phanerozoic strata of Grand Canyon. This is not the case, as indicated by the scarcity of Archean, 2000–1800 Ma, 1100 Ma, latest Proterozoic (Gondwanan), and Paleozoic (Appalachian) zircon in both Eocene and Oligocene–Miocene parts of the Sespe Formation. Rather, the ages and proportions of pre-arc zircon in the Sespe Formation are typical of Cretaceous to Paleogene strata in southern California that are inferred to have been derived from sources in southern California, southwestern Arizona, and/or northwestern Sonora (Jacobson et al., 2011; Ingersoll, et al., 2013, 2018; Sharman et al., 2015). Similarly, the Rainbow Gardens Formation of the Grand Wash Trough, which lies along the course of the modern Colorado River, shows no obvious evidence of sediment contribution from the Devonian and older rocks exposed in the deeper parts of Grand Canyon. Note age-axis scale break at 300 Ma. For the probability density plot (PDP) panels, the vertical scales also differ to the left and right of the scale break, such that equal area represents equal probability throughout graph. "N" and "n" as in previous figures.
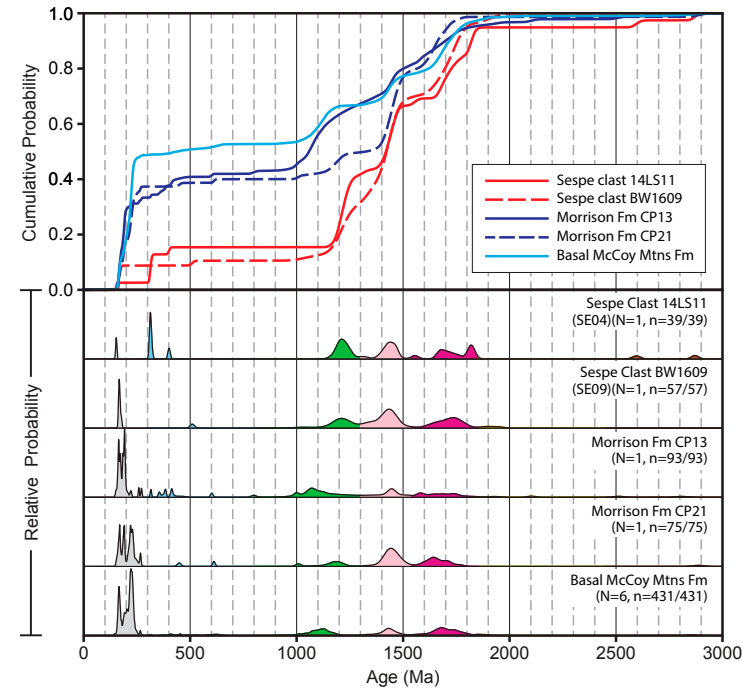
Figure 14. Sample 14LS11 has a maximum depositional age (MDA) of ca. 150 Ma, assuming the ages <500 Ma are not allochthonous. Sabbeth et al. (2019) concluded that this clast was derived from the Westwater Canyon Member of the Morrison Formation. Although not explicitly addressed by Sabbeth et al. (2019), we here also consider Sespe clast BW1609, which has a similar young apparent MDA. Both Sespe clasts have similar pre-arc age distributions as two samples of the Westwater Canyon member (CP13 and CP21) analyzed by Dickinson and Gehrels (2008a), but much lower proportions of arc-derived zircon, such that a correlation between the Sespe clasts and Morrison Formation is not compelling. Quartz arenite of Late Jurassic to Early Cretaceous age is exposed in several areas in southern California and southwestern Arizona. One example is the McCoy Mountains Formation (Barth et al., 2004; Spencer et al., 2011), but as with the Morrison Formation, the abundance of arc-derived zircon is much higher than in the Sespe clasts. Note that the above comparisons are constrained by only 39 and 57 dated zircon grains, respectively, from the two Sespe clasts.

Formation (CP13 and CP21; Dickinson and Gehrels, 2008a, 2008b). Sabbeth et al. (2019) said (p. 1991): "Similar to the Morrison, LS1114 [this sample also reported as 14LS11] has a moderate paleomagnetic inclination, scarcity of grains between 0.5 and 1 Ga in its detrital zircon spectrum, and is a well-indurated, light pinkish-gray, medium- to coarse-grained orthoquartzite. Although the Mesozoic peak in the Sespe spectrum is not as prominent as in the two Morrison spectra, the ratio of Mesozoic to Proterozoic grains is more similar between LS1114 and CP21, from the Morrison, than it is between the two Morrison samples."

This inference is problematic for several reasons. First, much of the Westwater Canyon sandstones are subarkosic (Cadigan, 1967). Furthermore, much of the Morrison Formation had been removed by erosion prior to deposition of the lower Upper Cretaceous Dakota Formation in the region of the proposed 20 Ma drainage such that any Morrison detritus would have had to come from the Four Corners region (Fig. 1; Dickinson, 2013, p. 10; Dickinson, 2018, his figures 93 and 94). In addition, whereas Sespe sample 14LS11 is broadly similar to Morrison samples CP13 and CP21 with respect to pre-Mesozoic age distributions (Fig. 14), the association of the Grenville, Picuris, and Yavapai-Mazatzal–age zircon is not particularly diagnostic (e.g., Gehrels and Pecha, 2014; Schwartz et al., 2019). The 1.2 Ga peak in sample 14LS11, based on only 39 total analyses for the entire sample, is not clearly diagnostic of the Morrison Formation. Most importantly, sample 14LS11 lacks the high percentage of Mesozoic arc-derived zircon that characterizes the Westwater Canyon Member of the Morrison Formation and other potential Triassic–Jurassic sources (Schwartz et al., 2019). The high Mismatch value of 0.59 between clast 14LS11 and the Morrison Formation (Fig. 7) challenges the notion that they are correlative.

We also compare sample 14LS11 to orthoquartzite in the basal part of the Upper Jurassic–Cretaceous McCoy Mountains Formation of southern California and southwestern Arizona (Barth et al., 2004; Spencer et al., 2011), which is exposed within the inferred catchment area of the Sespe drainage system (Fig. 1; Howard, 2000). As with Morrison samples CP13 and CP21, the basal McCoy includes substantially more arc-derived zircon than is found in sample 14LS11 (Fig. 14). In addition, the Grenville-age zircon in the basal McCoy Mountains Formation has a peak at ca. 1.1 Ga rather than 1.2 Ga. Upper Jurassic–Lower Cretaceous quartzose strata occur elsewhere in southern California, southwestern Arizona, and northwestern Sonora, Mexico, but are likewise enriched in Triassic–Jurassic arc detritus and/or ca. 600 Ma (Gondwanan) and 400 Ma (Appalachian) zircon typical of the Jurassic eolian deposits of the Colorado Plateau (Reis, 2009; Mauel et al., 2011; Peryam et al., 2012) and comprise poor matches to sample 14LS11. A source for clast 14LS11 thus remains unclear, assuming that the Phanerozoic ages are part of the detrital assemblage. Interestingly, the pre-arc zircon fraction in sample 14LS11 is similar to that in Sespe clast BW1609 (Fig. 14). Sample BW1609 likewise also includes Mesozoic ages, but in this case Sabbeth et al. (2019, p. 1991) interpreted the young ages as allochthonous. Perhaps they are also allochthonous in 14LS11. If so, 14LS11 could have been derived from one of the Neoproterozoic to Cambrian sequences discussed above (e.g., Fig. 10). Considering the above complexities, we conclude that the Sabbeth et al. (2019) extraordinary claim that pebbles

from Sespe can be traced to a Colorado Plateau source region to support the "Arizona River" hypothesis is unconvincing.

■ SUMMARY OF PROVENANCE EVIDENCE

In summary, the combined detrital zircon data from Sespe clasts and potential sources indicate the clasts were derived from more than one source, and there is no definitive match for the source of any individual Sespe clast. The most Shinumo-like clasts are more similar to Big Bear Group (Mismatch of 0.21) or Ontario Ridge metasedimentary rocks (Mismatch of 0.23) of the Transverse Ranges, and/or Troy Quartzite (Mismatch of 0.33) of central Arizona than the Shinumo Sandstone of Grand Canyon (Mismatch of 0.35). Unimodal spectra most closely resemble Pinto Mountain Quartzite (Mismatch of 0.21) and White Ledges Quartzite (Mismatch of 0.30) of these same regions rather than Shinumo (Mismatch of 0.56). The multiple sources are compatible with the conclusions of Howard (1996, 2000) and Ingersoll et al. (2018), to which we add probable Transverse Ranges sources. The potential Mesozoic clasts do not strongly resemble the Morrison Formation of the Colorado Plateau. Overall, the detrital zircon data from a more complete range of possible sources falsify the Sabbeth et al. (2019) assertion that Shinumo Sandstone is the only "plausible" source for Sespe orthoquartzite cobbles. Thus, the data also do not support the proposed Arizona River drainage connection between the Colorado Plateau and Sespe delta between 50 and 6 Ma.

■ REAPPRAISAL OF THERMOCHRONOLOGIC DATA ON INCISION HISTORY OF GRAND CANYON

This section addresses the persistent assertions by Sabbeth et al. (2019, p. 1995) that: "… Upper Granite Gorge of the eastern Grand Canyon had been eroded to within a few hundred meters of its current depth by early Miocene time ca. 20 Ma (p. 1995)…. as independently confirmed by (U-Th)/He thermochronology" and "…western Grand Canyon was carved to within a few hundred meters of its current depth no later than 20 Ma, and perhaps as early as Late Cretaceous/Paleocene time, based on thermochronological evidence (e.g., Flowers et al., 2008; Wernicke, 2011; Flowers and Farley, 2012)." More than a decade of work and multiple thermochronometric methods have now been applied to constrain time-temperature (t-T) paths in both eastern and western Grand Canyon. Such cooling data can model a grain's journey toward Earth's surface due to erosional exhumation of overlying strata to help visualize past, now-eroded, landscapes and the timing of carving of Grand Canyon. To help clarify the somewhat confusing past literature, Table 1 cites and summarizes prior thermochronologic studies. Figure 15 shows published t-T models that have led to alternative canyon carving histories. The questions addressed below, for eastern then western Grand Canyon, respectively, are: (1) when was eastern Grand Canyon cut deep enough to expose the Shinumo

TABLE 1. SUMMARY OF GRAND CANYON THERMOCHRONOLOGIC INTERPRETATIONS

Reference and Fig. 15 t-T path	Eastern Grand Canyon	Western Grand Canyon	Comments and future directions
Kelley et al. (2001) C, D, G	"…cooled during early Laramide deformation to temperatures of about 55 to 65 °C, … remained at these temperatures until 5 to 15 Ma" (p. 37)	"AFT data in western Grand Canyon record rapid Laramide cooling to temperatures <50 °C." (p. 37)	Western samples are from an uplifted Laramide block and do not necessarily record river incision; different cooling histories across faults need additional attention, especially for Hurricane fault.
Flowers et al. (2008) B	"Similar Early through mid-Tertiary temperatures in samples now separated by as much as 1500 m in both elevation and stratigraphic position imply that a kilometer-scale proto–Grand Canyon was carved in post-Paleozoic sediments during Early Tertiary time in the Upper Granite Gorge region." (p. 581)	"The single phase cooling history of the Lower Granite Gorge contrasts with the multiphase cooling history of the Upper Granite Gorge." (p. 578) "Cooling of the Kaibab surface below 45 °C occurred prior to 60 Ma in the western Grand Canyon" (p. 581)	South to north cooling was documented (due to cliff retreat), as was a potential mid-Tertiary paleocanyon across the Kaibab uplift. The interpretation that rim and river samples in eastern Grand Canyon were at similar temperatures in the Early Tertiary (hence a Laramide paleocanyon existed) is arguable depending on which t-T models are used (see below).
Wernicke (2010)	"Thus, rim and gorge samples ... that were at much different temperatures prior to 80 Ma, converged in temperature and accordingly had a common depth and thermal history after 70 Ma. … creating a canyon of roughly the same depth as the modern one, cut in younger strata now eroded away" (p. 1295)	"Given an apparent upper limit of 35 °C for the temperature of western Grand Canyon basement in the Diamond Creek area since 70 Ma," (p. 1303); "incision of a large canyon from a plain of low elevation and relief to a canyon of roughly the length and depth of modern Grand Canyon occurred primarily in Campanian time (80–70 Ma)." (p. 1288)	The conclusion of this paper that: "Colorado River did not play a significant role in excavating Grand Canyon." (p. 1312) was provocative and has motivated a continuing debate on the age, location, and geometry of prior paleocanyons. However, post–5 Ma carving of most of Grand Canyon by the Colorado River is supported by incision studies and geomorphic modeling.
Flowers and Farley (2012) B, E	"This history supports a model (Wernicke, 2011) in which much of the Grand Canyon was carved by an ancient Cretaceous river" (p. 1618), [but cf.] "This history is compatible with the suggestion that incision of much of the eastern half of the canyon occurred after 6 Ma" (p. 1617)	"… data for the western Grand Canyon provide evidence that it was excavated to within a few hundred meters of modern depths by ~70 Ma" (p. 1616)	Thermal histories were forced through 110° to 120°C peak temperatures at 80 to 85 Ma in E vs. 80 to 100 Ma in W, which was assumed to have resulted in complete annealing of apatite fission tracks at this time. This was a key unsupported assumption addressed by Fox and Shuster (2014).
Lee et al. (2013) C, D	"The new data suggest that the early Cenozoic landscape in eastern Grand Canyon was low in relief and does not indicate the presence of an early Cenozoic precursor to the modern Grand Canyon. However, there is evidence for the incision of a smaller-scale canyon across the Kaibab Uplift at 28–20 Ma. In contrast, just upstream in the area of Lee's Ferry, ~2 km of Mesozoic strata remained over the middle Cenozoic and were removed after 10 Ma." (p. 216)	"A robust AFT age of 62.8 ± 4.0 Ma for sample 01GC86 (river mile 243) with relatively long mean track lengths of 13.0 ± 0.4 µm coupled with 29.2–72.3 Ma AHe ages on low eU (11–17) grains constrain an episode of rapid cooling ca. 65–75 Ma, and residence at temperatures of ~50 °C through most of Cenozoic time." (p. 222)	Lee et al. (2013) had two age-elevation transects, one in the main canyon corridor and one near Tapeats Creek; these help define the length of the East Kaibab paleocanyon. Additional and more detailed age-elevation transects are needed to further resolve t-T paths for the Kaibab uplift and for the depth of the proposed East Kaibab paleocanyon along its length. Age-elevation transects in Mesozoic rocks near Lees Ferry are also needed.
Flowers and Farley (2013) E	"… similar temperatures from Late Cretaceous through mid-Tertiary time, compatible with the presence of a substantial eastern paleocanyon as proposed in Flowers et al. (2008)." (p. 143-c)	"all statistically acceptable paths requiring cooling to temperatures <30°C by ~70 Ma." (p. 143)	Additional ^{4}He/^{3}He data are needed and should be modeled as separate samples rather than groups of samples to distinguish any differences across faults and folds and to evaluate the possibility of ragged cliff retreat.
Karlstrom et al. (2014) C, D	"The 90–70 °C constraints indicate that rocks currently at river level were 1.8-4 km deep from 60 to 25 Ma and ... not carved to near modern depths by 70–55 Ma… rim and river cooling paths converge by ~20 Ma despite their 1.5 km difference in elevation. This provides evidence that a ~1.5 km-deep palaeocanyon was carved 25-15 Ma, which we call the East Kaibab palaeocanyon." (p. 240)	"AFT track length data (12.1 -13.0 µm) require that some of the rocks resided in the >60 °C AFT partial annealing zone, and AHe age-effective uranium concentration correlation also constrain higher temperatures of ~60 °C and, hence, 1.4–2.5 km burial depths…. this suggests that Westernmost Grand Canyon was not cut to near-modern depths until after 6 Ma." (p. 242)	"…palaeocanyon solution for carving Grand Canyon suggests that the 5–6 Ma Colorado River became integrated through two young (<6 Ma) segments (Marble Canyon and westernmost Grand Canyon), one 25–15 Ma segment (Eastern Grand Canyon), and a >50 Ma Hurricane segment…all segments were widened and Grand Canyon was deepened during semi-steady river incision over the past 4 Ma at rates of 100-200 m/Ma" (p. 243)
Fox and Shuster (2014) E	No data	"The possibility of incomplete annealing resolves the apparent conflicting time-temperature paths inferred over the last 70 Ma, although it requires temperatures during burial that are lower than predicted by apatite fission track data." (p. 174)	"If the annealing of alpha recoil damage and its effect on ^{4}He diffusivity in apatite is decoupled from existing models of fission track annealing, coexisting datasets for individual samples may be found to be more compatible with one another." (p. 182)
Fox et al. (2017) F	No data	"New data from westernmost Grand Canyon support a "young" Canyon model where rocks cooled from 80 to 50 °C in the Laramide, resided at about 50 °C, then cooled to near surface temperatures in the last 6 Ma" (p. 255)	"… limitation in quantifying radiation damage (and hence crystal retentivity) introduces non-uniqueness to interpreting time–temperature paths in rocks that resided in the apatite helium partial retention zone for long durations. Another source of non-uniqueness is due to unknown U and Th distributions within crystals." (p. 248)

(*continued*)

TABLE 1. SUMMARY OF GRAND CANYON THERMOCHRONOLOGIC INTERPRETATIONS (*continued*)

Reference and Fig. 15 t-T path	Eastern Grand Canyon	Western Grand Canyon	Comments and future directions
Winn et al. (2017) F, G	No data	… "thermochronologic data ….are reconciled via the integration of three methods of analysis on the same sample: AHe, ^{4}He/^{3}He, and AFT; …t–T paths show cooling from ~100 °C to 40–60 °C in the Laramide (70–50 Ma), long-term residence at 40–60 °C in the mid-Tertiary (50–10 Ma), and cooling to near-surface temperatures after 10 Ma, and thus support young incision of the westernmost Grand Canyon." (p. 257)	[To reconcile conflicting data] "we adjusted model parameters and uncertainties to account for uncertainty in the rate of radiation damage annealing in these apatites during sedimentary burial and the resulting variations in He retentivity." (p. 257) "A geologic hypothesis capable of explaining different t–T paths in these locations involves ragged cliff retreat of the Kaibab escarpment" (p. 270)
Karlstrom et al. (2017)	"Differential Laramide cooling [in the Little Colorado River (LCR) valley] suggests is carving of 70–30 Ma paleotopography by N- and E-flowing rivers whose pathways were partly controlled by strike valleys at the base of retreating Cretaceous cliffs. A second pulse of denudation is documented by apatite (U-Th)/He dates and thermal history models that indicate a broad LCR paleovalley was incised 25–15 Ma by an LCR paleoriver that flowed northwest and carved an East Kaibab paleovalley across the Kaibab uplift." (p. 49)	No data	In addition to the progressive cooling by NE cliff retreat, a pulse of denudation is recorded … near river level in the LCR valley; these [samples] remained >60 °C from 50 to 25 Ma, corresponding to preservation of 1–2 km of Mesozoic strata that still covered these rocks until ca. 25 Ma." (p. 62). Additional thermochronology at the LCR confluence in an age-elevation transect would help test the depth of the proposed East Kaibab paleocanyon.
Fitzgerald and Malusà (2019)	No data	"AFT and track-length data from basement several-hundred meters below the Cambrian unconformity in the Grand Wash trough were at 80-100 °C until rapid cooling about 17 Ma" (p. 183)	Wernicke (2011) compared thermal histories of rocks just below the Great Unconformity in Grand Canyon and the Gold Butte block; both he and Flowers and Farley (2012) assumed a higher peak Laramide burial temperature (110–120 °C) than Fitzgerald and Malusà (2019) did (80–100 °C).
Winn (2019) C, D	"Temperature interpolations on the Kaibab datum show that the south rim of this [East Kaibab] paleocanyon had been stripped of much of the Cretaceous and some Jurassic strata by 20 Ma, but the north Rim and the Kaibab uplift were at >50 °C until 10 Ma and still had Jurassic rocks above them." (p. 63)	"… a 40–140 °C Laramide (90–70 Ma) constraint box that allows the data to estimate the amount and timing of late Cretaceous maximum burial reheating. This approach allows for the build-up of radiation damage in crystals" (p. 54)	"cooling caused by erosional denudation .. took place 70–50 Ma; ~20 Ma, and <6 Ma …. These are also times of known paleorivers, geologically recorded erosion, and significant tectonic events…we conclude that episodes of uplift, base level fall, and river incision drove cliff retreat pulses." (p. 61)
Sabbeth et al. (2019)	[The Shinumo-Sespe connection] "is independently confirmed by (U-Th)/He thermochronology." (p. 1973)	"western Grand Canyon was carved to within a few hundred meters of its current depth no later than 20 Ma, and perhaps as early as Late Cretaceous/Paleocene time based on thermochronologic evidence" (p. 1995)	No new thermochronology was presented; they did not discuss or reconcile contradictions between the interpretation of Flowers and Farley versus the t-T models published in the post-2013 literature.

Abbreviations: LCR—Little Colorado River; t-T—time-temperature.

Sandstone; and (2) when did a paleocanyon pathway exist at that depth that could have transported Shinumo Sandstone to the Sespe delta? The overall goal of this section is to outline the limits of the resolving power of existing thermochronology and suggest future next steps.
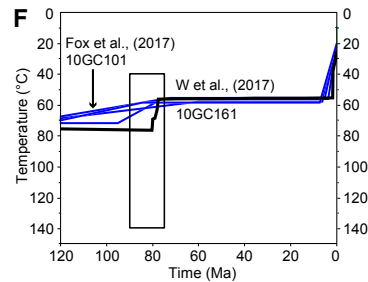
Eastern Grand Canyon

Flowers et al. (2008, p. 581) proposed that: "Similar Early through mid-Tertiary temperatures in samples now separated by as much as 1500 m in both elevation and stratigraphic position imply that a kilometer-scale proto–Grand Canyon was carved in post-Paleozoic sediments during Early Tertiary time in the Upper Granite Gorge region." This concept of an old Grand Canyon was applied to both 70 Ma and 55 Ma timeframes by Wernicke (2011), and his model was explicitly supported by Flowers and Farley (2012, 2013).

For eastern Grand Canyon, there is a general agreement of data and models with respect to t-T paths of upper Granite Gorge river–level rocks. Figure 15B shows a two-stage cooling path (Flowers and Farley, 2013) in a best-fit forward model derived from their ^{4}He/^{3}He data from four samples from the upper Granite Gorge. Basement rocks cooled from 100 to 60 °C in the Laramide, then resided at ~60 °C from 60 to 25 Ma. In Figure 15C, the Lee et al. (2013) weighted-mean paths based on combined apatite fission track (AFT) and He apatite (AHe) for the same area of the upper Granite Gorge suggest that rocks resided at ~80 °C. In Figure 15C, Marble Canyon AFT plus AHe weighted-mean paths suggest rocks were >110 °C until after 40 Ma (Kelley et al., 2001; Karlstrom et al., 2014; Winn, 2019). All data sets show that river-level rocks in eastern Grand Canyon were >60 °C, hence were >1.8 km deep (and still hotter in Marble Canyon) until after 20 Ma. Thus, these results are inconsistent with the hypotheses of a paleo–Grand Canyon between ca. 70 or 50 Ma that was carved to within a few hundred meters of its modern depths at these eastern Grand Canyon locations.
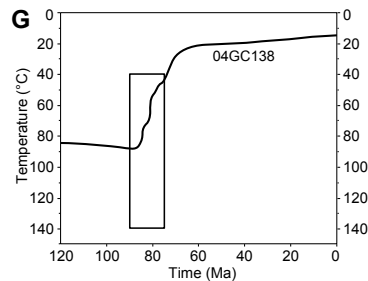
Western Grand Canyon
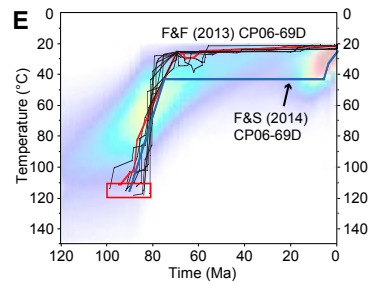
E. Westernmost Grand Canyon, ⁴He/³He Flowers & Farley (2013) versus Fox and Shuster (2014; colors), Separation Canyon.

F. Westernmost Grand Canyon, combined ⁴He/³He, AFT, and AHe, (Winn et al., 2017) and ⁴He/³He (Fox et al., 2017, blue), Separation Canyon.

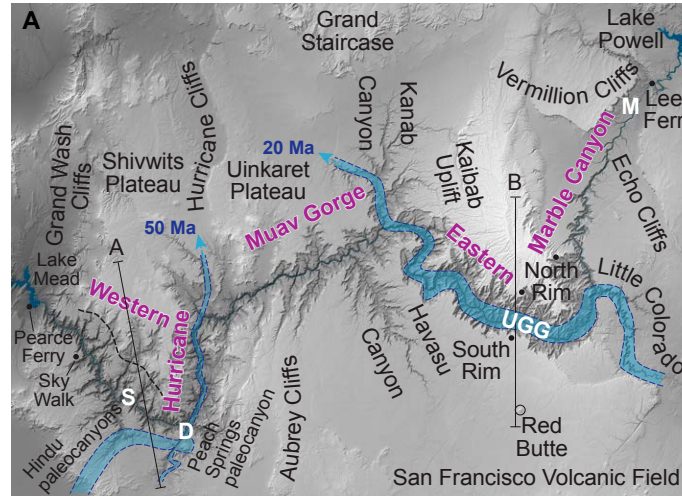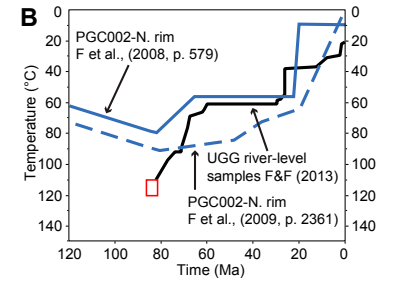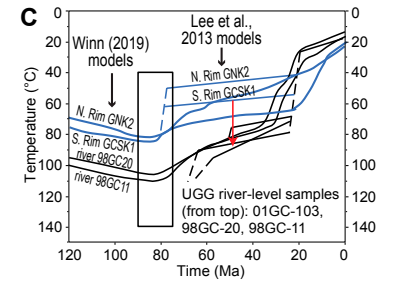G. Hurricane segment, 04GC138 AFT, Winn et al. (2017).

Eastern Grand Canyon

B. Eastern Grand Canyon, AHe and ⁴He/³He, Flowers and Farley (2013). Blue = rim samples.

C. Eastern Grand Canyon AHe and AFT, Lee et al. (2013), Winn (2019).

D. Marble Canyon (black) and Kaibab uplift (blue), Karlstrom et al. (2014); Winn (2019).

Figure 15. (A) Paleocanyon solution for the age of Grand Canyon suggests different segments of Grand Canyon (purple letters) have different ages and cooling histories. Blue colors are older paleocanyon segments of Karlstrom et al. (2014). Lines A and B are locations of cross-section lines in Figure 16. (B) Flowers et al. (2008, 2009) and Flowers and Farley (2012, 2013) interpretation that rim and river-level samples were at similar temperature since Late Cretaceous supporting the old Grand Canyon of Wernicke (2011). (C) Lee et al. (2013), Karlstrom et al. (2014), and Winn (2019) models suggest North and South Rim samples were ~30 °C cooler (red arrow) than river-level samples until 20 Ma when East Kaibab paleocanyon was carved across the Kaibab uplift, arguing against a 70 or 50 Ma Grand Canyon. (D) Apatite fission-track (AFT) data of Lee et al. (2013), Karlstrom et al. (2014), and Winn (2019) suggest Marble Canyon samples (M) were >110 °C until after 40 Ma, and North Rim samples were ~30 °C cooler (red arrow), arguing against a 70 or 50 Ma Grand Canyon. (E) Flowers and Farley (2012) ⁴He/³He data from Separation Canyon are compatible with alternative models with the difference being the Laramide constraint box (in red) imposed by Flowers and Farley (2012). (F) Precise ⁴He/³He data of Fox et al. (2017) and Winn et al. (2017) are best predicted by time-temperature (t-T) models compatible with a young westernmost Grand Canyon. (G) AFT data from Diamond Creek suggest that the Hurricane segment was partially carved by an older N-flowing paleoriver. S—Separation Canyon; D—Diamond Creek.
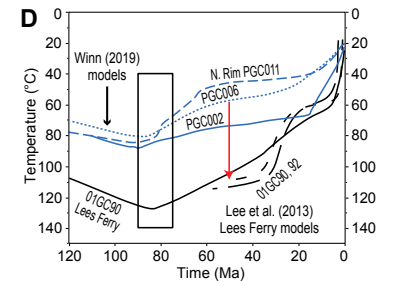
Karlstrom et al. | Shinumo-Sespe drainage connection

However, testing whether paleocanyons may have existed "in the air," i.e., in now-eroded Mesozoic rocks above eastern Grand Canyon, involves comparing rim and river-level t-T paths. Since the past thermal field would have been influenced by km-scale paleocanyon topography, comparative thermochronology of rocks at different modern elevations provides a test. Rocks at different elevations are predicted to be at comparable temperatures if the thermal field was strongly perturbed by paleotopography (Braun, 2003). Constraints from thermochronology in Figure 15B led Flowers and Farley (2012, 2013) to conclude that rim and river-level rocks were about the same temperature since the late Cretaceous and therefore that an old paleo–Grand Canyon existed since that time. In contrast, models in Figure 15C (Lee at al., 2013; Karlstrom et al., 2014; Winn, 2019) show rim samples were ~30–35 °C cooler than river-level samples, suggesting no paleocanyon existed until after 20 Ma. In the Figure 15C models, rim and river-level samples come to similar temperature 25–15 Ma leading to models for carving of an east Kaibab paleocanyon across the Kaibab uplift at this time (blue pathway of Fig. 15A; Karlstrom et al., 2014). Figure 15D suggests that the Lees Ferry area resided at ~100 °C until 25 Ma, then ~60 °C until 6 Ma, and was under several km of Mesozoic strata until after 6 Ma. Hence the Marble Canyon segment could not have been part of a 55 Ma (Wernicke, 2011, his figure 9A) or 20 Ma (Sabbeth et al., 2019, their figure 1) "Arizona River" flowing through Grand Canyon at near its modern depth.

The thermal evolution and eastern Grand Canyon depth after 20 Ma are not well resolved. Modeling of thermochronologic data suggests that modern-day rim and river-level rocks reached the same temperature (40–60 °C) 25–15 Ma due to carving of the ~1.5-km-deep East Kaibab paleocanyon, which had its rim in Jurassic rocks 0.6–1.4 km above the Kaibab surface and its floor below the Kaibab surface but still 0.6–1.4 km above river level (Flowers et al., 2008, their figure 8D; Lee et al., 2013, their figure 9). In these models, the highest outcrops of the Shinumo Sandstone that extend as high as 530 m above the river (1260 m elevation) in eastern Grand Canyon would not have been exposed. Karlstrom et al. (2017) suggested a speculative range of minimum elevations (maximum paleocanyon depths) for the ca. 6 Ma confluence to have been 500–900 m above modern river level (1200–1600 m), perhaps (marginally) allowing exposure of the Shinumo Sandstone by 6 Ma. However, the apatite thermochronology data currently do not have the needed resolving power at these low temperatures (below 30–40 °C), and conversion of temperature to depth has large uncertainties. Thus, existing thermochronology cannot independently confirm that the Shinumo Sandstone was exposed to erosion ca. 20 Ma.

Western Grand Canyon

There is no Shinumo Sandstone in western Grand Canyon, and the second question is, if Shinumo Sandstone was exposed for erosion at 20 Ma in eastern Grand Canyon, whether there was a major river through western Grand Canyon as proposed by Sabbeth et al. (2019) that connected to the Sepse delta (Fig. 1). Thermochronology of rocks in western Grand Canyon region

indicate that they cooled earlier than eastern Grand Canyon. This has been interpreted as due to Laramide removal of Mesozoic rocks from the Hualapai Plateau (Kelley et al., 2001; Young, 2001; Flowers et al., 2008). Figure 15E shows Flowers and Farley (2013) t-T models based on ^{4}He/^{3}He data for westernmost Grand Canyon data that favored an "old canyon" cooling path (Fig. 15E, red line). However, Figure 15EF also shows that their same data, as modeled by Fox and Shuster (2014), are consistent with both a young and an old canyon model, and that a young canyon t-T path (blue line) may be more probable (red background colors reflect higher probability). Fox and Shuster (2014) argued that the red constraint box of the Flowers and Farley model (Fig. 15E) was not necessarily justified and that, instead, models should include the long history of accumulation of radiation damage due to burial heating in the Phanerozoic. Figure 15F shows agreement of two different modeling efforts based on high-precision ^{4}He/^{3}He data from the Separation Canyon locality; the Fox et al. (2017) model is based on the ^{4}He/^{3}He data and the Winn et al. (2017) model combined AFT, AHe, and ^{4}He/^{3}He data. These models used only a very broad Laramide constraint box (black rectangle in Fig. 15F) to let the data resolve maximum pre-Laramide burial temperatures; they support a young canyon model and suggest that westernmost Grand Canyon basement rocks resided at ~60 °C until after 6 Ma. In contrast, the Hurricane fault segment of Grand Canyon (Fig. 15G) shows the "old canyon" cooling path and is interpreted to have been carved by a north-flowing 65–55 Ma Music Mountain paleoriver (Karlstrom et al., 2014). Thus, although paleocanyons existed in the 20 Ma landscape, available thermochronology data do not confirm that "western Grand Canyon was carved to within a few hundred meters of its current depth no later than 20 Ma, and perhaps as early as Late Cretaceous/Paleocene time" (Sabbeth et al., 2019, p. 1995).

Limitations of Thermochronologic Data

Several uncertainties have led to the conflicting interpretations and continue to limit the resolving power of Grand Canyon's thermochronologic data. The first involves understanding the annealing kinetics of radiation damage in apatite and how such lattice damage influences He diffusion kinetics, and hence, temperature sensitivity. The Flowers and Farley (2012, 2013) forward models of basement rocks in the Grand Canyon assumed that cooling of Precambrian apatite started in the imposed constraint boxes shown in the red boxes of Figures 15B and 15E, with assumed burial temperatures prior to 80 Ma of 110–120 °C. Newer modeling (Fox et al., 2017; Winn et al., 2017) suggests that this assumption may be valid for river-level rocks in eastern Grand Canyon (compare Figs. 15B–15D), but not for western Grand Canyon (compare Figs. 15E–15G). It was this assumption (and the constraint box in their models) that appears to have led to their western Grand Canyon ^{4}He/^{3}He t-T models for an "old canyon" (red curve in Fig. 15E) in which rocks cooled quickly in the Laramide and resided from 70 Ma to present at 20–30 °C, potentially only a few hundred meters below the surface. However, Fox and Shuster (2014)

Karlstrom et al. | Shinumo-Sespe drainage connection

showed that t-T paths rely on model parameters such as Rmr0 (Ketcham, 2005) that have large laboratory uncertainty reflecting uncertainty in understanding helium diffusion systematics and kinetics, especially for conditions of moderate prograde heating before the Laramide and incomplete annealing of lattice damage.

Even if t-T paths are well resolved, a major geologic uncertainty is converting paleotemperature to paleodepth. This requires assumptions about both time-averaged surface temperature and geothermal gradient (Karlstrom et al., 2014, their supplementary table 2). It is unlikely that any average values accurately characterizes this time of transition from flat-slab refrigeration of western North America (75–55 Ma; Dumitru et al., 1991), higher heat flow during the 38–25 Ma ignimbrite flare-up (Best et al., 2016), and major Cenozoic climate changes (Cather et al., 2011). But, following recent papers, we use a geothermal gradient of 25 °C/km and an average surface temperature of 25 °C to compare region to region (Wernicke, 2011; Karlstrom et al., 2014; Winn et al., 2017). This results, for 50 °C, in a paleodepth of 1 km. Alternatively, 50 °C could correspond to a depth of 1.6–2.0 km (10 °C and 25–20 °C/km) or ~800 m (25 °C and 30 °C/km). However, interpreting rocks at 50 °C to reflect <500 m depth, as needed to reconcile the 20 Ma Shinumo-Sepse connection, would require unlikely time-averaged values, for example, of 40 °C surface temperature and 20 °C/km geothermal gradient.

To further present thermochronologic progress and limitations, Figure 16 shows cross-section reconstructions of eastern and western Grand Canyon paleosurfaces through time using weighted-mean paths from Figure 15 and applying a 25 °C/km geotherm and 25 °C surface temperature to the samples

shown. These hypothetical paleosurfaces change by hundreds of meters depending on which sample and which t-T model is chosen, and also shift a similar amount depending on assumptions of geothermal gradient and surface temperature. Stratigraphic thicknesses from nearby areas are from Karlstrom et al. (2017), with thinner Jurassic section in western Grand Canyon region due to stripping prior to deposition of the 95 Ma Dakota Sandstone (Dickinson, 2013). In both cross sections, the reconstructed paleosurfaces do not agree well with stratigraphic heights shown for the 95 and 75 Ma upper Cretaceous paleosurfaces, which themselves are subject to large thickness extrapolation uncertainties.

In eastern Grand Canyon, consensus conclusions are that a 70–50 Ma paleocanyon, if one existed, would have been "in the air" in now-eroded Mesozoic strata and that a ca. 20 Ma paleocanyon may have notched through the Kaibab surface to as much as one third to half the depth of modern Grand Canyon (Flowers and Farley, 2012; Lee et al., 2013). In western Grand Canyon, cooling was mainly by cliff retreat; Hualapai Plateau was stripped of most of the Mesozoic section by ca. 60 Ma as shown by the ca. 65–55 Ma Music Mountain (Young and Hartman, 2014) paleodrainage that flowed north through the >600-m-deep Milkweed-Hindu paleocanyon to the Hurricane segment of Grand Canyon. Geologic data, plus the more recent and precise $^4He/^3He$ data (Fox et al., 2017; Winn et al., 2017), suggest that upper Paleozoic and Triassic strata remained over the westernmost position of the modern Grand Canyon, keeping river-level rocks at 40–60 °C until after 6 Ma. Retreat of the Kaibab escarpment by at least 8 km northward from the rim of the Milkweed-Hindu paleocanyon continued to widen the Shivwits Plateau during the retreat of
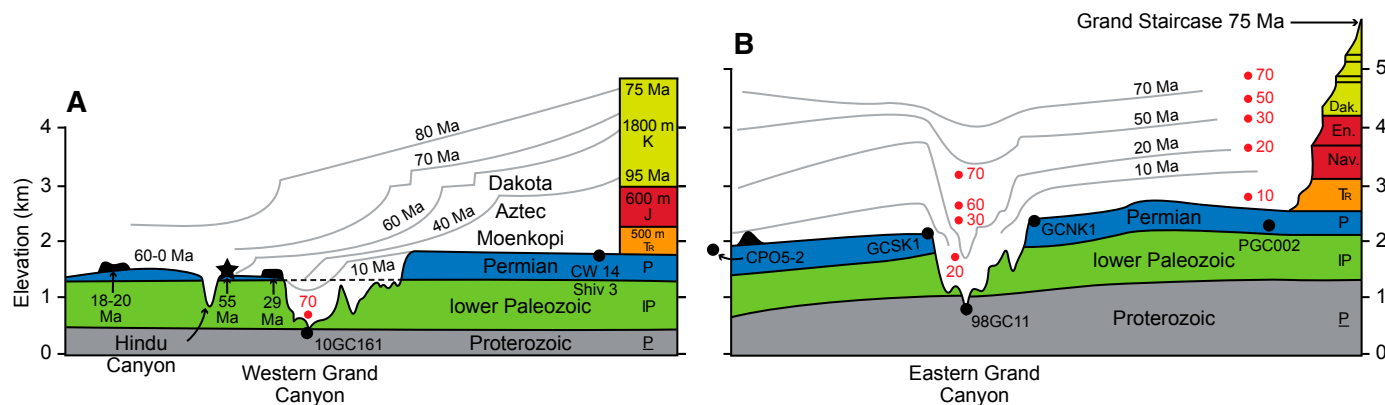

Figure 16. Evolution of paleosurfaces in eastern and western Grand Canyon based on applying a 25 °C surface temperature and 25 °C/km geothermal gradient to the time-temperature (t-T) models and along the cross-section lines shown in Figure 15. Samples and models used for the gray lines were: 10GC161 (Winn et al., 2017), CW-14Shiv3 (Winn, 2019), CP05-2, GCSK1, GCNK1, 98GC11, and PGC002 (Winn, 2019). The models for river-level samples in eastern Grand Canyon from Figure 15B from Flowers and Farley (2012) would predict different paleosurface heights through time (red dots) especially before 30 Ma such that the evidence for a 50–70 Ma paleocanyon in Mesozoic strata is permissive but arguable based on thermochronologic data. For western Grand Canyon, alternative hypotheses are that cooling history prior to 6 Ma river incision was driven by episodes of cliff retreat (Winn et al., 2017) as opposed to early deep fluvial incision by 70 Ma (red dot; Wernicke, 2011; Flowers and Farley, 2012, 2013).

the Kaibab escarpment to its present north-rim position within the past 6 m.y. (Young and Crow, 2014).

■ PALEOGEOGRAPHY OF THE SOUTHWESTERN COLORADO PLATEAU

The Shinumo-Sespe hypothesis highlights persistent research questions about the drainage evolution of the Colorado Plateau. Many workers have assumed that uplift of the Colorado Plateau and Rocky Mountains during Laramide time would likely have established continental-scale ancestral rivers that drained these uplifted regions (e.g., Galloway et al., 2011), including various configurations of an ancestral Colorado River (Hunt, 1956; McKee et al., 1967; Wernicke, 2011). The following section explores an alternative paradigm, supported by models for multi-stage uplift of the Rocky Mountain–Colorado Plateau region (Karlstrom et al., 2008, 2011; Cather et al., 2011), that most of the Colorado Plateau region was internally drained for much of the Cenozoic, until the Colorado River became integrated through Grand Canyon 5–6 Ma. Here we use the term paleoriver (e.g., Brazos and Platte paleorivers) for rivers ancestral to modern rivers, and we use the formation name of fluvial sedimentary deposits for the paleorivers that deposited them (e.g., Music Mountain paleoriver; Young and Hartman, 2014).

Early Eocene (50 Ma) Paleogeography

In the Late Cretaceous, east-, northeast-, and north-flowing rivers flowed from the continental divide on the Nevadaplano and Mogollon highlands onto the Colorado Plateau toward the retreating Western Interior Seaway in New Mexico, Colorado, and Wyoming (Goldstrand, 1994; Young, 2001; Saleeby, 2003; DeCelles, 2004; Davis et al., 2010; Wernicke, 2011; Sharman et al., 2015; Lawton, 2019). This pattern was severely altered during the Late Cretaceous–Paleogene Laramide orogeny. Uplift of the Rocky Mountains caused emergence of a region of dominantly internal drainage (Spencer et al., 2008; Lawton, 2019), although there may have been some flow-through lakes (Galloway et al., 2011).

Davis et al. (2010) proposed a "California River" that flowed north from the Mojave region to the Colton Formation of the Uinta Basin, as suggested by similar detrital zircon distributions in the Colton Formation and the upper McCoy Mountains Formation. However, this interpretation has been challenged given the more abundant 100–85 Ma zircon in the Colton that was more likely sourced from the Sierran arc rather than ca. 75 Ma zircon expected from abundant Laramide plutons in the Mojave region (Jacobson et al., 2011; Ingersoll et al., 2013; Sharman et al., 2015; Shulaker et al., 2019). These workers also showed from detrital zircon studies of Eocene strata in southern California that the likely eastern limit for Eocene streams that flowed west to the paleo–Pacific Ocean through the disrupted Mojave-Salinia segment of the Cretaceous batholith was the Mogollon highlands and the related mountainous region in eastern

California and southwestern Arizona (Fig. 17B). Paleorivers may have flowed northeast from this divide, roughly parallel to the Sevier thrust belt highland (Shulaker et al., 2019) to deposit the sand-dominated deltas in Lake Uinta until ca. 49 Ma (Smith and Dowling, 2008; Lawton, 2019). Wernicke (2011, p. 1288) used the same name "California River" for a different 80–70 Ma NE-flowing paleoriver that he envisioned to have "cut to within a few hundred meters of its modern erosion level in western Grand Canyon, and to the level of Lower Mesozoic strata in eastern Grand Canyon." Similarly, Potochnik (2001) and Cather et al. (2008) proposed a paleoriver pathway from the Mogollon highlands to the San Juan Basin. As summarized above, thermochronologic data indicate that any such paleoriver would have been flowing across Cretaceous strata 1–2 km higher than the Kaibab surface in the eastern Grand Canyon area, and hence potential pathways through the Grand Canyon region remain speculative.

The most critical region of middle Eocene paleogeography for this paper is western Grand Canyon and adjacent parts of southern Nevada, western Arizona, and eastern California (Figs. 12 and 17). The Kingman Uplift was cored by Paleoproterozoic crystalline basement punctured by numerous Laramide intrusions (72–65 Ma). To the southeast, this uplift merged with the Mogollon Highlands (Beard and Faulds, 2011); to the north, it likely merged with the Nevadaplano via a series of thrust sheets, although paleogeographic details are scarce. Remnants of the early and middle Eocene drainage-system deposits exist in paleoriver deposits in several localities. The Music Mountain Formation is early Paleocene to early Eocene based on fossil evidence (Young and Hartman, 2014), although U-Pb dating of the same fossiliferous carbonate indicates ages as old as 65 Ma (Hill et al., 2016). This paleoriver carved a major canyon, Milkweed-Hindu paleocanyon (Young, 2011), that was incised through the Kaibab surface to the level of Cambrian rocks on the Hualapai Plateau (Fig. 16). Paleocurrents document northerly sediment transport as do the Precambrian clasts, which could only have been derived from uplifts to the south and southwest (Young, 2011). Remnants of other paleorivers are preserved farther southeast along the Mogollon Slope that have been referred to as the "Rim Gravels" (Young, 2001). In contrast to the 65–55 Ma Music Mountain Formation, other "Rim Gravels" are younger, such as the 37–22 Ma Mogollon Rim Formation (Potochnik, 2001). In Figure 17B, we use the term Baca paleorivers for the early Eocene ancestors of these eastern Rim Gravels that likely flowed into the Baca Basin and perhaps flowed at times to the Gulf of Mexico (Cather, 2009; Galloway et al., 2011). A key conclusion of our paper is that a Mogollon highlands–Kingman uplift–Nevadaplano drainage divide persisted through the Eocene and sourced paleorivers that carried sediment both southward to the Sespe Formation and northward onto the lower elevation Colorado Plateau.

Early Miocene (20 Ma) Paleogeography

Figure 18 shows tectonic and paleogeographic maps at ca. 20 Ma (Early Miocene). Drainage reorganization was under way due to development of the Pacific–North American transform boundary and extension in the Great Basin
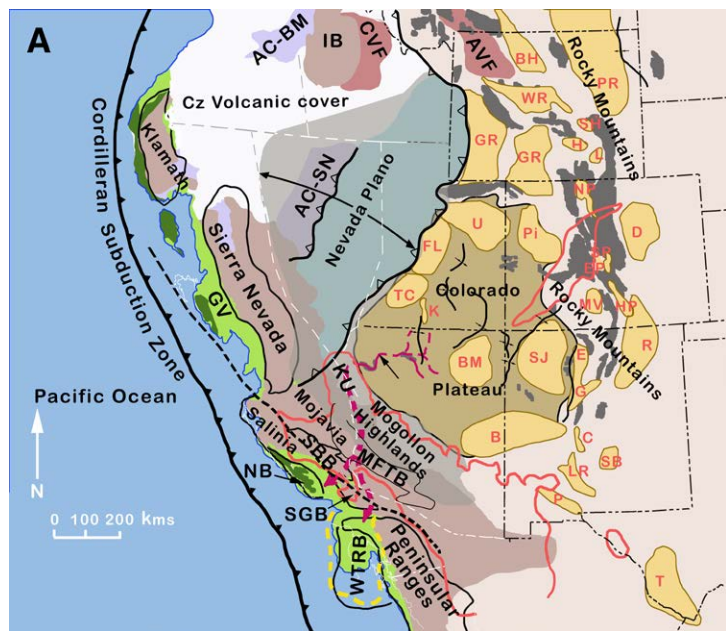
Figure 17. (A) Eocene paleotectonic features ca. 50 Ma. The region was bifurcated by major highlands—the Nevadaplano, Kingman Uplift (KU), and Mogollon Highlands—that extended from southern Idaho to southeast Arizona. Streams sourced from the western margin of the highlands flowed west into the Pacific Ocean; streams sourced from the eastern margin flowed into the array of Laramide basins, some of which at various times may have connected to the Gulf of Mexico (Galloway et al., 2011). Parts of the Rocky Mountains formed a complex divide that evolved rapidly during the Paleogene and early Eocene. Shown in yellow with red letters are Laramide sedimentary basins (Lawton, 2019). Basin and other abbreviations are: AC-BM— Paleozoic–Mesozoic accretionary terranes of Blue Mountains; AC-SN—Paleozoic–Mesozoic accretionary terranes of Sonoman and Antler orogenies; AVF—Absaroka volcanic field; B—Baca; BM—Black Mesa; BH—Big Horn; C—Carthage; CVF—Challis volcanic field; D—Denver; E—El Rito; EP—Echo Park; FL—Flagstaff; G—Galisteo; GR—Green River; GV—Great Valley; H—Hanna; HP—Huerfano Park; IB—Idaho Batholith; K—Kaiparowits; L—Laramie; LR—Love Ranch; MFTB—Maria fold and thrust belt (with thin black outlines); MV—Monte Vista; NB—Nacimiento Block (displaced Franciscan); NP—North Park; P—Potrillo; PI—Piceance; PR—Powder River; R—Raton; SB—Sierra Blanca; SBB—San Bernardino Block; SGB—San Gabriel Block; SH—Shirley; SJ—San Juan; SP—South Park; T—Tomillo; TC—Table Cliffs (Claron); U—Uinta; WR—Wind River; WTRB—Western Transverse Ranges Block. Additional patterns: solid red line—Laramide plutons (Colorado Mineral Belt in Colorado); heavy black dashed line—trace of future San Andreas fault; heavy yellow dashed line—maximum extent of Eocene–Miocene Sespe delta; dark-gray areas—Laramide Rocky Mountain uplifts. Sources of data: Howard (1995, 2000); Saleeby (2003); McQuarrie and Wernicke (2005); Davis et al. (2010); Dickinson et al. (2012); Young and Crow (2014); Sharman et al. (2015); Best et al. (2016); Ingersoll et al. (2018); Lawton (2019). (B) Early Eocene paleogeography ca. 50 Ma. Red dashed lines indicate drainage divides at 50 Ma showing paleorivers (blue lines and arrows) and lakes (light blue). Not all rivers were active at same time and drainage divides migrated rapidly. Several river systems entrenched in Klamath and Sierra Nevada regions fed Eocene basins in the Great Valley region.
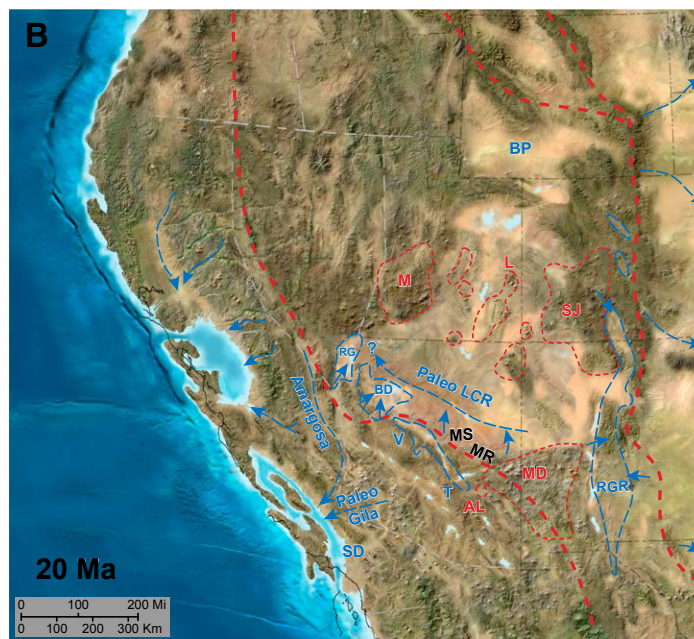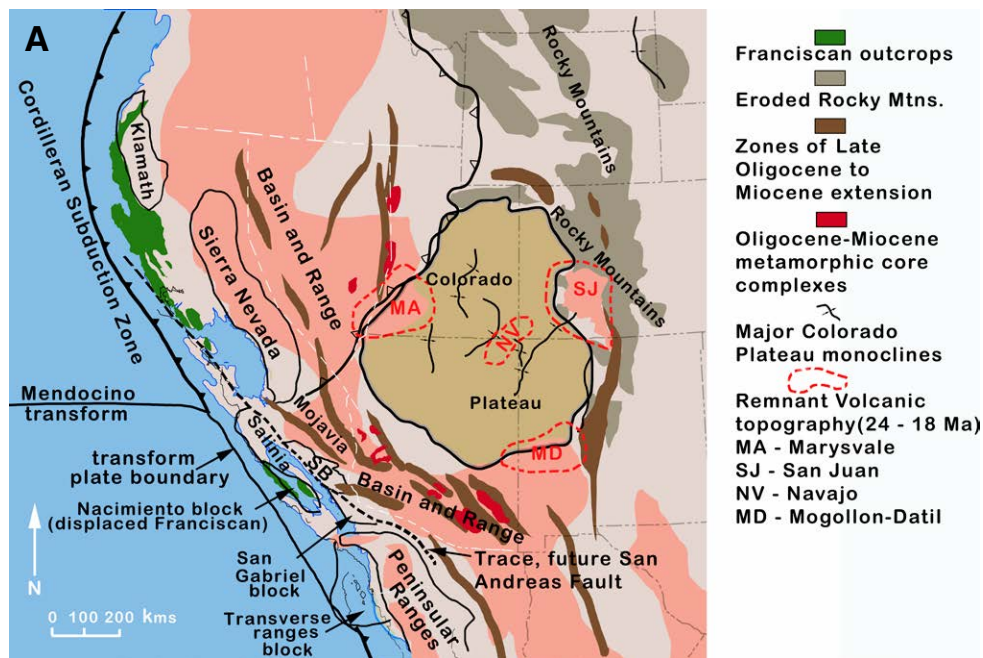
Figure 18. (A) Miocene paleotectonic features ca. 20 Ma. Basin and Range extension dismembered much of the Nevadaplano, Kingman Uplift, and Mogollon Highlands as volcanism waned, but remnant volcanic highlands remained from the caldera complexes, which were active in southern Arizona from 28 to 14 Ma and peaked between 24 and 18 Ma and mark the general location of the Nevadaplano divide. The western plate boundary of North America was a subduction margin to the north and a transform margin to the south of the Mendocino fracture zone. SB—San Bernardino block. Data from Behl (1999), McQuarrie and Wernicke (2005), and Best et al. (2016). (B) Miocene paleogeography ca. 20 Ma. Volcanics (24–18 Ma) are a waning expression of 38–23 Ma caldera-related volcanic activity of the ignimbrite flare-up (red). On the Colorado Plateau, scattered eolian sand and scattered lakes (shown hypothetically) likely mantled the internally drained landscape. Rainbow Gardens Formation and Buck and Doe Conglomerate represent drainages that flowed into internally drained basins. Major ash flow sheets of the 18.8 Ma Peach Spring Tuff flowed east and west from its source across the hypothetical path of the Arizona River. Paleo–Little Colorado River flowed across the Kaibab uplift through the East Kaibab paleocanyon with Jurassic rocks forming its north rim. An evolving Mogollon Rim escarpment separated the N-flowing Mogollon slope paleorivers from late Oligocene and early Miocene fluvial-lacustrine deposits in extensional basins. Rio Grande rift was the locus of sedimentation into fault-bounded internally drained lacustrine basins. Along the California coast, rapidly subsiding elongate basins mostly parallel to the coast received clastic sediment from intra-basinal uplifts that exposed Franciscan rocks, from uplands of the volcanic arc, and from basement catchments in the Mojave region. Upper Sespe sandstone reflects relatively nearby sources compared with lower Sespe deposits that had distant sources, including the flanks of the Mogollon Highlands. Data from Cather et al. (2008), Ingersoll et al. (2018), and Ott et al. (2018). Abbreviations: AL—Apache Leap Tuff; BD—Buck and Doe Conglomerate; BP—Browns Park Formation; LCR—Little Colorado River; M—Marysvale volcanic field; MD—Mogollon Datil volcanic field; MR—Mogollon Rim; MS—Mogollon slope; SJ—San Juan volcanic field; RG—Rainbow Gardens Formation; RGR—Rio Grande rift; SD—Sespe delta; T—Tonto Basin; V—Verde Valley.

and Basin and Range and Rio Grande rift (Dickinson, 1996, 2006; Atwater and Stock, 1998). Wasatch and proto–Grand Wash faults were beginning to emerge as boundaries between the Colorado Plateau and Basin and Range (18–16 Ma; Faulds et al., 2001). The western Nevadaplano continental divide was collapsing due to core-complex extension; high regions remained, and low regions were occupied by playas and internally drained lakes. Erosion of volcanic highlands from the 38–25 Ma Oligocene ignimbrite flare-up caused regional aggradation because of sediment oversupply to rivers. Volcanism was less prominent at ca. 20 Ma, but caldera complexes of the Superstition Mountains and Peach Spring Tuff (Young, 1999, 2011) erupted at ca. 19–18 Ma, and basaltic volcanism took place in volcanic fields around the Colorado Plateau (Young and Brennan, 1974; Crow et al., 2011). Internally drained basins in the Colorado Plateau region and remnants of the Chuska erg (Cather et al., 2008) were likely present, and it is unclear if there were any major rivers from the Colorado Plateau region reaching either the Pacific or Gulf of Mexico. Ancestral rivers continued to drain the east side of the Rockies to the Gulf of Mexico (Galloway et al., 2011). Rift flanks of the Rio Grande rift were rapidly unroofing ca. 20 Ma (Ricketts et al., 2016), and subsiding rift basins were internally drained with complex divides likely.

As shown in Figure 18B, based on combined U-Pb zircon and K-feldspar Pb isotopic provenance studies (Shulaker et al., 2019), rapidly evolving drainage patterns in the forearc region took place as North America interacted with the East Pacific rise and/or Mendocino fracture zone, the transform margin, inboard regions extended, and a gap in the subducting slab formed and widened eastwards (Dickinson and Snyder, 1979; Nicholson et al., 1994; Ingersoll and Rumelhart, 1999a, 1999b). These studies support several conclusions of our paper: that a drainage divide existed along the collapsing Nevadaplano-Mogollon highlands, and that the Sespe Formation and other forearc deposits tapped multiple cratonal basement catchments, including the Mojave Desert region, in addition to the predominance of arc-derived material. Drainage in the central Colorado Plateau was influenced by volcanic highlands and a paleo–Little Colorado river is proposed to have cut across the subdued Kaibab uplift at the foot of a northward-retreating paleo–Vermillion cliffs of the Grand Staircase of Mesozoic strata (Fig. 16B; Karlstrom et al., 2014, 2017; Winn, 2019). The Mogollon Rim and Mogollon Slope defined the south margin (Holm, 2001; Ott et al., 2018), while north-flowing paleorivers such as the paleo–Salt River were disrupted by normal faulting to form internal drainage (Potochnik, 2001).

The hypothesized west- and south-flowing 20 Ma Arizona River pathway in the Grand Canyon and northwestern Arizona regions (Sabbeth et al., 2019) is not supported here for several reasons. The 25–17 Ma Rainbow Gardens Formation and 34–19 Ma Buck and Doe Conglomerate were locally derived and deposited by north-flowing rivers, opposite to the proposed Arizona River drainage. The Buck and Doe Formation gravel on the Hualapai Plateau shows southerly source regions: lower units were derived mostly from the local Paleozoic sedimentary rocks; upper units (Peach Spring Member) tapped basement rocks (Young, 2011). Likewise, 20–18 Ma basalts and the Peach Spring Tuff flowed north onto the Colorado Plateau resulting in subdued topography and weakening of north-flowing drainage. Thick pyroclastic flows of Peach Spring

Tuff at 18.8 Ma directly crossed the proposed path of the Arizona River, extending as far west as Barstow, California, and eastward onto the SW Colorado Plateau (Fig. 12). The absence of both pre–1.8 Ga grains from Vishnu basement and the full range of 300–1100 Ma detrital zircon detritus in the Rainbow Gardens or Sespe formations, along the proposed Arizona River flow path, further preclude their derivation from Grand Canyon and the Colorado Plateau.

■ SUMMARY

The Shinumo Sandstone is not the "only plausible" source for a subset of lower Miocene Sespe Formation clasts that have moderate paleoinclination and the three regionally common detrital zircon peaks of ca. 1.8–1.6, 1.5–1.4, and 1.2–1.1 Ga, as portrayed by Sabbeth et al. (2019). Their extraordinary claim is that a 20 Ma paleoriver existed in the same place as the modern Colorado River, connected the Colorado Plateau to the Sespe delta, and carved Grand Canyon to within a few hundred meters of its modern depth. However, this claim is not supported by sufficient evidence to overturn the large body of geologic and thermochronologic evidence that such a pathway did not exist prior to 6 Ma (Young, 1999, 2001, 2011; Ingersoll et al., 2013; Karlstrom et al., 2014, 2017; Young and Crow, 2014; Crossey et al., 2015; Lamb et al., 2018). This paper questions the Shinumo-Sespe drainage connection by evaluating each data set. We show that the paleomagnetic inclination data from Sespe orthoquartzite clasts are ambiguous because the magnetization is not demonstrated to be primary, and measured inclinations are not demonstrated to be relative to horizontal bedding rather than cross bedding. Further, the large dispersion in measured clast paleoinclinations of 0°–78° cannot be convincingly related to the Shinumo Sandstone because of the small sample size and lack of characterization of other potential source terranes. Our analysis of the detrital zircon spectra of the 12 clasts reported from the Sespe Formation also causes us to reject the Arizona River hypothesis. No clast has its best statistical detrital zircon match to the Shinumo Sandstone. Rather, the best statistical matches for the four most "Shinumo-like" polymodal detrital zircon spectra of the Sespe clasts are Big Bear Group and Ontario Ridge quartzites of the Transverse Ranges, Horsethief Springs Sandstone from Death Valley, and Troy Quartzite of central Arizona. Three Sespe clasts with unimodal detrital zircon spectra are statistically most similar to White Ledges Formation of central Arizona and Pinto Mountain quartzites of the Transverse Ranges. Sespe clasts with grains younger than the Shinumo Sandstone can be tentatively matched to Cambrian Tapeats and/or Zabriskie sandstones and the Horsethief Springs Formation of Death Valley. Clasts with Mesozoic zircon do not match the Morrison Formation and hence do not provide convincing evidence for a drainage connection between the Colorado Plateau and the Sespe Formation. Instead, we find that Sespe clasts are statistically different from each other showing derivation from diverse sources in central Arizona, the Transverse Ranges, and the Death Valley region and/or equivalent then-exposed terranes in southern California and southwestern Arizona.

The 55 Ma "Arizona River," and the "old" Grand Canyon implied by it, are not supported by the Sabbeth et al. (2019) data, but the last sentence of the paper indicates that they still support an Arizona River in western Grand Canyon "perhaps as early as Late Cretaceous/Paleocene time." This notion of an "old" (70–50 Ma) Grand Canyon is falsified by several lines of evidence as summarized in this paper. Rivers of this age (Music Mountain Formation) were north-flowing, counter to the inferred 55 Ma drainage system proposed by Wernicke (2011, p. 1301). Thermochronology indicates that Marble Canyon and eastern Grand Canyon segments were >100 °C, buried beneath Mesozoic strata of the Grand Staircase, and hence not deeply incised at this time. Basement rocks of the westernmost Grand Canyon segment, as well as the area of Grand Wash trough (Fitzgerald and Malusà, 2019, p. 183), were 50–100 °C and buried by more than 1 km of Paleozoic and Mesozoic strata. The oldest detritus in the Eocene Sespe Formation of coastal California is 42 Ma (Ingersoll et al., 2018) and hence could not have been derived from Colorado Plateau or Grand Canyon sources via a 55 Ma paleoriver.

We also argue against the 20 Ma "Arizona River" hypothesis. The paleogeography of Oligocene and early Miocene time involved internally drained basins and north-flowing aggrading drainages opposite to the proposed throughgoing, south-flowing drainage system from the Colorado Plateau to the Sespe delta. The hypothesized "asymmetric drainage divide" is refuted by paleocurrent and provenance data from north-flowing 25–19 Ma fluvial systems on Hualapai Plateau. Fluvial deposits of the 25–17 Ma Rainbow Gardens Formation were part of an internally aggrading system with fluvial input from both the north and south (Beard, 1996; Lamb et al., 2018); the 34–19 Ma Buck and Doe Conglomerate also had northerly paleoflow and was an aggradational package with no evidence for a lower base level in a paleo–Grand Canyon (Young and Crow, 2014). Basement rocks of eastern Grand Canyon were >40–50 °C such that the floor of the East Kaibab paleocanyon (25–15 Ma; Karlstrom et al., 2014) was >600 m above the modern river level, in agreement with speleothem data (Polyak et al., 2008), and not likely carved to the depths of the Shinumo Sandstone that extends in a few places to 530 m above the river but is mainly <300 m above the river. Basement rocks of westernmost Grand Canyon were >50 °C, not carved to within a few hundred meters of their modern depth at 20 Ma to allow a Shinumo-Sespe drainage connection.

Instead, the hypothesis favored here is that downward integration of the Colorado River and carving of Grand Canyon took place after opening of the Gulf of California 6–5 Ma (Oskin and Stock, 2003; Pearthree and House, 2014; Dorsey et al., 2018; Kimbrough et al., 2015; Crossey et al., 2015; Crow et al., 2019a, 2019b), in part utilizing preserved older paleovalley segments across the Kaibab uplift and along the Hurricane fault (Karlstrom et al., 2014).

REFERENCES CITED

Amidon, W.H., Burbank, D.W., and Gehrels, G.E., 2005, U–Pb zircon ages as a sediment mixing tracer in the Nepal Himalaya: Earth and Planetary Science Letters, v. 235, p. 244–260.

Applegate, J.D., and Hodges, K.V., 1995, Mesozoic and Cenozoic extension recorded by metamorphic rocks in the Funeral Mountains, California: Geological Society of America Bulletin, v. 107, p. 1063–1076, https://doi.org/10.1130/0016-7606(1995)107<1063:MACERB>2.3.CO;2.

Atwater, T., and Stock, J., 1998, Pacific–North America plate tectonics of the Neogene southwestern United States: An update: International Geology Review, v. 40, no. 5, p. 375–402, https://doi.org/10.1080/00206819809465216.

Barth, A.P., Wooden, J.L., Coleman, D.S., and Fanning, C.M., 2000, Geochronology of the Proterozoic basement of southwestern most North America, and the origin and evolution of the Mojave crustal province: Tectonics, v. 19, p. 616–629, https://doi.org/10.1029/1999TC001145.

Barth, A.P., Wooden, J.L., Jacobson, C.E., and Probst, K., 2004, U-Pb geochronology and geochemistry of the McCoy Mountains Formation, southeastern California: A Cretaceous retroarc foreland basin: Geological Society of America Bulletin, v. 116, p. 142–153, https://doi.org/10.1130/B25288.1.

Barth, A.P., Wooden, J.L., Coleman, D.S., and Vogel, M.B., 2009, Assembling and disassembling California: A zircon and monazite geochronologic framework for Proterozoic crustal evolution in southern California: The Journal of Geology, v. 117, p. 221–239, https://doi.org/10.1086/597515.

Beard, L.S., 1996, Paleogeography of the Horse Spring Formation in relation to the Lake Mead fault system, Virgin Mountains, Nevada and Arizona, in Beratan, K.K., ed., Reconstructing the History of Basin and Range Extension Using Sedimentology and Stratigraphy: Geological Society of America Special Paper 303, p. 27–60, https://doi.org/10.1130/0-8137-2303-5.27.

Beard, L.S., and Faulds, J.E., 2011, Kingman Uplift, paleovalleys and extensional foundering in northwest Arizona, in Beard, L.S., Karlstrom, K.E., Young, R.A., and Billingsley, G.H., eds., 2011, CRevolution 2—Origin and Evolution of the Colorado River System, Workshop Abstracts: U.S. Geological Survey Open-File Report 2011-1210, p. 28–37.

Behl, R.J., 1999, The Miocene Monterey Formation of California revisited, in Moores, E.M., Sloan, D., and Stout, D.L., eds., Classic Cordilleran Concepts: A View from California: Geological Society of America Special Paper 338, p. 301–313, https://doi.org/10.1130/0-8137-2338-8.301.

Best, M.G., Christiansen, E.H., de Silva, S., and Lipman, P.W., 2016, Slab-rollback ignimbrite flareups in the southern Great Basin and other Cenozoic American arcs: A distinct style of arc volcanism: Geosphere, v. 12, p. 1097–1135, https://doi.org/10.1130/GES01285.1.

Blackwelder, E., 1934, Origin of the Colorado River: Geological Society of America Bulletin, v. 45, p. 551–566, https://doi.org/10.1130/GSAB-45-551.

Bloch, J.D., Timmons, J.M., Gehrels, G.E., Karlstrom, K.E., and Crossey, L.J., 2006, The Petrology of Mesoproterozoic Unkar Group shales and detrital zircon geochronology of interbedded sandstones, Grand Canyon Supergroup: Grenvillian influence on sedimentation of inboard Rodinia: Journal of Sedimentary Research, v. 76, https://doi.org/10.2110jsr.2006.107.

Bouse, R.M., Ruiz, J., Titley, S.R., Tosdal, R.M., and Wooden, J.L., 1999, Lead isotope compositions of Late Cretaceous and Early Tertiary igneous rocks and sulfide minerals in Arizona: Implications for the sources of plutons and metals in porphyry copper deposits: Economic Geology and the Bulletin of the Society of Economic Geologists, v. 94, p. 211–244, https://doi.org/10.2113/gsecongeo.94.2.211.

Brady, R., Wernicke, B., and Fryxell, J., 2000, Kinematic evolution of a large-offset continental normal fault system, South Virgin Mountains, Nevada: Geological Society of America Bulletin, v. 112, no. 9, p. 1375–1397, https://doi.org/10.1130/0016-7606(2000)112<1375:KEOALO>2.0.CO;2.

Braun, J., 2003, Pecube: A new finite-element code to solve the 3D heat transport equation including the effects of a time-varying, finite amplitude surface topography: Computers & Geosciences, v. 29, p. 787–794, https://doi.org/10.1016/S0098-3004(03)00052-9.

Burns, B.A., 1987, The sedimentology and significance of a middle Proterozoic braidplain: Chediski Sandstone Member of the Troy Quartzite, central Arizona [MS thesis]: Flagstaff, Northern Arizona University, 143 p.

Cadigan, R.A., 1967, Petrology of the Morrison Formation in the Colorado Plateau Region: U.S. Geological Survey Professional Paper 556, 113 p., https://doi.org/10.3133/pp556.

Cather, S.M., 2009, Stratigraphy and structure of the Laramide Carthage–La Joya Basin, central New Mexico, *in* Lucas, S.G., and Chamberlin, R.M., eds., Geology of the Chupadera Mesa, Lueth, Virgil: New Mexico Geological Society Guidebook, v. 60, p. 227–234.

Cather, S.M., Connell, S.D., Chamberlin, R.M., McIntosh, W.C., Jones, G.E., Potochnik, A.R., Lucas, S.G., and Johnson, P.S., 2008, The Chuska erg: Paleogeomorphic and paleoclimatic implications of an Oligocene sand sea on the Colorado Plateau: Geological Society of America Bulletin, v. 120, p. 13–33, https://doi.org/10.1130/B26081.1.

Cather, S.M., Chapin, C.E., and Kelley, S.A., 2011, Diachronous episodes of Cenozoic erosion in southwestern North America and their relationship to surface uplift, paleoclimate, paleodrainage, and paleoaltimetry: Geosphere, v. 8, p. 1177–1206, https://doi.org/10.1130/GES00801.1.

Chapman, J.B., Dafov, M.N., Gehrels, G., Ducea, M.N., Valley, J.W., and Ishida, A., 2018, Lithospheric architecture and tectonic evolution of the southwestern U.S. Cordillera: Constraints from zircon Hf and O isotopic data: Geological Society of America Bulletin, v. 130, p. 2031–2046, https://doi.org/10.1130/B31937.1.

Cohen, J., 1977, Statistical Power Analysis for the Behavioral Sciences: New York, Academic Press, 490 p.

Cox, R., Martin, M.W., Comstock, J.C., Dickerson, L.S., Ekstrom, I.L., and Sammons, J.H., 2002, Sedimentology, stratigraphy, and geochronology of the Proterozoic Mazatzal Group, central Arizona: Geological Society of America Bulletin, v. 114, p. 1535–1549, https://doi.org/10.1130/0016-7606(2002)114<1535:SSAGOT>2.0.CO;2.

Crossey, L.C., Karlstrom, K.E., Dorsey, R., Pearce, J., Wan, E., Beard, L.S., Asmerom, Y., Polyak, V., Crow, R.S., Cohen, A., Bright, J., and Pecha, M.E., 2015, The importance of groundwater in propagating downward integration of the 6–5 Ma Colorado River System: Geochemistry of springs, travertines and lacustrine carbonates of the Grand Canyon region over the past 12 million years: Geosphere, v. 11, no. 3, p. 660–682, https://doi.org/10.1130/GES01073.1.

Crow, R., Karlstrom, K., Asmerom, Y., Schamndt, B., Polyak, V., and DuFrane, S.A., 2011, Shrinking of the Colorado Plateau via lithospheric mantle erosion: Evidence from Nd and Sr isotopes and geochronology of Neogene basalts: Geology, v. 39, p. 27–30, https://doi.org/10.1130/G31611.1.

Crow, R., Schwing, J., Karlstrom, K.E., Heizler, M., Pearthree, P.A., Houses, P.K., Dulin, S., Stelten, M., and Crossey, L., 2019a, Redefining the age of the Colorado River: Geological Society of America Abstracts with Programs, v. 51, no. 5, https://doi.org/10.1130/abs/2019AM-339026.

Crow, R.S., Howard, K.A., Beard, L.S., Pearthree, P.A., House, P.K., Karlstrom, K.E., Peters, L., McIntosh, W., Cassidy, C., Felger, T.J., and Block, D., 2019b, Insights into post-Miocene uplift of the western margin of the Colorado Plateau from the stratigraphic record of the lower Colorado River: Geosphere, v. 15, no. 6, p. 1826–1845, https://doi.org/10.1130/GES02020.1.

Daneker, T.M., 1975, Sedimentology of the Precambrian Shinumo Sandstone, Grand Canyon, Arizona [MS thesis]: Flagstaff, Northern Arizona University, 195 p.

Davis, S.J., Dickinson, W.R., Gehrels, G.E., Spencer, J.E., Lawton, T.F., and Carroll, A.R., 2010, The Paleogene California River: Evidence of Mojave-Uinta paleodrainage from U-Pb ages of detrital zircons: Geology, v. 38, p. 931–934, https://doi.org/10.1130/G31250.1.

DeCelles, P., 2004, Late Jurassic to Eocene evolution of the Cordilleran thrust belt and foreland basin system, western U.S.A.: American Journal of Science, v. 304, p. 105–168, https://doi.org/10.2475/ajs.304.2.105.

Dehler, C., Gehrels, G., Porter, S., Heizler, M., Karlstrom, K.E., Cox, G., Crossey, L.C., and Timmons, J.M., 2017, Synthesis of the 780–740 Ma Chuar, Uinta Mountain, and Pahrump groups (ChUMP), western USA: Implications for Laurentia-wide cratonic marine basins: Geological Society of America Bulletin, v. 129, p. 607–624, https://doi.org/10.1130/B31532.1.

Dickinson, W.R., 1996, Kinematics of Transrotational Tectonism in the California Transverse Ranges and Its Contribution to Cumulative Slip along the San Andreas Transform Fault: Geological Society of America Special Paper 305, 46 p., https://doi.org/10.1130/0-8137-2305-1.1.

Dickinson, W.R., 2006, Geotectonic evolution of the Great Basin: Geosphere, v. 2, p. 353–368, https://doi.org/10.1130/GES 00054.1.

Dickinson, W.R., 2013, Rejection of the lake spillover model for initial incision of the Grand Canyon, and discussion of alternatives: Geosphere, v. 9, p. 1–20, https://doi.org/10.1130/GES00839.1.

Dickinson, W.R., 2018, Tectonosedimentary Relations of Pennsylvanian to Jurassic Strata on the Colorado Plateau: Geological Society of America Special Paper 553, 184 p., https://doi.org/10.1130/SPE533.

Dickinson, W.R., and Gehrels, G.E., 2003, U-Pb ages of detrital zircons from Permian and Jurassic eolian sandstones of the Colorado Plateau, USA: Paleogeographic implications: Sedimentary Geology, v. 163, p. 29–66, https://doi.org/10.1016/S0037-0738(03)00158-1.

Dickinson, W.R., and Gehrels, G.E., 2008a, Sediment delivery to the Cordilleran foreland basin: Insights from U-Pb ages of detrital zircons in Upper Jurassic and Cretaceous strata of the Colorado Plateau: American Journal of Science, v. 308, p. 1041–1082, https://doi.org/10.2475/10.2008.01.

Dickinson, W.R., and Gehrels, G.E., 2008b, U-Pb ages of detrital zircons in relation to paleogeography: Triassic paleodrainage networks and sediment dispersal across Southwest Laurentia: Journal of Sedimentary Research, v. 78, p. 745–764, https://doi.org/10.2110/jsr.2008.088.

Dickinson, W.R., and Gehrels, G.E., 2009, U-Pb ages of detrital zircons in Jurassic eolian and associated sandstones of the Colorado Plateau: Evidence for transcontinental dispersal and intraregional recycling of sediment: Geological Society of America Bulletin, v. 121, p. 408–433, https://doi.org/10.1130/B26406.1.

Dickinson, W.R., and Snyder, W.S., 1979, Geometry of subducted slabs related to San Andreas transform: The Journal of Geology, v. 87, p. 609–627, https://doi.org/10.1086/628456.

Dickinson, W.R., Lawton, T.F., Pecha, M., Davis, S.J., Gehrels, G.E., and Young, R.A., 2012, Provenance of the Paleogene Colton Formation (Uinta Basin) and Cretaceous–Paleogene provenance evolution in the Utah foreland: Evidence from U-Pb ages of detrital zircons, paleocurrent trends, and sandstone petrofacies: Geosphere, v. 8, p. 854–880, https://doi.org/10.1130/GES00763.1.

Doe, M.F., Jones, J.V., III, Karlstrom, K.E., Thrane, K., Frei, D., Gehrels, G., and Pecha, M., 2012, Basin formation near the end of the 1.6–1.45 Ga tectonic gap in southern Laurentia: Mesoproterozoic Hess Canyon Group of Arizona and implications for 1.5 Ga supercontinent configurations: Lithosphere, v. 4, p. 77–88, https://doi.org/10.1130/L160.1.

Doe, M.F., Jones, J.V., III, Karlstrom, K.E., Dixon, B., Gehrels, G., and Pecham, M., 2013, Using detrital zircon ages and Hf isotopes to identify 1.48–1.45 Ga sedimentary basins and fingerprint sources of exotic 1.6–1.5 Ga grains in southwestern Laurentia: Precambrian Research, v. 231, p. 409–421, https://doi.org/10.1016/j.precamres.2013.03.002.

Donadini, F., Pesonen, L.J., Korhonen, K., Deutsch, A., and Harlan, S.S., 2011, Paleomagnetism and paleointensity of the 1.1 Ga old diabase sheets from central Arizona: Geophysica, v. 47, p. 3–30.

Dorsey, R.J., O'Connell, B., McDougall, K., and Homan, M.B., 2018, Punctuated sediment discharge during early Pliocene birth of the Colorado River: Evidence from regional stratigraphy, sedimentology, and paleontology: Sedimentary Geology, v. 363, p. 1–33, https://doi.org/10.1016/j.sedgeo.2017.09.018.

Dumitru, T.A., Gans, P.B., Foster, D.A., and Miller, E.L., 1991, Refrigeration of the western Cordilleran lithosphere during Laramide shallow-angle subduction: Geology, v. 19, p. 1145–1148, https://doi.org/10.1130/0091-7613(1991)019<1145:ROTWCL>2.3.CO;2.

Elston, D.P., and Bressler, S.L., 1977, Paleomagnetic poles and polarity zonation from Cambrian and Devonian strata of Arizona: Earth and Planetary Science Letters, v. 36, p. 423–433, https://doi.org/10.1016/0012-821X(77)90067-X.

Elston, D.P., and Grommé, C.S., 1994, Middle Proterozoic magnetostratigraphic polar path and polarity zonation from Grand Canyon, Northern Arizona: unpublished manuscript prepared for U.S. Geological Survey Bulletin, Menlo Park, 69 p.

Elston, D.P., Link, P.K., Winston, D., Horodyski, R.J., and Reed, J.C., 1993, Correlations of Middle and Late Proterozoic successions, *in* Reed, J.C., Jr., et al., eds., Precambrian: Conterminous U.S.: Boulder, Colorado, Geological Society of America, Geology of North America, C-2, p. 468–487.

Elston, D.P., Enkin, R.J., Baker, J., and Kisilevsky, D.K., 2002, Tightening the Belt: Paleomagnetic-stratigraphic constraints on deposition, correlation, and deformation of the Middle Proterozoic (ca. 1.4 Ga) Belt-Purcell Supergroup, United States and Canada: Geological Society of America Bulletin, v. 114, p. 619–638, https://doi.org/10.1130/0016-7606(2002)114<0619:TTBPSC>2.0.CO;2.

Eyster, A.E., Weiss, B.P., Karlstrom, K.E., Kremers, J.K., and Macdonald, F.A., 2020, Paleomagnetism of the Chuar Group and evaluation of the 780–720 Ma apparent polar wander path of Laurentia with implications for the makeup and breakup of Rodinia: Geological Society of America Bulletin, v. 132, p. 710–738, https://doi.org/10.1130/B32012.1.

Farmer, G.L., Bowring, S.A., Matzel, J., Espinosa Maldonado, G., Fedo, C., and Wooden, J., 2005, Paleoproterozoic Mojave province in northwestern Mexico?: Isotopic and U-Pb zircon geochronologic studies of Precambrian and Cambrian crystalline and sedimentary rocks, Caborca, Sonora, *in* Anderson, T.H., ed., The Mojave-Sonora Megashear Hypothesis: Development, Assessment, and Alternatives: Geological Society of America Special Paper 393, p. 183–198, https://doi.org/10.1130/0-8137-2393-0.183.

Faulds, J.E., Feuerbach, D.L., Miller, C.F., and Smith, E.I., 2001, Cenozoic evolution of the northern Colorado River extensional corridor, southern Nevada and northwest Arizona, *in* Erskine, M.C., Faulds, J.E., Bartley, J.M., and Rowely, P.D., eds., The Geologic Transition, High Plateaus to Great Basin, the Mackin Symposium: Pacific Section of the American Association of Petroleum Geologists Publication GB 78 (also Utah Geological Association Publication 30), p. 239–272.

Fitzgerald, P.G., and Malusà, M.G., 2019, Concept of the exhumed partial annealing (retention) zone and age-elevation profiles in thermochronology, *in* Malusà, M.G., and Fitzgerald, P.G., eds., Fission-Track Thermochronology and Its Application to Geology: Springer International Publishing, p. 165–189, https://doi.org/10.1007/978-3-319-89421-8_9.

Flowers, R.M., and Farley, K.A., 2012, Apatite ⁴He/³He and (U-Th)/He evidence for an ancient Grand Canyon: Science, v. 338, p. 1616–1619, https://doi.org/10.1126/science.1229390.

Flowers, R.M., and Farley, K.A., 2013, Response to comments on "Apatite ⁴He/³He and (U-Th)/He evidence for an ancient Grand Canyon: Science, v. 340, p. 143, https://doi.org/10.1126/science.1234203.

Flowers, R.M., Wernicke, B.P., and Farley, K.A., 2008, Unroofing, incision, and uplift history of the southwestern Colorado Plateau from apatite (U-Th)/He thermochronology: Geological Society of America Bulletin, v. 120, p. 571–587, https://doi.org/10.1130/B26231.1.

Flowers, R.M., Ketcham, R.A., Shuster, D.L., and Farley, K.A., 2009, Apatite (U Th)/He thermochronometry using a radiation damage accumulation and annealing model: Geochimica Cosmochimica Acta v. 73, p. 2347–2365.

Fox, M., and Shuster, D., 2014, The influence of burial heating on the (U-Th)/He system in apatite: Grand Canyon case study: Earth and Planetary Science Letters, v. 397, p. 174–183, https://doi.org/10.1016/j.epsl.2014.04.041.

Fox, M., Tripathy-Langa, A., Shuster, D.L., Winn, C., Karlstrom, K.E., and Kelley, S., 2017, Westernmost Grand Canyon incision: Testing thermochronometric resolution: Earth and Planetary Science Letters, v. 474, p. 248–256, https://doi.org/10.1016/j.epsl.2017.06.049.

Galloway, W.E., Whiteaker, T.L., and Ganey-Curry, P., 2011, History of Cenozoic North American drainage basin evolution, sediment yield, and accumulation in the Gulf of Mexico basin: Geosphere, v. 7, p. 938–973, https://doi.org/10.1130/GES00647.1.

Gehrels, G., and Pecha, M., 2014, Detrital zircon U-Pb geochronology and Hf isotope geochemistry of Paleozoic and Triassic passive margin strata of western North America: Geosphere, v. 10, p. 49–65, https://doi.org/10.1130/GES00889.1.

Gehrels, G., Valencia, V., and Pullen, A., 2006, Detrital zircon geochronology by laser-ablation multicollector ICPMS at the Arizona LaserChron Center: The Paleontological Society Papers, v. 12, p. 67–76, https://doi.org/10.1017/S1089332600001352.

Gehrels, G.E., Valencia, V.A., and Ruiz, J., 2008, Enhanced precision, accuracy, efficiency, and spatial resolution of U-Pb ages by laser ablation–multicollector–inductively coupled plasma–mass spectrometry: Geochemistry, Geophysics, Geosystems, v. 9, p. 1–13, https://doi.org/10.1029/2007GC001805.

Gehrels, G.E., Blakey, R., Karlstrom, K., Timmons, M., Kelley, S., Dickinson, W.R., and Pecha, M., 2011, Detrital zircon U-Pb geochronology of Paleozoic strata in the Grand Canyon: Lithosphere, v. 3, p. 183–200, https://doi.org/10.1130/L121.1.

Goldstrand, P.M., 1994, Tectonic development of Upper Cretaceous to Eocene strata of Southwest Utah: Geological Society of America Bulletin, v. 106, p. 145–154, https://doi.org/10.1130/0016-7606(1994)106<0145:TDOUCT>2.3.CO;2.

Hamilton, W., 1987, Mesozoic geology and tectonics of the Big Maria Mountains region, southeastern California, *in* Dickinson, W.R., and Klute, M.A., eds., Mesozoic Rocks of Southern Arizona and Adjacent Areas: Arizona Geological Society Digest, v. 18, p. 33–47.

Helsley, C.E., and Spall, H., 1972, Paleomagnetism of 1140 to 1150 million-year diabase sills from Gila County, Arizona: Journal of Geophysical Research, v. 77, p. 2115–2128, https://doi.org/10.1029/JB077i011p02115.

Hereford, R., 1977, Deposition of the Tapeats Sandstone (Cambrian) in central Arizona: Geological Society of America Bulletin, v. 88, p. 199–211, https://doi.org/10.1130/0016-7606(1977)88<199:DOTTSC>2.0.CO;2.

Hill, C.A., Polyak, V.J., Asmeroim, Y., and Proviencio, P.P., 2016, Constraints on a Late Cretaceous uplift, denudation, and incision of the Grand Canyon region, southwestern Colorado Plateau, USA, from U-Pb dating of lacustrine limestone: Tectonics, v. 35, p. 896–906, https://doi.org/10.1002/2016TC004166.

Hillhouse, J.W., 2010, Clockwise rotation and implications for northward drift of the western Transverse Ranges from paleomagnetism of the Piuma Member, Sespe Formation, near Malibu, California: Geochemistry, Geophysics, Geosystems, v. 11, https://doi.org/10.1029/2010GC003047.

Holland, M.E., Karlstrom, K.E., Doe, M.F, Gehrels, G.E., Pecha, M., Shufeldt, O.P., Begg, G., Griffin, W.L., and Belousova, E., 2015, An imbricate midcrustal suture zone: The Mojave-Yavapai Province boundary in Grand Canyon, Arizona: Geological Society of America Bulletin, v. 127, p. 1391–1410, https://doi.org/10.1130/B31232.1.

Holland, M.E., Karlstrom, K.E., Gehrels, G., Shufeldt, O.P., Begg, G., Griffin, W., and Belousova, E., 2018, The Paleoproterozoic Vishnu basin in southwestern Laurentia: Implications for supercontinent reconstructions, crustal growth, and the origin of the Mojave crustal province: Precambrian Research, v. 308, https://doi.org/10.1016/j.precamres.2018.02.001.

Holm, R.F., 2001, Cenozoic paleogeography of the central Mogollon Rim–southern Colorado Plateau region, Arizona, revealed by Tertiary gravel deposits, Oligocene to Pleistocene lava flows, and incised streams: Geological Society of America Bulletin, v. 113, p. 1467–1485, https://doi.org/10.1130/0016-7606(2001)113<1467:CPOTCM>2.0.CO;2.

Howard, J.L., 1987, Paleoenvironments, Provenance and Tectonic Implications of the Sespe Formation, Southern California [Ph.D. thesis]: Santa Barbara, California, University of California, 306 p.

Howard, J.L., 1995, Conglomerates of the Upper Middle Eocene to Lower Miocene Sespe Formation along the Santa Ynez fault—Implications for the Geologic History of the Eastern Santa Maria Basin Area, California: U.S. Geological Survey Bulletin 1995H, 37 p.

Howard, J.L., 1996, Paleocene to Holocene paleodeltas of ancestral Colorado River offset by the San Andreas fault system, southern California: Geology, v. 24, no. 9, p. 783–786, https://doi.org/10.1130/0091-7613(1996)024<0783:PTHPOA>2.3.CO;2.

Howard, J.L., 2000, Provenance of quartzite clasts in the Eocene–Oligocene Sespe Formation: Paleogeographic implications for southern California and the ancestral Colorado River: Geological Society of America Bulletin, v. 112, p. 1635–1649, https://doi.org/10.1130/0016-7606(2000)112<1635:POQCIT>2.0.CO;2.

Hunt, C.B., 1956, Cenozoic geology of the Colorado Plateau: U.S. Geological Survey Professional Paper 279, 99 p.

Ingersoll, R.V., and Rumelhart, P.E., 1999a, Three-stage evolution of the Los Angeles Basin, southern California: Geology, v. 27, p. 593–596, https://doi.org/10.1130/0091-7613(1999)027<0593:TSEOTL>2.3.CO;2.

Ingersoll, R.V., and Rumelhart, P.E., 1999b, Correction: Three-stage evolution of the Los Angeles Basin, southern California: Geology, v. 27, p. 864, https://doi.org/10.1130/0091-7613(1999)027%3C0864:C%3E2.3.CO;2.

Ingersoll, R.V., Grove, M., Jacobson, C.E., Kimbrough, D.L., and Hoyt, J.F., 2013, Detrital zircons indicate no drainage link between southern California rivers and the Colorado Plateau from mid-Cretaceous through Pliocene: Geology, v. 41, p. 311–314, https://doi.org/10.1130/G33807.1.

Ingersoll, R.V., Spafford, C.D., Jacobson, C.E., Grove, M., Howard, J.L., Hourigan, J., and Pedrick, J., 2018, Provenance, paleogeography and paleotectonic implications of the mid-Cenozoic Sespe Formation, coastal southern California, USA, *in* Ingersoll, R.V., Lawton, T.F., and Graham, S.A., eds., Tectonics, Sedimentary Basins, and Provenance: A Celebration of the Career of William R. Dickinson: Geological Society of America Special Paper 540, p. 441–462, https://doi.org/10.1130/2018.2540(20).

Jacobson, C.E., Grove, M., Vućić, A., Pedrick, J.N., and Ebert, K.A., 2007, Exhumation of the Orocopia Schist and associated rocks of southeastern California: Relative roles of erosion, synsubduc-tion tectonic denudation, and middle Cenozoic extension, *in* Cloos, M., et al., eds., Convergent Margin Terranes and Associated Regions: A Tribute to W.G. Ernst: Geological Society of America Special Paper 419, p. 1–37, https://doi.org/10.1130/2007.2419(01).

Jacobson, C.E., Grove, M., Pedrick, J.N., Barth, A.P., Marsaglia, K.M., Gehrels, G.E., and Nourse, J.A., 2011, Late Cretaceous–early Cenozoic tectonic evolution of the southern California margin inferred from provenance of trench and forearc sediments: Geological Society of America Bulletin, v. 123, p. 485–506, https://doi.org/10.1130/B30238.1.

Kapp, J., Miller, C.F., and Miller, J.S., 2002, Ireteba Pluton, Eldorado Mountains, Nevada: Late, deep-source, peraluminous magmatism in the Cordilleran interior: The Journal of Geology, v. 110, p. 649–669, https://doi.org/10.1086/342864.

Karlstrom, K.E., Crow, R, Crossey, L.J., Coblentz, D., and van Wijk, J., 2008, Model for tectonically driven incision of the less than 6 Ma Grand Canyon: Geology, v. 36, p. 835–838, https://doi.org/10.1130/G25032A.1.

Karlstrom, K.E., Coblentz, D., Dueker, K., Ouimet, W., Kirby, E., Van Wijk, J., Schmandt, B., Kelley, S., Lazear, G., Crossey, L.J., Crow, R., Aslan, A, Darling, A., Aster, R., MacCarthy, J., Hansen, S.M., Stachnik, J., Stockli, D.F., Hoffman, M., McKeon, R., Feldman, J., Heizler, M., Donahue, M.S., and the CREST working group, 2011, Surface response to mantle convection beneath the Colorado Rocky Mountains and Colorado Plateau: Lithosphere, v. 4, p. 3–22, https://doi.org/10.1130/L150.1.

Karlstrom, K.E., Lee, J., Kelley, S., Crow, R., Crossey, L.J., Young, R., Lazear, G., Beard, L.S., Ricketts, J., Fox, M., and Shuster, D., 2014, Formation of the Grand Canyon 5 to 6 million years ago through integration of older palaeocanyons: Nature Geoscience, v. 7, p. 239–244, https://doi.org/10.1038/ngeo2065.

Karlstrom, K.E., Crossey, L.J., Embid, E., Crow, R., Heizler, M., Hereford, R., Beard, L.S., Ricketts, J.W., Cather, S., and Kelley, S., 2017, Cenozoic incision history of the Little Colorado River: its role in carving Grand Canyon and onset of rapid incision in the last ~2 Ma in the Colorado River System: Geosphere, v. 13, no. 1, p. 49–81, https://doi.org/10.1130/GES01304.1.

Karlstrom, K.E., Hagadorn, J., Gehrels, G.G., Mathews, W., Schmitz, M., Madronich, L., Mulder, J., Pecha, M., Geisler, D., and Crossey, L.J., 2018, Cambrian Sauk transgression in the Grand Canyon region redefined by detrital zircons: Nature Geoscience, v. 11, p. 438–443, https://doi.org/10.1038/s41561-018-0131-7.

Kelley, S.A., Chapin, C.E., and Karlstrom, K.E., 2001, Laramide cooling histories of Grand Canyon, Arizona, and the Front Range, Colorado, determined from apatite fission-track thermochronology, *in* Young, R.A., and Spamer, E.E., eds., Colorado River Origin and Evolution: Grand Canyon Association, p. 37–42.

Ketcham, R.A., 2005, Forward and inverse modeling of low-temperature thermochronometry data: Reviews in Mineralogy and Geochemistry, v. 58, p. 275–314, https://doi.org/10.2138/rmg.2005.58.11.

Kimbrough, D.L., Grove, M., Gehrels, G.E., Dorsey, R.J., Howard, K.A., Lovera, O., Aslan, A., House, P.K., and Pearthree, P.A., 2015, Detrital zircon U-Pb provenance of the Colorado River: A 5 m.y. record of incision into cover strata overlying the Colorado Plateau and adjacent regions: Geosphere, v. 11, p. 1719–1748, https://doi.org/10.1130/GES00982.1.

Kuiper, N.H., 1960, Tests concerning random points on a circle, *in* Proceedings van de Koninklijke Nederlandse Akademie van Wetenschappen: v. 63, no. 1, p. 38-47.

Labotka, T.C., 1980, Petrology of a medium-pressure regional metamorphic terrane, Funeral Mountains, California: The American Mineralogist, v. 65, p. 670–689.

Lamb, M.A., Beard, L.S., Dragos, M., Hanson, A.D., Hickson, T.A., Sitton, M., Umhoefer, P.J., Karlstrom, K.E., Dunbar, N., and McIntosh, W., 2018, Provenance and paleogeography of the 25–17 Ma Rainbow Gardens Formation: Evidence for tectonic activity at ca. 19 Ma and internal drainage rather than throughgoing paleorivers on the southwestern Colorado Plateau: Geosphere, v. 14, p. 1592–1617, https://doi.org/10.1130/GES01127.1.

Lang, J., and Titley, S., 1998, Isotopic and geochemical characteristics of Laramide magmatic systems in Arizona and implications for the genesis of porphyry copper deposits: Economic Geology and the Bulletin of the Society of Economic Geologists, v. 93, p. 138–170, https://doi.org/10.2113/gsecongeo.93.2.138.

Lawton, T.F., 2019, Laramide Sedimentary Basins and Sediment-Dispersal Systems, *in* Miall, A.D., ed., The Sedimentary Basins of the United States and Canada (second edition): Amsterdam, Elsevier, p. 529–557, https://doi.org/10.1016/B978-0-444-63895-3.00013-9.

Lee, J.P., Stockli, D.F., Kelley, S.A., Pederson, J.L., Karlstrom, K.E., and Ehlers, T.A., 2013, New Thermochronometric Constraints on the Tertiary Landscape Evolution of Central and Eastern Grand Canyon, Arizona: Geosphere, v. 9, no. 2, p. 216–228, https://doi.org/10.1130/GES00842.1.

Longwell, C.R., 1946, How old is the Colorado River?: American Journal of Science, v. 244, p. 817–835, https://doi.org/10.2475/ajs.244.12.817.

Lucchitta, I., 1966, Cenozoic geology of the Lake Mead area adjacent to the Grand Wash Cliffs [Ph.D. dissertation]: College Station, Pennsylvania State University, 218 p.

Lucchitta, I., 1972, Early history of the Colorado River in the Basin and Range Province: Geological Society of America Bulletin, v. 83, p. 1933–1948, https://doi.org/10.1130/0016-7606(1972)83[1933:EHOTCR]2.0.CO;2.

Lucchitta, I., 2013, Comment on apatite ⁴He-³He and (U-Th)/He evidence for an ancient Grand Canyon: Science, v. 340, p. 143, https://doi.org/10.1126/science.1234567.

Mackey, G.N., Horton, B.K., and Milliken, K.L., 2012, Provenance of the Paleocene–Eocene Wilcox Group, western Gulf of Mexico basin: Evidence for integrated drainage of the southern Laramide Rocky Mountains and Cordilleran arc: Geological Society of America Bulletin, v. 124, p. 1007–1024, https://doi.org/10.1130/B30458.1.

Mahon, R.C., Dehler, C.M., Link, P.K., Karlstrom, K.E., and Gehrels, G.E., 2014a, Geochronologic and stratigraphic constraints on the Mesoproterozoic and Neoproterozoic Pahrump Group, Death Valley, California: A record of the assembly, stability, and breakup of Rodinia: Geological Society of America Bulletin, v. 126, no. 5–6, p. 652–664, https://doi.org/10.1130/B30956.1.

Mahon, R.C., Dehler, C.M., Link, P.K., Karlstrom, K.E., and Gehrels, G.E., 2014b, Detrital zircon provenance and paleogeography of the Pahrump Group and overlying strata, Death Valley, California: Precambrian Research, v. 251, p. 102–117, https://doi.org/10.1016/j.precamres.2014.06.005.

Mako, C.A., Williams, M.L., Karlstrom, K.E., Doe, M.F., Powicki, D., Holland, M.E., Gehrels, G.E., and Pecha, M., 2015, Polyphase Proterozoic deformation in the Four Peaks area, central Arizona, and relevance for the Mazatzal orogeny: Geosphere, v. 11, p. 1975–1995, https://doi.org/10.1130/GES01196.1.

Massey, F.J., Jr., 1951, The Kolmogorov-Smirnov test for goodness of fit: Journal of the American Statistical Association, v. 46, p. 68–78.

Matthews, W., Guest, B., and Madronich, L., 2018, Latest Neoproterozoic to Cambrian detrital zircon facies of western Laurentia: Geosphere, v. 14, p. 243–264, https://doi.org/10.1130/GES01544.1.

Mauel, D.J., Lawton, T.F., González-León, C.M., Iriondo, A., and Amato, J.M., 2011, Stratigraphy and age of Upper Jurassic strata in north-central Sonora, Mexico: Southwestern Laurentian record of crustal extension and tectonic transition: Geosphere, v. 7, p. 390–414, https://doi.org/10.1130/GES00600.1.

McKee, E.D., and Resser, C.E., 1945, Cambrian History of the Grand Canyon Region: Washington, D.C., Carnegie Institute Publications, v. 563, 232 p.

McKee, E.D., Wilson, R.F., Breed, W.J., and Breed, C.S., eds., 1967, Evolution of the Colorado River in Arizona: Museum of Northern Arizona Bulletin 44, 67 p.

McQuarrie, N., and Wernicke, B.P., 2005, An animated tectonic reconstruction of southwestern North America since 36 Ma: Geosphere, v. 1, p. 147–172, https://doi.org/10.1130/GES00016.1.

Miller, C.F., D'Andrea, J.L., Ayers, J.C., Coath, C.D., and Harrison, T.M., 1997, BSE imaging and ion probe geochronology of zircon and monazite from plutons of the Eldorado and Newberry Mountains, Nevada—Age, inheritance, and subsolidus modification: Eos (Transactions. American Geophysical Union), v. 78, p. F783.

Mulder, J.A., Karlstrom, K.E., Fletcher, K., Heizler, M.T., Timmons, J.M., Crossey, L.J., Gehrels, G.E., and Pecha, M., 2017, The syn-orogenic sedimentary record of the Grenville Orogeny in southwest Laurentia: Precambrian Research, v. 294, p. 33–52, https://doi.org/10.1016/j.precamres.2017.03.006.

Mulder, J.A., Karlstrom, K.E., Halpin, J.A., Spencer, C.J., Berry, R.F., Merdith, A.S., Gehrels, G.E., Pecha, M., and McDonald, B., 2018, Rodinian devil in disguise: Correlation of 1.25−1.10 Ga strata between Tasmania and Grand Canyon refines Rodinia: Geology, v. 46, p. 991–994, https://doi.org/10.1130/G45225.1.

Nicholson, C., Sorlien, C.C., Atwater, T., Crowell, J.C., and Luyendyk, B.P., 1994, Microplate capture, rotation of the western Transverse Ranges, and initiation of the San Andreas transform as a low-angle fault system: Geology, v. 22, p. 491–495, https://doi.org/10.1130/0091-7613(1994)022<0491:MCROTW>2.3.CO;2.

Oskin, M., and Stock, J., 2003, Pacific–North America plate motion and opening of the Upper Delfín basin, northern Gulf of California, Mexico: Geological Society of America Bulletin, v. 115, p. 1173–1190, https://doi.org/10.1130/B25154.1.

Ott, R.F., Whipple, K.X., and van Soest, M., 2018, Incision history of the Verde Valley region and implications for uplift of the Colorado Plateau (central Arizona): Geosphere, v. 14, no. 4, p. 1690–1709, https://doi.org/10.1130/GES01640.1.

Pearthree, P.A., and House, P.K., 2014, Paleogeomorphology and evolution of the early Colorado River inferred from relationships in Mohave and Cottonwood valleys, Arizona, California, and Nevada: Geosphere, v. 10, p. 1139–1160, https://doi.org/10.1130/GES00988.1.

Peryam, T.C., Lawton, T.F., Amato, J.M., González León, C.M., and Mauel, D.J., 2012, Lower Cretaceous strata of the Sonora Bisbee Basin: A record of the tectonomagmatic evolution of northwestern Mexico: Geological Society of America Bulletin, v. 124, p. 532–548, https://doi.org/10.1130/B30456.1.

Polyak, V.J., Hill, C.A., and Asmerom, Y., 2008, Age and evolution of the Grand Canyon revealed by U-Pb dating of water table-type speleothems: Science, v. 319, p. 1377–1380, https://doi.org/10.1126/science.1151248.

Potochnik, A.R., 2001, Paleogeomorphic evolution of the Salt River region: Implications for Cretaceous-Laramide inheritance for ancestral Colorado River drainage, *in* Young, R.A., and Spamer, E.E., eds., Colorado River Origin and Evolution: Grand Canyon Association, p. 17–24.

Pullen, A., Ibáñez-Mejía, M., Gehrels, G.E., Ibáñez-Mejía, J.C., and Pecha, M., 2014, What happens when n = 1000? Creating large-n geochronological datasets with LA-ICP-MS for geologic investigations: Journal of Analytical Atomic Spectrometry, v. 29, p. 971–980.

Reis, J.H., 2009, Jurassic and Cretaceous Tectonic Evolution of the Southeast Castle Dome Mountains, Southwest Arizona [MS thesis]: Ames, Iowa State University, 106 p.

Ricketts, J.W., Kelley, S., Karlstrom, K.E., Schmandt, B., Donahue, M., and van Wijk, J., 2016, Synchronous opening of the Rio Grande rift along its entire length at 25–10 Ma supported by apatite (U-Th)/He and fission-track thermochronology, and evaluation of possible driving mechanisms: Geological Society of America Bulletin, v. 128, p. 397–424, https://doi.org/10.1130/B31223.1.

Rose, E.C., 2011, Modification of the nomenclature and a revised depositional model for the Cambrian Tonto Group of the Grand Canyon, Arizona, *in* Hollingsworth, J.S., Sundberg, F.A., and Foster, J.R., eds., Cambrian Stratigraphy and Paleontology of Northern Arizona and Southern Nevada: Museum of Northern Arizona Bulletin, p. 77–98.

Sabbeth, L., Wernicke, B.P., Raub, T.D., Grover, J.A., Lander, E.B., and Kirschvink, J.L., 2019, Grand Canyon provenance for orthoquartzite clasts in the lower Miocene of coastal southern California: Geosphere, v. 15, p. 1973–1998, https://doi.org/10.1130/GES02111.1.

Saleeby, J., 2003, Segmentation of the Laramide Slab—Evidence from the southern Sierra Nevada region: Geological Society of America Bulletin, v. 115, p. 655–668, https://doi.org/10.1130/0016-7606(2003)115<0655:SOTLSF>2.0.CO;2.

Salem, A.C., 2009, Mesozoic Tectonics of the Maria Fold and Thrust Belt and McCoy Basin, Southeastern California: An Examination of Polyphase Deformation and Synorogenic Response [Ph.D. thesis]: Albuquerque, University of New Mexico, 284 p.

Satkoski, A.M., Wilkinson, B.H., Hietpas, J., and Samson, S.D., 2013, Likeness among detrital zircon populations—An approach to the comparison of age frequency data in time and space: Geological Society of America Bulletin, v. 125, p. 1783–1799, https://doi.org/10.1130/B30888.1.

Saylor, J.E., and Sundell, K.E., 2016, Quantifying comparison of large detrital geochronology data sets: Geosphere, v. 12, p. 203–220, https://doi.org/10.1130/GES01237.1.

Saylor, J.E., Stockli, D.F., Horton, B.K., Nie, J., and Mora, A., 2012, Discriminating rapid exhumation from syndepositional volcanism using detrital zircon double dating: Implications for the tectonic history of the Eastern Cordillera, Colombia: Geological Society of America Bulletin, v. 124, p. 762–779, https://doi.org/10.1130/B30534.1.

Saylor, J.E., Jordan, J.C., Sundell, K.E., Wang, X., Wang, S., and Deng, T., 2018, Topographic growth of the Jishi Shan and its impact on basin and hydrology evolution, NE Tibetan Plateau: Basin Research, v. 30, p. 544–563.

Schwartz, T.M., Schwartz, R.K., and Weislogel, A.L., 2019, Orogenic recycling of detrital zircons characterizes age distributions of North American Cordilleran strata: Tectonics, v. 38, p. 4320–4334, https://doi.org/10.1029/2019TC005810.

Sharman, G.R., Graham, S.A., Grove, M., Kimbrough, D.L., and Wright, J.E., 2015, Detrital zircon provenance of the Late Cretaceous–Eocene California forearc: Influence of Laramide low-angle subduction on sediment dispersal and paleogeography: Geological Society of America Bulletin, v. 127, p. 38–60, https://doi.org/10.1130/B31065.1.

Sharman, G.R., Sharman, J.P., and Sylvester, Z., 2018, detritalPy: A Python-based toolset for visualizing and analyzing detrital geo-thermochronologic data: The Depositional Record: A Journal of Biological, Physical and Geochemical Sedimentary Processes, v. 4, p. 202–215, https://doi.org/10.1002/dep2.45.

Shulaker, D.Z., Grove, M., Hourigan, J.K., Van Buer, N., Sharman, G., Howard, K., Miller, J., and Barth, A.P., 2019, Detrital K-feldspar Pb isotopic evaluation of extraregional sediment transported through an Eocene tectonic breach of southern California's Cretaceous batholith: Earth and Planetary Science Letters, v. 508, p. 4–17, https://doi.org/10.1016/j.epsl.2018.11.040.

Smith, G.R., and Dowling, T.E., 2008, Correlating hydrographic events and divergence times of speckled dace (Rhinichthys: Teleostei: Cyprinidae) in the Colorado River drainage, *in* Reheis, M.C., Hershler, R., and Miller, D.M., eds., Late Cenozoic Drainage History of the Southwestern Great Basin and Lower Colorado River Region: Geologic and Biotic Perspectives: Geological Society of America Special Paper 439, p. 301–317, https://doi.org/10.1130/2008.2439(13).

Spencer, C.J., Kirkland, C.L., and Taylor, R.J.M., 2016a, Strategies towards statistically robust interpretations of in situ U-Pb zircon geochronology: Geoscience Frontiers, v. 7, p. 581–589, https://doi.org/10.1016/j.gsf.2015.11.006.

Spencer, J.E., and Reynolds, S.J., 1991, Tectonics of mid-Tertiary extension along a transect through west central Arizona: Tectonics, v. 10, p. 1204–1221, https://doi.org/10.1029/91TC01160.

Spencer, J.E., Smith, G.R., and Dowling, T.E., 2008, Middle to late Cenozoic geology, hydrography, and fish evolution in the American Southwest, *in* Reheis, M.C., Hershler, R., and Miller, D.M., eds., Late Cenozoic Drainage History of the Southwestern Great Basin and Lower Colorado River Region: Geologic and Biotic Perspectives: Geological Society of America Special Paper 439, p. 279–299, https://doi.org/10.1130/2008.2439(12).

Spencer, J.E., Richard, S.M., Gehrels, G.E., Gleason, J.D., and Dickinson, W.R., 2011, Age and tectonic setting of the Mesozoic McCoy Mountains Formation in western Arizona, USA: Geological Society of America Bulletin, v. 123, p. 1258–1274, https://doi.org/10.1130/B30206.1.

Spencer, J.E., Pecha, M.E., Gehrels, G.E., Dickinson, W.R., Domanik, K.J., and Quade, J., 2016b, Paleoproterozoic orogenesis and quartz-arenite deposition in the Little Chino Valley area, Yavapai tectonic province, central Arizona, USA: Geosphere, v. 12, p. 1774–1794, https://doi.org/10.1130/GES01339.1.

Stewart, J.H., Gehrels, G.E., Barth, A.P., Link, P.K., Christie-Blick, N., and Wrucke, C.T., 2001, Detrital zircon provenance of Mesoproterozoic to Cambrian arenites in the western United States and northwestern Mexico: Geological Society of America Bulletin, v. 113, p. 1343–1356, https://doi.org/10.1130/0016-7606(2001)113<1343:DZPOMT>2.0.CO;2.

Swanson-Hysell, N.L., Ramezani, J., Fairchild, L.M., and Rose, I., 2019, Failed rifting and fast drifting: Midcontinent Rift development, Laurentia's rapid motion and the driver of Grenvillian orogenesis: Geological Society of America Bulletin, v. 131, no. 5–6, p. 913–940, https://doi.org/10.1130/B31944.1.

Timmons, J.M., Karlstrom, K.E., Heizler, M., Bowring, S.A., and Crossey, L.C., 2005, Tectonic inferences from the ca. 1254–1100 Ma Unkar Group and Nankoweap Formation, Grand Canyon: Intracratonic deformation and basin formation during protracted Grenville orogenesis: Geological Society of America Bulletin, v. 117, p. 1573–1595, https://doi.org/10.1130/B25538.1.

Van Alstine, D.R., and Gillett, S.L., 1979, Paleomagnetism of upper Precambrian sedimentary rocks from the Desert Range, Nevada: Journal of Geophysical Research, v. 84, p. 4490–4500, https://doi.org/10.1029/JB084iB09p04490.

Vermeesch, P., 2013, Multi-sample comparison of detrital age distributions: Chemical Geology, v. 341, p. 140–146, https://doi.org/10.1016/j.chemgeo.2013.01.010.

Wallace, M.A., Faulds, J.E., and Brady, R.J., 2005, Geologic Map of the Meadview North Quadrangle, Mohave County, Arizona, and Clark County, Nevada: Nevada Bureau of Mines and Geology Map 154, scale 1:24,000, 1 sheet.

Weil, A.B., Geissman, J.W., and Van der Voo, R., 2004, Paleomagnetism of the Neoproterozoic Chuar Group, Grand Canyon Supergroup, Arizona: Implications for Laurentia's Neoproterozoic APWP and Rodinia break-up: Precambrian Research, v. 129, p. 71–92, https://doi.org/10.1016/j.precamres.2003.09.016.

Weil, A.B., Geissman, J.W., and Ashby, J.M., 2006, A new paleomagnetic pole for the Neoproterozoic Uinta Mountain Supergroup, central Rocky Mountain States, USA: Precambrian Research, v. 147, p. 234–259, https://doi.org/10.1016/j.precamres.2006.01.017.

Wernicke, B., 2011, The California River and its role in carving Grand Canyon: Geological Society of America Bulletin, v. 123, p. 1288–1316, https://doi.org/10.1130/B30274.1.

Winn, C., 2019, Landscape evolution of the southern Colorado Plateau using low-temperature apatite thermochronology and detrital zircon and sanidine provenance studies [Ph.D. dissertation]: Albuquerque, University of New Mexico, 265 p.

Winn, C., Karlstrom, K.E., Shuster, D.K., Kelley, S., and Fox, M., 2017, 6 Ma Age of carving Westernmost Grand Canyon: Reconciling geologic data with combined AFT, (U-Th)/He, and ^{4}He/^{3}He thermochronologic data: Earth and Planetary Science Letters, v. 474, p. 257–271, https://doi.org/10.1016/j.epsl.2017.06.051.

Young, R.A., 1999, Nomenclature and ages of Late Cretaceous(?)–Tertiary strata in the Hualapai Plateau region, northwest Arizona, *in* Billingsley, G.H., Wenrich, K.J., Huntoon, P.W., and Young, R.A., Breccia Pipe and Geologic Map of the Southwestern Part of the Hualapai Indian Reservation and Vicinity, Arizona: Appendix for U.S. Geological Survey Miscellaneous Investigations Series Map I-2554, p. 21–50.

Young, R.A., 2001, Geomorphic, structural, and stratigraphic evidence for Laramide uplift of the southwestern Colorado Plateau margin in northwestern Arizona, *in* Erskine, M.C., Faulds, J.E., Bartley, J.M., and Rowley, P.D., eds., The Geologic Transition Colorado Plateau to Great Basin—A Symposium and Field Guide (The Mackin Volume): Utah Geological Association Publication 30, p. 227–237.

Young, R.A., 2011, Brief Cenozoic geologic history of the Peach Spring Quadrangle and the Hualapai Plateau (Hualapai Indian Reservation): Arizona Geological Survey Contributed Report CR-11-O, p. 1–28, map, cross-section. (Available at Arizona Geological Survey as "repository.azgs.az.gov/uri_gin/azgs/dlio/1362".)

Young, R.A., and Brennan, W.J., 1974, The Peach Spring Tuff: Its bearing on the structural evolution of the Colorado Plateau and development of Cenozoic drainage in Mohave County, Arizona: Geological Society of America Bulletin, v. 85, p. 83–90, https://doi.org/10.1130/0016-7606(1974)85<83:PSTIBO>2.0.CO;2.

Young, R.A., and Crow, R., 2014, Paleogene Grand Canyon incompatible with Tertiary paleogeography and stratigraphy: Geosphere, v. 10, p. 664–679, https://doi.org/10.1130/GES00973.1.

Young, R.A., and Hartman, J.H., 2014, Paleogene rim gravel of Arizona: Age and significance of the Music Mountain Formation: Geosphere, v. 10, p. 870–891, https://doi.org/10.1130/GES00971.1.

Zylstra, S., 2017, Late Cretaceous Metamorphic and Plutonic Overprint of Proterozoic Metasediments of Ontario Ridge, San Gabriel Mountains, California [MS thesis]: Pomona, California State Polytechnic University, 121 p.